Project Title:

Evaluation of Bridge Decks Using Non-Destructive Evaluation (NDE) at Near Highway Speeds for Effective Asset Management

FINAL REPORT

Sponsoring Organization: Michigan Department of Transportation

Research Agency:

Michigan Technological University
1400 Townsend Drive
Houghton, MI 49931

Principal Investigator(s):

Theresa M. Ahlborn, PhD, FACI, FPCI
Professor
Civil & Environmental Engineering
Director, Center for Structural Durability

Colin N. Brooks, MEM
Research Scientist
Manager, Environmental Science Lab
Michigan Tech Research Institute

Date Submitted: June 30, 2015

Michigan Tech

1. Report No. RC-1617	**2. Government Accession No.** N/A	**3. MDOT Project Manager** Eric Burns
4. Title and Subtitle Evaluation of Bridge Decks using Non-Destructive Evaluation (NDE) at Near Highway Speeds for Effective Asset Management – FINAL REPORT		**5. Report Date** March 31, 2015 **6. Performing Organization Code** N/A
7. Author(s) Theresa (Tess) M. Ahlborn and Colin N. Brooks		**8. Performing Org. Report No.** N/A
9. Performing Organization Name and Address Michigan Technological University 1400 Townsend Drive Houghton, Michigan 49931		**10. Work Unit No. (TRAIS)** N/A **11. Contract No.** 2010-0295 **11(a). Authorization No.** Z7
12. Sponsoring Agency Name and Address Michigan Department of Transportation Office of Research and Best Practices 425 West Ottawa Street Lansing MI 48933		**13. Type of Report & Period Covered** Final Report 11/1/2012 – 3/31/2015 **14. Sponsoring Agency Code** N/A
15. Supplementary Notes None		

16. Abstract

Remote sensing technologies allow for the condition evaluation of bridge decks at near highway speed. Data collection at near highway speed for assessment of the top of the concrete deck and proof of concept testing for the underside of the deck was conducted for surface and subsurface evaluation. 3-D photogrammetry was combined with passive thermography to detect spalls, cracks and delaminations for the top of the concrete bridge deck, while active thermography was investigated for bottom deck surface condition assessment. Successful field demonstrations validated results comparable to MDOT inspections. Recommendations for immediate implementation for condition assessment of the top of a concrete deck are included for introducing the BridgeViewer Remote Camera System into current bridge inspections to provide a photo inventory of the bridge deck captured at 45mph and above using GoPro cameras. The combined optical photogrammetry (3DOBS) and passive thermography technologies provide an objective analysis of spalls, cracks and suspected delaminations while traveling at near highways speed. Using the same 3DOBS technology with higher resolution cameras and slower speeds, cracks can be detected as small as 1/32 in. Laboratory and field demonstrations show active thermography would benefit from further development as a remote sensing technology for condition assessment on the underside of the bridge deck.

17. Key Words inspection, concrete, concrete bridge deck, remote sensing, condition assessment, field demonstration	**18. Distribution Statement** No restrictions. This document is available to the public through the Michigan Department of Transportation.

19. Security Classification - report Unclassified	**20. Security Classification - page** Unclassified	**21. No. of Pages** 547	**22. Price** N/A

Acknowledgements

The Michigan Department of Transportation is recognized for their support in the research efforts. Also acknowledged is the work by project partners including the Michigan Tech Research Institute, Department of Civil & Environmental Engineering at Michigan Technological University, and BridgeGuard, Inc.

Michigan Department of Transportation:
Eric Burns, Project Manager
Michael Townley, Research Manager
Research Advisory Panel members Jim Covey, Dave Juntunen, Bob Kelley, John Lobbestael, Linda Reed and Nate VanDrunen
Rich Stack and Numerous Field Personnel

Michigan Tech Research Institute:
David Banach, Dave Dean, Rick Dobson, Nate Jesse, Amy Rohman and Blaine Stormer

Department of Civil & Environmental Engineering, Michigan Technological University:
Jason Cattelino and Khatereh Vaghefi

BridgeGuard, Inc.:
Gary Howard, Jay Ruohonen, Chase Sturos, David Torola, and Field Technicians

Disclaimer

This publication is disseminated in the interest of information exchange. The Michigan Department of Transportation (hereinafter referred to as MDOT) expressly disclaims any liability, of any kind, or for any reason, that might otherwise arise out of any use of this publication or the information or data provided in the publication. MDOT further disclaims any responsibility for typographical errors or accuracy of the information provided or contained within this information. MDOT makes no warranties or representations whatsoever regarding the quality, content, completeness, suitability, adequacy, sequence, accuracy or timeliness of the information and data provided, or that the contents represent standards, specifications, or regulations.

1. Table of Contents

List of Figures

Page

List of Tables

Page

Executive Summary

Just over 30% of the U.S. transportation infrastructure has passed its expected service life soon (FHWA 2011). The rate at which we build new bridges has subsided in the past decades as the nation has changed to a focus on preservation of the infrastructure. Enhanced inspection techniques for bridge condition assessment are directly related to this focus as effective assessment management is founded on quality objective bridge inspection techniques.

Development of commercially available and rapidly advancing technologies has lead to a renewed interest in remote sensing. Remote sensing applications for bridge inspection means the ability to evaluate the condition of a bridge in a hands-off manner without traffic disruption. Such applications can increase public mobility and safety of inspectors, as well as reduce inspection times and improve subjective inspection methods and reporting. Enhanced inspections lead to effective asset management through improved data for decision support and prioritization of preservation projects.

From a maintenance and preservation perspective, the bridge deck is the critical component in protecting the remaining superstructure and substructure from the environment and contaminants while taking on a primary role for load transfer. As a result, one of the first elements besides bridge deck joints of a bridge to deteriorate and consequently require attention is the deck. Therefore, thorough assessment of the condition of this component is necessary to ensure the integrity of the bridge structure. To accurately assess the condition of this major component, it is equally important to evaluate both the top and bottom of the deck. Only after thorough evaluation of both can the integrity and remaining service life of the bridge be determined.

This research project investigated non-destructive evaluation (NDE) techniques deployable at- or near-highway speed augmenting bridge deck inspection programs, by detecting and quantifying delaminations, cracks and spalls, for the top surface of the concrete bridge deck. In addition, the condition of the concrete deck bottom surface was evaluated in a hands-off manner using remote sensing technologies including 3-D photogrammetry and active thermography. Outreach activities included training sessions for MDOT personnel to understand and implement these technologies.

Condition Assessment of the Top Surface of Concrete Bridge Decks

Health indicators for distress in concrete bridge decks include spalls, cracking and delaminations. The top surface of the deck is typically visually inspected while subsurface degradation is often determined by sounding with hammer or with a chain drag. Principals of photogrammetry and thermography, both non-destructive remote sensing technologies, were demonstrated as tools for condition assessment of health indicators.

Passive thermal imaging and a 3-D Optical Bridge-evaluation System (3DOBS, an application of 3-D photogrammetry) were combined for detecting spalls and delaminations on the top deck surface at near-highway speeds. Passive thermography is a more mature technology used to locate suspected delaminations and is capable of operating at highway speed. The 3DOBS system, previously used at walking speed, was upgraded to a camera system with a high frame rate for implementation at near highway speed to detect spalls. Using a higher resolution 3DOBS system at slower speeds, crack size and location detection was demonstrated on cracks as small as 1/32 in. In addition, the Bridge Viewer Remote Camera System (BVRCS), also an optical system using Go-Pro cameras, was developed to provide a high-resolution photo inventory of the top deck surface while travelling at highway speed.

Two field deployments of the non-destructive testing methods were conducted. Emphasis during the first deployment was on the evaluation of individual technologies including the 3DOBS high-resolution system to detect spalls and cracking, and evaluation of the passive infrared thermography to detect delaminations. The results of the first deployment were used as a basis for comparison for the second deployment. The remote sensing techniques were evaluated, systems upgraded, vehicular mounting system improved, and lab testing was conducted between deployment phases.

Figure ES-1: Deployment without traffic disruption

The second deployment allowed for further evaluation of the 3DOBS low-resolution system and passive infrared thermography conducted simultaneously at near highway speeds, demonstrating the data collection process without traffic disruption (see Figure 1). This deployment also allowed for implementation and evaluation of the 3DOBS high-resolution system at slower speeds for more refined crack evaluation. For comparison purposes, an MDOT certified bridge inspector was present for the Maryland Ave field tests to establish ground-truth information. Results from the remote sensing tests were evaluated based on the inspector's findings.

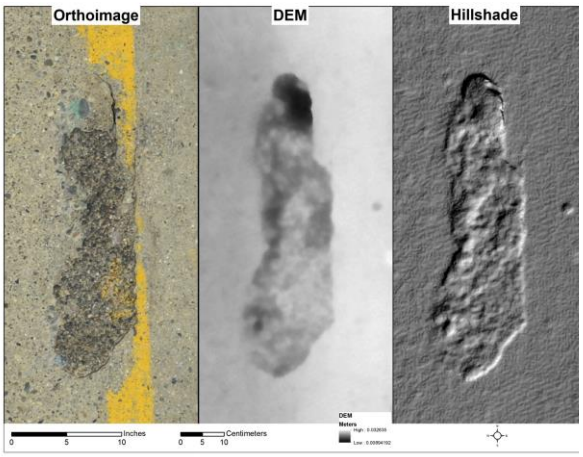

Figure ES-2: Generated data layers

Eight layers of georeferenced datasets from the collected imagery is available for decision support. The layers include an

orthoimage, digital elevation model (DEM), hillshade of DEM, LAS point cloud of the bridge deck, thermal mosaic, detected spalls, detected cracks, and potential delaminations. A combination of these layers could enable MDOT to perform a change detection analysis on the distresses and provide objective data to assist in generating condition states assessments and NBI ratings for the top surface of the concrete bridge deck.

The BridgeViewer Remote Camera System (BVRCS) was developed and successfully demonstrated for documenting the top surface of the bridge deck with a high resolution geo-tagged photo inventory using GoPro cameras at operating speeds of 45 mph and above. By incorporating BVRCS into bridge deck assessments, MDOT can quickly obtain temporally accurate imagery of bridge decks and store the information into photo inventories. These inventories can be accessed for use prior to the next inspection or during preliminary bridge scoping.

Condition Assessment of the Bottom Surface of Concrete Bridge Decks

The condition of the bottom surface of the deck is subjected to the same types of distress as the top surfaces including subsurface spalls and cracks, and delaminations. However, access can be limited and techniques applicable for condition of the top surface may not be effective for assessment of the bottom surface. Active thermography involves an external heat source rather than the sun to impart heat on the system. 3DOBS photogrammetry was used in conjunction with the active thermal IR testing method to evaluate the bottom surface of the deck. Laboratory tests focused on reducing inspection time and the portability of equipment. The results validated the method for a proof of concept field demonstration.

Field testing was performed to evaluate the bottom surface of the deck using active thermal IR. Weather conditions during the field demonstration dictated that a pier cap be evaluated rather than a fascia beam in addition to the bottom deck surface.

Results indicate that this remote sensing technology is acceptable for detecting and quantifying delaminations. A simple polygon method for analysis was developed to quantify delamination areas for comparison to MDOT ground truth. In all cases, the current MDOT hammer sounding method of inspection for estimating the area of delamination was conservative relative to active thermography results.

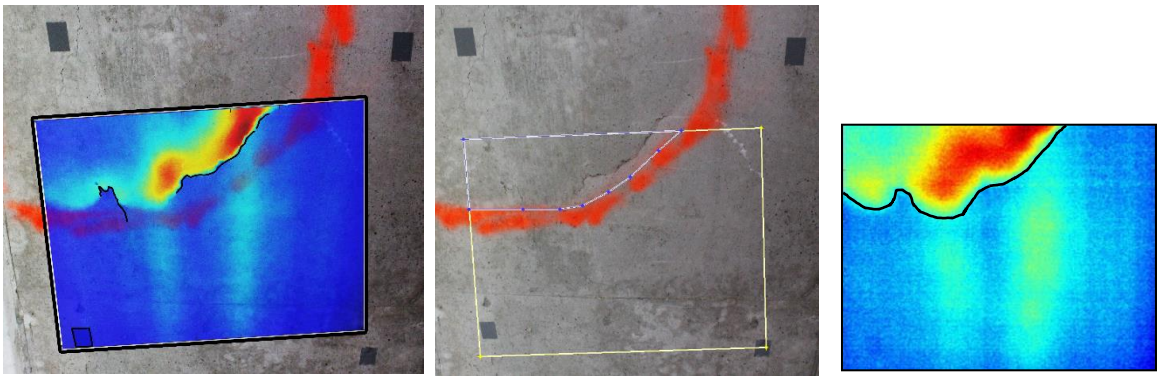

Figure ES-3: Results of active thermography testing on the underside of a concrete bridge deck

As with technologies deployed for the top deck surface evaluation, implementation of this remote sensing technology can best be realized through further development prior to implementation. Improvements in data analysis, repeatability of the test method and results, and reduced testing time are parameters that need to be further addressed.

Outreach Activities

With an objective of gaining an understanding of the field readiness and demand for technologies by current bridge inspectors, a general training session was conducted to provide a hands-on equipment demonstration of the 3DOBS, BVRCS and active IR thermography systems. The presentation slides are presented in an appendix. Outcomes included the request for an additional training session specific to the data processing for the 3DOBS photogrammetry imagery, which was provided. Attendees, including inspectors, region bridge engineers and photogrammetry experts, agreed that BVRCS was ready for deployment and requested an additional training session and a "How To" manual for use (Appendix H). The combined technologies of 3DOBS and passive thermography for top of deck condition assessment are near ready for implementation and will require additional pilot studies prior to full implementation. Bottom of deck assessment techniques were recommended for further study.

1. Introduction

As the nation's concrete highway bridges age, bridge inspectors and engineers demand easily deployable condition assessment technologies. Effective asset management facilitated by a comprehensive evaluation method for bridge decks and structures is not only a priority for transportation departments, but also a major factor in determining the priority of bridge preservation activities. While these evaluation methods provide engineers with valuable information regarding the remaining service life of structures and whether maintenance should be performed, it is important that inspections and assessments be conducted consistently and accurately to inform good decisions.

Non-destructive evaluation (NDE) techniques have been long sought after to provide complete and accurate assessment of bridge condition. Remote sensing, a subset of NDE, can be of even more benefit to the bridge inspection and management community by providing an avenue for collection of bridge health data, without direct contact, leading to little or no traffic disruption (Ahlborn et al. 2012). Therefore, to the bridge industry, the term *remote sensing* can be used interchangeably with NDE when NDE does not come into contact with the element being inspected. To the bridge inspector, remote sensing provides an opportunity to assess the condition of the bridge without traffic disruption.

Numerous indicators of bridge condition can be assessed using remote sensing technologies. For example, concrete delamination is one of the indicators of steel reinforcement deterioration within concrete bridge elements. Quantifying the area of delamination can result in a more accurate estimate of the deck deficiency allowing for a more suitable National Bridge Inventory (NBI) rating. Significant deficient area (>10%) on the bottom side of the bridge deck results in a poor condition rating of the bridge deck. In the case of excessive delaminated areas on the bottom side of the concrete deck, false decking is installed over the travel lane to prevent damage to the traffic underneath the bridge (MDOT 2008), and in many cases bridge decks will be scheduled for replacement instead of rehabilitation practices.

Routine bridge inspection usually involves visual inspection of bridge elements and taking notes of deficient areas. In the case of excessive indicators of deterioration, an in-depth inspection is scheduled. In general, an in-depth bridge inspection for the underside of a bridge deck includes the use of conventional inspection practices such as hammer sounding, which is labor intensive, subjective, and often requires traffic lane closures resulting in mobility concerns such as transit disruptions and safety concerns for inspectors. Delaminated areas reveal hollow sounds when tapped with a hammer compared to a sharp tone of intact concrete allowing inspectors to locate and quantify defective areas.

It is recognized that no single technology can assess the complete condition of a highway bridge. While some technologies remain in their infancy for use in bridge inspections, many such as optical, thermal, and ground penetrating radar, have had some success in determining the condition of concrete bridge elements. Combining remote sensing technologies with

current common practices has been found to be beneficial to detecting surface and subsurface indicators for specific bridge elements (Vaghefi et. al, 2012).

Using remote sensing technologies at highway speed can eliminate the need for lane closures, reduce mobility costs and improve safety. But little research has been conducted at highway speed. In fact, most studies have considered static testing or testing at walking speed. The current study presented herein combines three technologies (thermal, photographic and photogrammetric) by evaluating their performance at various speeds, including near-highway speed, to assess bridge deck health indicators.

1.1 Objectives

This research was conducted to:

1. Investigate non-destructive evaluation (NDE) techniques that can be deployed at- or near-highway speed augmenting bridge deck inspection programs, by detecting and quantifying delaminations, cracks and spalls, for the top surface of the concrete bridge deck.
2. Investigate the condition of the concrete deck bottom surfaces and fascia beams in a hands-off manner using remote sensing technologies.
3. Provide MDOT employees with training to deploy acceptable technologies.

1.2 Scope

To accomplish the objectives, the research team took a multifaceted approach dividing the effort among several tasks. Because the technologies are changing and improving quickly in today's market, a comprehensive literature review centered on what is being done commercially and academically in the area of remote sensing for bridge condition assessment. The review includes a general assessment of common types of deterioration of concrete bridge decks, as well as the current MDOT methods of practice and an overview of NDE assessment methods including the current state of remote sensing technologies for assessing the condition of concrete bridge decks and fascia elements.

Individual technologies, specifically thermal and optical imaging, were considered for further evaluation. Upgrading equipment and data fusion of these technologies for a combined assessment was first performed in the laboratory environment before conducting field demonstrations at near highway speed. Primary tasks were divided into two groups considering the top surface of the bridge deck with testing at near highway speed, and the bottom surface and fascia beams.

Passive thermal imaging and a 3-D Optical Bridge-evaluation System (3DOBS, an application of 3-D photogrammetry) were combined for detecting spalls and delaminations on the top deck surface at near-highway speeds. Passive thermography is a more mature technology used to

locate suspected delaminations and is capable of operating at highway speed. The 3DOBS system, previously used at walking speed, was implemented at near-highway speed to detect spalls using a lower resolution camera system. Using a higher resolution system and slower speeds, crack size and location was investigated. In addition, the Bridge Viewer Remote Camera System (BVRCS), also an optical system using Go-Pro cameras, was enhanced to provide a high-resolution photo inventory of the top deck surface while travelling at highway speed.

Assessing the condition of the bottom surface of the deck was more challenging and was not intended to operate in transit. Rather, active thermography (using an external heat source) was investigated in the laboratory prior to the proof-of-concept field demonstration to detect subsurface delaminations. Combining active thermography with 3DOBS allowed for data to be overlaid such that cracking and delaminations could be assessed in a combined fashion.

Educating a workforce of bridge inspectors was an integral part of this research project. Training, including equipment demonstration, was provided for MDOT personnel showing all remote-sensing technologies investigated. Further training was specifically developed for bridge inspectors to implement BVRCS. Additional training was provided to assist MDOT personnel in understanding data fusion and processing such that MDOT can begin implementation.

Combining technologies results in a bridge inspection suite of tools that represents a highly integrated, multi-spectral, and multi-sensor inspection system that provides an assessment of several health indicators for surface and subsurface issues. The vetting of these technologies, individually and combined, through laboratory studies and field demonstrations are described herein, along with conclusions and recommendations for implementation.

2. Literature Review

2.1 Review of Previous Research

The maintenance, preservation, and improvement of transportation infrastructure is a growing challenge for state and local governments, particularly for bridges. Billions of dollars are needed to repair and replace aging bridges, with one recent estimate at $140 billion (AASHTO 2008). Following the I-35W bridge collapse in August 2007, the deteriorating condition of bridges has been under increased scrutiny by government officials, as well as the public. This emphasis is warranted considering that approximately 25 percent of the nation's 600,000 bridges are either structurally deficient or functionally obsolete. In Michigan, 12 percent of the state's 11,000 bridges are structurally deficient. This statistic highlights the need for upgrading and replacing existing infrastructure, and underscores the importance of quality inspection and assessment mechanisms to prioritize these efforts.

Many methods have been applied to the inspection of bridge deck systems, including coring of the pavement, conductivity tests, and pavement sounding using acoustical devices and ground penetrating radar (GPR). These techniques are generally time consuming, labor intensive, tedious, operator dependent and cost prohibitive. Furthermore, traffic control dilemmas caused by current bridge deck inspection techniques increase safety and mobility concerns for both inspection teams and the traveling public alike.

The primary components of a bridge can be categorized as the bridge deck, superstructure and substructure. The superstructure is responsible for supporting the bridge deck by means of beams and the substructure transfers loads from the superstructure to the ground through abutments and piers. While all three components are essential to the performance of a bridge, the bridge deck is of major interest due to the primary role of transferring loads to the superstructure and substructure and determines when preservation activities are to be performed to a specific structure. From a maintenance and condition evaluation perspective, bridge decks serve as the driving surface while also providing protection from the environmental and contaminant impacts (e.g., salts and chemicals) to the superstructure and substructure elements below. As a result, the first element of a bridge to deteriorate and consequently require attention is frequently the deck. Therefore, thorough assessment of the condition of this component is necessary to ensure the integrity of the bridge structure. To accurately assess the condition of this major component, it is equally important to evaluate both the top and bottom of the deck. Only after thorough evaluation of both can the integrity and remaining service life of the bridge be determined.

During routine bridge inspections, decks are evaluated visually and if an in-depth inspection is needed, a more detailed study is conducted. Sounding by hammer or by chain dragging are MDOT's current methods for conducting a delamination study and are only as effective as the

person who is conducting or reading the tests. Because the separated layers inside concrete can cause an interruption in sound wave transmission through the concrete, sounding methods are the most common techniques for detecting delaminated areas. Tapping concrete with a metal rod or a light weight hammer on concrete bridge elements and dragging a chain across the concrete bridge deck are the most common methods for detecting delaminations during a bridge inspection. Delaminated areas reveal hollow sounds when tapped with a hammer compared to a sharp tone of intact concrete and this can indicate the defective area. The chain drag method involves dragging a heavy chain across the bridge deck and marking the hollow sounding area with spray paint similar to the hammer sounding technique (Ryan et al. 2006; Jana 2007).

Both assessment techniques are labor intensive, require traffic control over the bridge deck and are dependent on the inspector's training and experience. These bridge deck evaluations determine the presence of not only delaminations, but also cracking, spalling, scaling, and even fascia and expansion joint conditions throughout the structure.

Evaluation of bridge deck cracking is also a labor intensive. During detailed scoping inspections when lanes are closed, inspectors evaluate the entire bridge deck for cracking. This involves the inspector walking down each lane, drawing cracking patterns, measuring crack widths and estimating length and location on the deck. Crack widths are measured using a crack gauge which has to be held up the crack for accurate measurements. Smaller hairline cracking can be missed during the inspection due to lighting conditions or the ability of the inspector to see small cracks.

No less important is the condition of the deck bottom surface. While the bridge deck riding surface is the most prominent topic of discussion in bridge condition assessment, problems with the bottom surface and fascia can be disastrous and possibly fatal. Ascertaining their condition periodically is extremely important when considering the possibility of bridge debris falling on passing traffic. Current underside in-depth inspection techniques are limited to hammer-soundings. This method provides both access challenges and safety concerns to inspectors working over traffic lanes. In addition, such inspections are time consuming and subject to an individual inspectors training and experience.

A combination of thermal imaging and electro-optical technologies allows inspectors to assess surface and subsurface health indicators in a less subjective manner. These new inspection methods will improve consistency among inspectors and provide more accurate quantitative results. With the potential of these sensors being mounted to vehicles, these technologies offer DOTs the ability to collect data while driving across bridges. The purpose of this report is to provide background on bridge health indicators and overview of application of thermal and electro-optical imagery to assess health indicators of the bridge deck, fascia beams and underside. This is done by evaluating prior research on these technologies including the findings from the recent USDOT/RITA project "Bridge Condition Assessment Using Remote Sensors" (www.mtri.org/bridgecondition).

2.1.1 Common types of deterioration of concrete bridge decks

Within the state of Michigan, 79% of total bridge deck systems are either concrete cast- in-place or precast concrete panels (FHWA 2011). Therefore, evaluation of the concrete bridge decks is the main focus of this report. A bridge deck can be classified, to a certain extent, as a sacrificial element because it can be replaced as it degrades. However, as the integrity of the deck is compromised during the degradation process, the protection afforded to the superstructure and substructure elements also diminishes, often providing a catalyst for deterioration or accelerating degradation of these elements.

In general, assessing the condition of a bridge deck includes detecting deck health indicators such as spalls, scaling, map cracking and delaminations as well as monitoring the vertical and horizontal cracks on the bridge deck and expansion joints condition. These health indicators are classified as surface and subsurface measures that-indicate the condition of both the top and bottom surfaces of the deck as well as the deck fascia.

Current practice for detecting bridge deck health indicators during bridge inspections includes visual inspection, chain dragging the bridge deck top surface and hammer sounding the bridge deck top, bottom and fascia. Not all bridges undergo an in-depth inspection using chain dragging and hammer sounding techniques. The severity of the bridge deck condition is identified through visual inspections and financial demands related to traffic control are considered before in-depth inspections are performed.

2.1.2 Bridge health indicators

Table 2-1 shows bridge health indicators used to assign condition for concrete bridge deck and fascia based on the guidelines provided by MDOT for the National Bridge Inventory (NBI) rating (MDOT 2011) and AASHTO for Pontis condition state rating (AASHTO 2011). Methods that are listed in this table are the tools generally being used by transportation agencies to conduct an in-depth inspection survey and rate bridges in NBI scheme. However, in more critical cases and where a NDE tool is available, an in-depth inspection with a NDE tool may be conducted to provide additional information regarding the deck deficiency.

Table 2-1: Bridge Health Indicators for Concrete Bridges

Location		*Bridge Health Indicator*	*Required Measurements*	*Current practice methods*
Deck Top	Surface	Spalls, scaling	1/4" depth * 6" diameter **	Visual inspection
		Cracking	1/32" wide *	Visual inspection
		Map cracking	spacing of 1ft **	Visual inspection
	Subsurface	Delamination	6" diameter **	Chain drag, Hammer sound
Deck Bottom	Surface	Spalls, scaling	1/4" depth * 6" diameter **	Visual inspection
		Cracking	1/32" wide *	Visual inspection
		Map cracking	spacing of 1ft **	Visual inspection
	Subsurface	Delamination	6" diameter **	Hammer sound
Fascia (prestressed concrete beam)	Surface	Spalls, scaling	1/4" depth * 6" diameter **	Visual inspection
		Cracking	0.004" wide **	Visual inspection
		Map cracking	spacing of 1ft **	Visual inspection
	Subsurface	Delamination	6" diameter **	Hammer sound

* reference: MDOT 2011
** reference: AASHTO 2011

2.1.2.1 Delaminations

Delaminations are separations of concrete layers generally over and near the top layer of rebar. Delaminations can express themselves as horizontal cracked planes in concrete slabs that at times deflect vertically to represent on the deck surface. As these cracked planes are so small

in size and virtually undetectable to the human eye, determining the exact location and area of delamination during visual bridge inspections involves numerous challenges and difficulties. Corrosion of reinforcing steel in concrete bridges has been highlighted as the main cause of delamination in literature (FHWA 2006; Jana 2007). Freeze-thaw cycles and overstress in a member are other factors that can also cause delaminations. Delaminated areas can completely separate from the concrete bridge elements and develop into spalls; thus, it is important to identify the location and size of these areas accurately.

2.1.2.2 Map Cracking

Map cracking is the distress of concrete decks in which the surface has a pattern of cracks caused by material failure. Traditional inspection techniques used for the assessment of map cracking include visual evaluation, ultrasonic testing, and impact- echo (FHWA 2006). According to the *AASHTO Manual for Bridge Element Inspection*, cracking on the bridge can be assessed based on the crack width and density, and then classified into four different condition states for repair decision-making process, see Figure 2-1. Detecting areas of map cracking is critical for bridge deck condition assessment as these areas can indicate a delaminated area or rebar corrosion underneath. Map cracking at the bottom surface of the deck can be more critical due to the safety issue for underneath traffic. Also, identifying areas of cracking allows for preventative maintenance actions to prevent further chloride ingress and corrosion inside concrete.

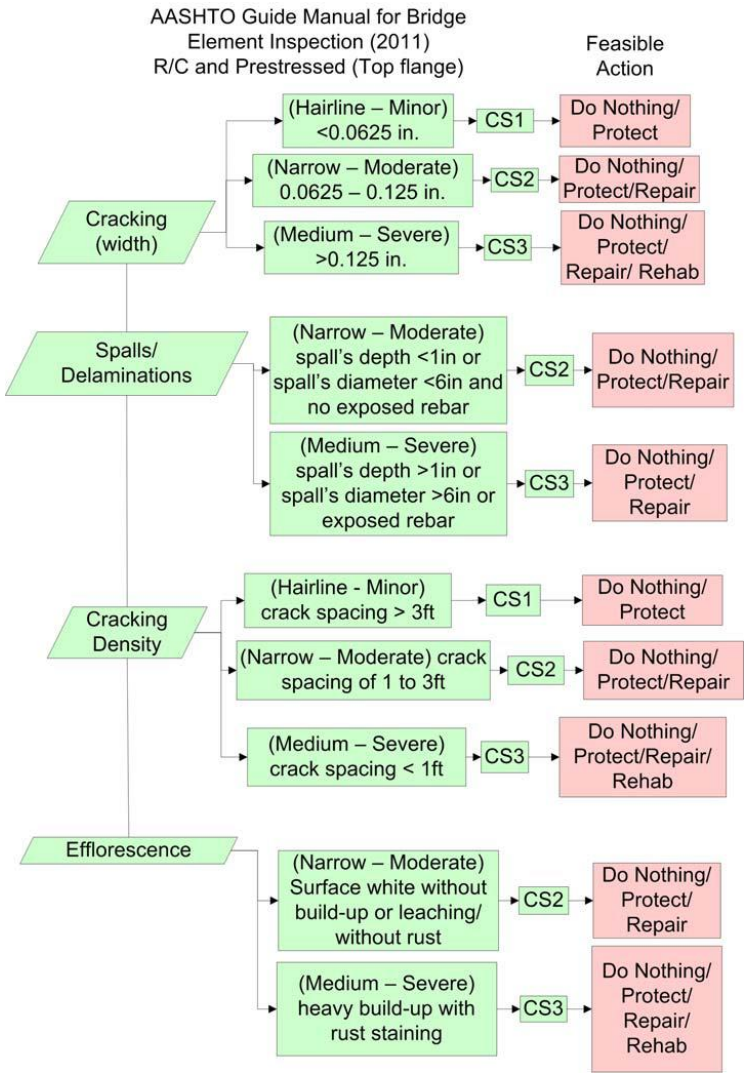

Figure 2-1: Summary of the AASHTO Repair Guideline for Concrete Bridge Decks and Top Flange of Prestressed Concrete Bridges.

2.1.2.3 Spalling and Scaling

Spalling and scaling on the bridge top and bottom surfaces of the deck are defined as the loss of material due to corrosion of rebar or distress on the concrete deck surface. For the purpose of this document and research, spalling is considered on the order of magnitude of 1/4 to 1 inch in depth (FHWA 2006; MDOT 2011) and 6 inches in diameter (AASHTO 2011). The current method for identifying the amount of spalling on a bridge structure is visual assessment. Detecting spalls is necessary over the bridge deck, specifically on the wheel path and riding surfaces. Also, spalls and scaling on the top or bottom surface of the bridge deck can indicate the presence of subsurface defects such as a large area of delamination and can be significantly important for bridge deck condition assessment and the decision to proceed with preservation activities.

2.1.2.4 Deck Fascia Condition

According to the MDOT Bridge Element Inspection Manual, condition of the bridge deck fascia can be assessed and classified into four different condition states based on the amount of spalling and cracking on the fascia, possibility of large spalls dropping of the bridge, and strength of the railing (MDOT 2007). The current methods of deck fascia inspection are primarily visual and hammer sounding, with the use of crack width gauge where accessible and needed.

Detecting delaminated areas on the bridge deck fascia is more critical to determining the condition of this structural component than identifying cracks. Delaminated areas on the fascia can turn into spalls and can raise safety issues for traffic passing underneath the bridge.

2.1.2.5 Expansion Joint Condition

There are several different types of distress related to the expansion joints of a bridge that are also common indicators of overall bridge health. These include torn or missing seals, armored plate damage, chemical leaching on joint bottoms, cracks within two feet of the joint and spalls within two feet of the joint. The magnitude threshold of cracking and spalling is identical to those for surface cracking (1/16 to 3/16 inch in width) and spalling (1/4 to 1 inch in depth) (FHWA 2006).

2.1.3 Current MDOT practice methods for bridge condition assessment

Bridge inspection information is recorded in the bridge safety inspection report, the *Michigan Bridge Element Inspection Report,* and in the detailed scoping documents. The *MDOT Bridge Deck Preservation Matrix and Project Scoping Manual* provides various maintenance activity decision guidelines and an associated fixed life for each activity (MDOT 2009; MDOT 2011).

During biennial bridge inspections, both top and bottom surface of the bridge deck are inspected and total percent deck deficiency is included in the bridge safety inspection reports. Also, qualitative assessment of the deteriorating conditions, such as location and significance of the spalls, cracks or delaminations, is explained for each bridge element. Michigan Bridge Deck Preservation Matrix provides guidance for bridge deck condition decision (Table 2-2). Referring to this matrix, deficiency percent is defined as total percent of deck surface area that is spalled, delaminated or patched with temporary patch materials. This matrix was created from element deterioration data, and the intellect of individuals from Construction and Technology, Maintenance and Design Support Areas, and FHWA. The guidelines established by this matrix lead to an economical repair decision, which can be Capital Scheduled Maintenance (CSM), Capital Preventive Maintenance (CPM), Rehabilitation or Replacement (MDOT 2008). Current bridge inspection practices usually involve visual

inspection of the bridge elements and quantification of crack widths and spall dimensions. Inspections are conducted over accessible areas on the bridge as traffic allows.

Table 2-2: Bridge Deck Preservation Matrix

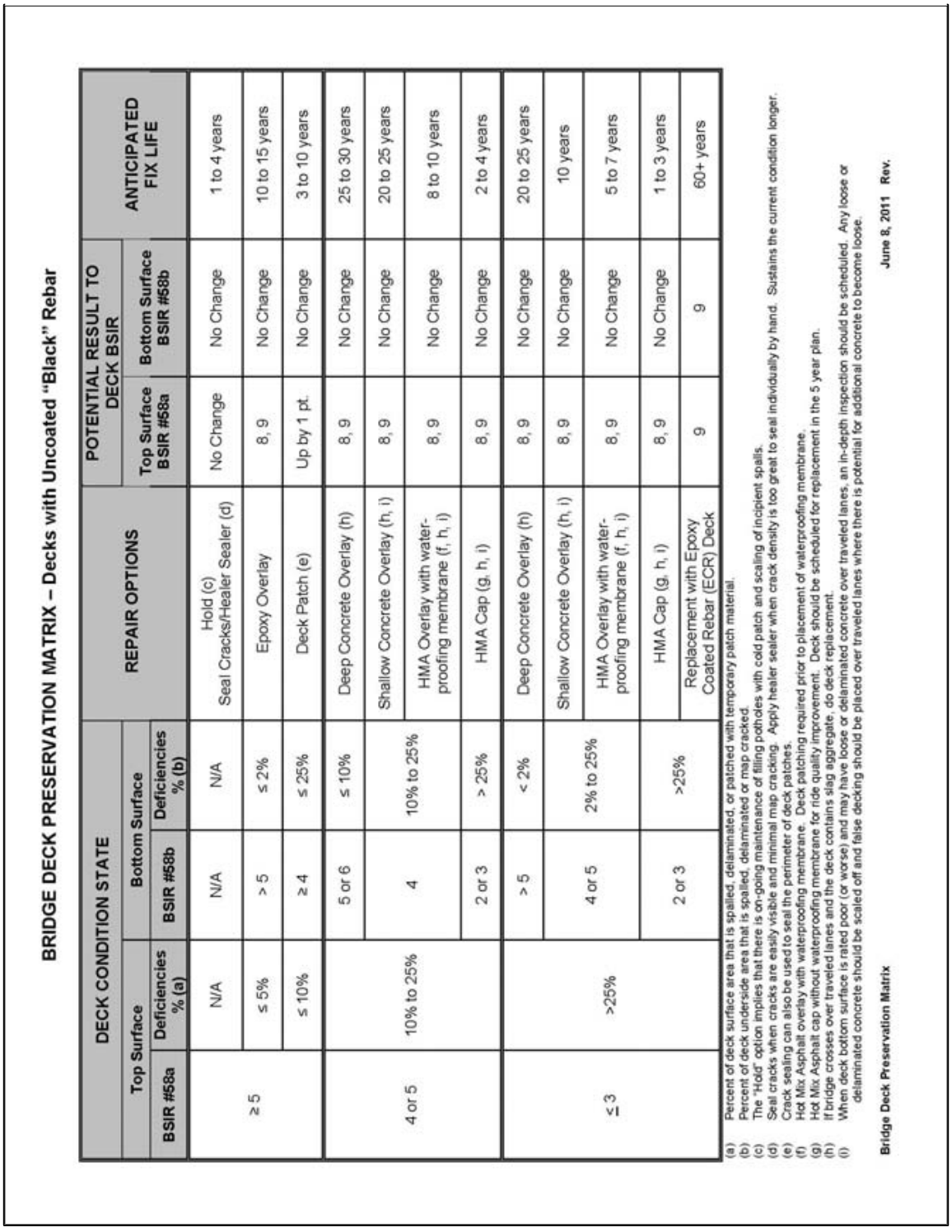

BRIDGE DECK PRESERVATION MATRIX – Decks with Uncoated "Black" Rebar

DECK CONDITION STATE				REPAIR OPTIONS	POTENTIAL RESULT TO DECK BSIR		ANTICIPATED FIX LIFE
Top Surface		Bottom Surface			Top Surface BSIR #58a	Bottom Surface BSIR #58b	
BSIR #58a	Deficiencies % (a)	BSIR #58b	Deficiencies % (b)				
≥ 5	N/A	N/A	N/A	Hold (c) Seal Cracks/Healer Sealer (d)	No Change	No Change	1 to 4 years
	≤ 5%	> 5	≤ 2%	Epoxy Overlay	8, 9	No Change	10 to 15 years
	≤ 10%	≥ 4	≤ 25%	Deck Patch (e)	Up by 1 pt.	No Change	3 to 10 years
4 or 5	10% to 25%	5 or 6	≤ 10%	Deep Concrete Overlay (h)	8, 9	No Change	25 to 30 years
		4	10% to 25%	Shallow Concrete Overlay (h, i)	8, 9	No Change	20 to 25 years
				HMA Overlay with water-proofing membrane (f, h, i)	8, 9	No Change	8 to 10 years
		2 or 3	> 25%	HMA Cap (g, h, i)	8, 9	No Change	2 to 4 years
≤ 3	>25%	> 5	< 2%	Deep Concrete Overlay (h)	8, 9	No Change	20 to 25 years
		4 or 5	2% to 25%	Shallow Concrete Overlay (h, i)	8, 9	No Change	10 years
				HMA Overlay with water-proofing membrane (f, h, i)	8, 9	No Change	5 to 7 years
		2 or 3	>25%	HMA Cap (g, h, i)	8, 9	No Change	1 to 3 years
				Replacement with Epoxy Coated Rebar (ECR) Deck	9	9	60+ years

(a) Percent of deck surface area that is spalled, delaminated, or patched with temporary patch material.
(b) Percent of deck underside area that is spalled, delaminated or map cracked.
(c) The "Hold" option implies that there is on-going maintenance of filling potholes with cold patch and scaling of incipient spalls.
(d) Seal cracks when cracks are easily visible and minimal map cracking. Apply healer sealer when crack density is too great to seal individually by hand. Sustains the current condition longer.
(e) Crack sealing can also be used to seal the perimeter of deck patches.
(f) Hot Mix Asphalt overlay with waterproofing membrane. Deck patching required prior to placement of waterproofing membrane.
(g) Hot Mix Asphalt cap without waterproofing membrane for ride quality improvement. Deck should be scheduled for replacement in the 5 year plan.
(h) If bridge crosses over traveled lanes and the deck contains slag aggregate, do deck replacement.
(i) When deck bottom surface is rated poor (or worse) and may have loose or delaminated concrete over traveled lanes, an in-depth inspection should be scheduled. Any loose or delaminated concrete should be scaled off and false decking should be placed over traveled lanes where there is potential for additional concrete to become loose.

Bridge Deck Preservation Matrix

June 8, 2011 Rev.

Biennial routine inspection is the most common method of bridge inspection practices. During a routine bridge inspection, a bridge inspector visually observes the bridge and makes notes of deficient areas. These notes along with general measurements of the bridge are included in Bridge Safety Inspection Report (BSIR). Because this type of inspection relies on assessing the bridge visually, there are some limitations for evaluating areas that are not sufficiently visible or that raise safety issues for inspectors. Although routine bridge inspection focuses on overall condition of all the bridge components, the main attention is mostly on the deficient areas that were found in previous inspections and were indicated in the inspection report (Fu 2005). In-depth inspections, which include chain dragging, hammer sounding or the use of other NDE methods, are more comprehensive than biennial inspections, require lane closure over or under the bridge and are conducted more regularly on poor condition bridges. However, these types of inspections are not a required practice during a biennial inspection and are only completed when additional condition information is required and preservation activities become a priority. Chain dragging and hammer sounding along with the more commercialized version of an electro-mechanical sounding cart are standardized in ASTM D4580 – *Standard Practice for Measuring Delaminations in Concrete Bridge Decks by Sounding*. The main components of an electro mechanical cart include a battery, two tapping wheels, two sonic receivers and a strip recorder (ASTM 1997). This device can detect delaminations up to 2.6 inches below the surface (Jana 2007).

An investigation of the reliability of routine and in-depth visual inspection for highway bridges (Moore et al. 2000), reported significant variability in deck delamination surveys conducted by 22 bridge inspection teams. Basic hammer and chain dragging were the only tools used in this survey and the range of delamination percentage results varied from 2 to 35%. Studies such as this highlight the inconsistency current techniques due to differences in training and experience and reveal the need for an easy to use inspection tool to help bridge inspectors locate and sketch delaminations more accurately and objectively.

2.1.4 Overview of NDE assessment methods

Previous evaluations of NDE methods demonstrate the potential of these techniques to detect deteriorations, provide more accurate assessments, and reduce inspection time of concrete bridge decks (Vaghefi et al. 2012). These methods include: Ground Penetrating Radar, infrared thermography, LiDAR, aerial photogrammetry, UAV photogrammetry, impact echo, visual inspection, chain drag and hammer sounding. Previous studies related to bridge condition assessment have established that there is no single technology available that can provide sufficient information for both surface and subsurface bridge deck defects (Ahlborn et al. 2012; Gucunski et al. 2013). Therefore, the focus of this study is the combination of two NDE technologies for comprehensive detection and quantification of bridge deck deterioration. Infrared thermography and electro-optical imagery showed the great promise for practical use at near-highway speed, based on Ahlborn's previous USDOT-RITA study. Infrared thermography improves the accuracy of quantifying subsurface defects and electro-optical

imagery enhances visual inspection significantly by reducing inspection times, ability to collect subjective and repeatable measurements and provide high resolution datasets for evaluation.

2.1.4.1 Infrared Thermography

Infrared thermography is a technology based on collecting the radiant surface temperature and converting that temperature measurement into a visual image. Thermal infrared radiant energy is emitted from all objects that have a temperature greater than absolute zero. The radiant temperature (T_{rad}) of an object is defined by the amount of electromagnetic energy exiting the object in the range of two electromagnetic spectrum windows: 3-5μm and 8-14μm. This value is slightly lower than the true kinetic temperature (T_{kin}) of any object due to the fact that objects are not perfect emitters (Jenson 2007).

An object that radiates the absorbed energy at a maximum possible rate is called a blackbody. This theoretical construct helps to define the amount of heat that can be radiated from an object. According to the Stefan-Boltzmann law, the amount of radiant energy exiting a blackbody is proportional to the fourth power of its temperature and expressed as:

$$M_b = \sigma {T_{rad}}^4 \qquad \text{Equation 2-1}$$

where, M_b is the total emitted radiation of a blackbody which is equal to the kinetic temperature; T_{rad} is the radiant temperature and σ is the Stefan-Boltzmann constant (5.6697×10^{-8} $Wm^{-2}k^{-4}$). However, for real objects the amount of radiated energy is lower than the amount of absorbed energy. Therefore, the radiant temperature of the real object is lower than the true kinetic temperature. Emissivity of the material is the factor that affects the radiant temperature measurement of the material surface and defines the correlation between the true kinetic temperature and the radiant temperature of an object. This correlation defines with the equation below.

$$\varepsilon = \left(\frac{T_{rad}}{T_{kin}}\right)^4 \qquad \text{Equation 2-2}$$

Radiant flux is defined as the amount of electromagnetic energy exiting an object. Emissivity depends on the amount of radiant flux emitted from a material and has the value between 0 and 1. This value is almost equal to 1 for a blackbody; therefore, the radiant temperature for a blackbody is almost equal to the true kinetic temperature.

The value for emissivity of concrete is typically considered to be greater than 0.9 for concrete. Characteristics such as surface roughness, color, moisture content, viewing angle and field of view are some of the factors that can influence the emissivity of objects (Jenson 2007). Objects with darker colors absorb and emit more energy than lighter colored objects due

to the higher emissivity of darker colored objects. Surface roughness can influence the amount of radiant energy absorbed and emitted from an object, therefore, it influences the emissivity and radiant temperature of an object. Objects with higher moisture content have higher emissivity, thus absorb and emit more electromagnetic energy. Also, the emissivity can change based on the viewing angle; this mostly affects the measurements under the bridge and between the bridge girders. A smaller field of view results in a higher spatial resolution compared to a larger field of view; it will be different to look at a 2ft by 2ft concrete surface compared to looking at the whole bridge in one image.

A thermal IR camera is a tool for collecting the radiant surface temperature data of an object and generating a thermal IR image. Each pixel on a thermal infrared image is designated with a temperature data. Commonly, a range of minimum to maximum temperature on each image is shown as a sidebar on the image and assigned with false color values to create a visual image. Radiation, conduction and convection are three methods of heat transfer that can affect the heat flow through concrete. Although radiated energy is the parameter that can be measured by a thermal IR camera, the heat conductivity within the concrete and heat convection around the concrete can also influence this measurement.

The estimated emissivity value of 0.95 for concrete can be considered for collecting thermal IR images with the purpose of detecting subsurface abnormalities and defects as the actual temperature values are not of interest in this data collection. The emissivity value is inserted as an input on the thermal IR camera software while collecting data to achieve temperature results close to the true kinetic temperature. In measuring the defective areas in concrete, the temperature difference between sound concrete and defective area is in the interest of the inspector. Materials with reflective surface, such as duct tape, have lower emissivity compared to concrete; therefore, it will appear with lower temperature on the thermal infrared image.

Two approaches considered in conducting an infrared thermography test include passive and active. In the literature mostly related to the non-destructive testing (NDT) field, passive infrared thermography is generally defined as a method to detect the flaws in materials without using an external heater. In the passive method, an object radiates heat due to its internal heating system or properties. Inspecting the insulation of building envelops, heating floors and gas leaks are some of the applications of passive infrared thermography. On the other hand, active infrared thermography is described as a method to collect thermal infrared images after heating the object with an external heating system. In this method, the radiated heat is different from the defective and sound areas. Therefore, defective areas are revealed on the thermal infrared image (Maldague 1993; Starnes 2002). Recording the time is crucial in active infrared thermography to allow for resolving the depth and size of the flaw and obtain quantitative information.

The concept behind the application of passive infrared thermography in concrete bridge evaluation is that the anomalies and subsurface delaminations interrupt the heat transfer through the concrete and appear with different temperatures on the thermal IR image compared to the

area of surrounding sound concrete. During the day, as the ambient temperature increases, concrete absorbs heat and starts emitting radiant energy.

Delaminations and air voids within the concrete-resist the heat transfer and warm up at a faster rate than surrounding sound concrete, thus they appear as hot areas on the thermal IR image if captured during the day. However, during the night, as the ambient temperature decreases, sound concrete around delaminations lose heat at a lower rate compared to the defected area, thus the delaminations appear as cold areas on the thermal IR images (Washer et al. 2009 a). This concept is illustrated in Figure 2-2.

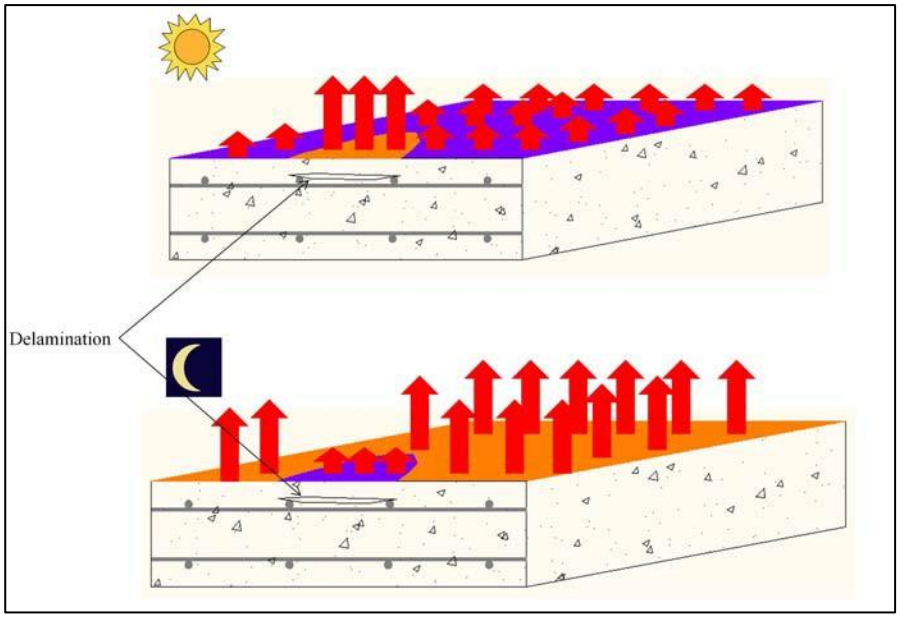

Figure 2-2: Emitted Thermal Infrared Energy from a Concrete Deck during the Day and Night.

Infrared thermography has the potential to be and effective inspection technique on both the top and bottom surfaces of the concrete bridge deck as well as other concrete elements such as prestressed or reinforced concrete girders and piers.

2.1.4.1. 1 Application to Bridge Decks

Infrared thermography has been cited in the ACI 222 report as a potential tool for detecting delaminations (ACI 2001). Additionally ASTM D4788 describes the test method, equipment and environmental conditions for detecting delaminations on the topside of the concrete bridge decks using this technology (ASTM 2007). This remote sensing technology can yield both qualitative and quantitative indicators of condition. A delamination map, created from the outputs of a thermal IR bridge inspection, can help to document relative shapes of these indicators and can be used to determine the total area and percentage of delaminations over the entire bridge deck.

According to the ASTM D4788 – *Standard Test Method for Detecting Delaminations in Bridge Decks Using Infrared Thermography*, a thermal IR camera (0.1˚F thermal resolution), video recorder, video camera, distance measurement device, test vehicle and contact thermometer are required for passive infrared thermography testing over the bridge deck. The thermal IR camera is mounted to a vehicle along with a video camera in a way that provides a minimum image width of 14ft. The vehicle mounted thermal IR camera and a video recorder are driven over the center of each lane on a bridge deck at near highway speeds while assessment information is acquired. The conventional video camera images are integrated with corresponding infrared images on the bridge deck to separate patches and surface defects from subsurface defects. From the collected information, image processing techniques are performed and delamination maps are prepared. These maps are then georeferenced to corresponding locations on the bridge deck and a composite image is generated. Bridge deck dryness is a factor that has to be considered during data collection with this method, as moisture on the surface can affect emissivity and reduce the thermal contrast on the thermal IR image (ASTM 2007).

Time of data collection is the most critical factor in a thermal IR survey. Different materials in the environment have different responses to ambient temperature change and this causes the variation in diurnal radiant temperature measures for different materials. Two thermal crossover times can be identified in the diurnal graphs of radiant temperature of materials. These two times are roughly the local sunrise and local sunset time; when the radiant temperatures of the materials are the same and appear with the same temperature on the thermal IR image. Concrete materials and delaminated areas on a bridge have similar behavior with respect to ambient temperature changes. In a study conducted by Washer et al. (2009) on developing thermal IR inspection technology for concrete bridges, it was found that the effective time to perform a thermal IR test depends on the depth of the delamination. The most contrast appears on the thermal IR image approximately 4 hours after sunrise for a 2 in. deep delamination and 7 hours after sunrise for a 3 in. deep delamination (Washer et al. 2009 a).

2.1.4.1.1.1 Advantages

Capable of detecting subsurface defects and delaminations, commercial availability, remote sensing, and ease of data collection and image interpretation are the advantages of the passive infrared thermography technique. This method of condition assessment provides an objective methodology to detect subsurface defects that is independent of inspector training and experience. In addition, inspection time is significantly reduced making this assessment technique less disruptive to traffic routes than other methods such as closing lanes to conduct hammer soundings. These advantages and the fact that infrared thermography provides in-depth condition information highlights the benefits of applying this technique in biennial bridge inspection practices (Ahlborn et al. 2012). Lab studies of passive infrared thermography for concrete slabs show that this technique is capable of detecting shallow (up to 3 inches from the top surface) delaminations which can help bridge inspectors identify areas of unsound concrete before they turn into spalls (Ahlborn et al. 2012).

Evaluating the top subsurface of concrete bridge decks has been mentioned in the literature as the main application of passive infrared thermography for bridge inspection as this element is exposed to direct sunlight (Gucunski et al. 2013). This technology also has the potential to be applied at near highway speed over the bridge deck with more advanced cameras, which can help to conduct quicker, safer, more frequent inspections. Another advantage associated with the use of infrared thermography is that the results from a delamination survey can typically be easily imported and stored in a standard GIS software such as ArcGIS, thus enabling a bridge management team to review the bridge information easier for decision making (Ahlborn et al. 2012).

2.1.4.1.1.2 Limitations

Previous studies on passive infrared thermography applications for bridge inspection have reported several limitations that should be considered. Clark et al. highlighted the fact that emissivity of the concrete surface can vary based on different materials found on the surface, thus the appearance of what might seem like a subsurface defect on thermal images is not necessarily an indication of such defects (Clark et al. 2003). Soil, moisture, oil spills, and staining on the concrete surface can appear as hot spots and affect the results of passive infrared thermography; therefore, taking optical (visual) images of the concrete surface is necessary to enable the inspector to separate these areas from delaminations.

Wind speed, solar energy, ambient temperature and humidity are environmental factors that influence thermal IR images (Washer et al. 2009 b). More advanced thermal IR camera models have the option to adjust the image based on the relevant humidity and ambient temperature occurring at the time of data collection. The minimum ambient temperature of 32˚F and the maximum wind velocity of 30 mph have been defined as upper limits on environmental criteria for performing passive infrared thermography of concrete bridge decks in ASTM D4788 (ASTM 2007). Washer et al. investigated the effects of variable environmental conditions on concrete bridge inspections and suggested a maximum wind speed of 8 mph on a sunny day and 10 mph when the surface is not directly exposed to solar energy. Also, it has been noted that consistent solar loading on the concrete can provide a better contrast on a thermal IR image (Washer et al. 2009 b).

Infrared thermography inspection is mostly applied for shallow delaminations. The maximum depth of 3 inches has been mentioned in the literature as a limitation of this technology in detecting delaminations (Vaghefi et al. 2013). When interpreting a thermal IR image, consideration must be taken to the fact that temperature variations of subsurface defects decrease with depth.

Determining the quantitative measures with passive infrared thermography is also a challenge that has to be considered while analyzing the results. Although generally more variables are involved in conducting a passive infrared thermography test, some previous studies suggest that

processing methods that are applicable for active thermography tests have the potential to be used for passive thermography as well (Abdel-Qader et al. 2008).

2.1.4.1.2 Application to Fascia Beams and Underside

Several studies have demonstrated that passive infrared thermography can also be applied for detecting deterioration on the deck bottom surface and on the bridge soffits (Washer 2010). Locating and mitigating damaged areas can be critical for the safe passage of traffic under the bridge.

Although most of the previous field applications of the infrared thermography in civil engineering have focused on passive thermal IR techniques, Pollock et al. (2008) investigated the possibility of using external heaters as part of an active thermal IR system to warm up prestressed concrete bridge girders before collecting the thermal IR images. Two methods were considered to perform this test on the bridge. In the first method, a heater was placed inside the prestressed box girder and thermal IR images were taken from the external box girder surface underneath the bridge. In this method, irregularities appeared as cold spots in the thermal IR images. Performing this test with this method is not always possible, as it requires access inside the box beams. The second method involved heating the underside of the bridge box girders by placing a heater on a lift truck platform and heating the girders for one to three hours before taking thermal IR images. Both of these methods showed promise for detecting delaminations in prestressed girders; however cost and accessibility are two factors that need to be considered in applying active thermal IR imaging for bridge inspection (Pollock et al. 2008). A variety of controllable heating sources, including hot air guns, quartz lamps and heat blankets can be used to produce thermal excitation on the test specimen. Solar energy has been mentioned by some researchers as a potential external heat resource (Spring et al. 2011).

2.1.4.1.2.1 Advantages

Remote sensing characteristic of infrared thermography can reduce traffic disruption and lane closures on and specifically underneath the bridge, as no direct contact is required. This allows for the inspector to collect condition information from a distance, either from a moving vehicle or outside of the traffic lanes. Previous study shows that passive thermography can be easily applied for inspecting fascia beams from the shoulders and without using an aerial truck (Ahlborn et al. 2012). Figure 2-3 shows a possible delamination on the fascia beam of Willow Rd. as collected form a hand held thermal camera.

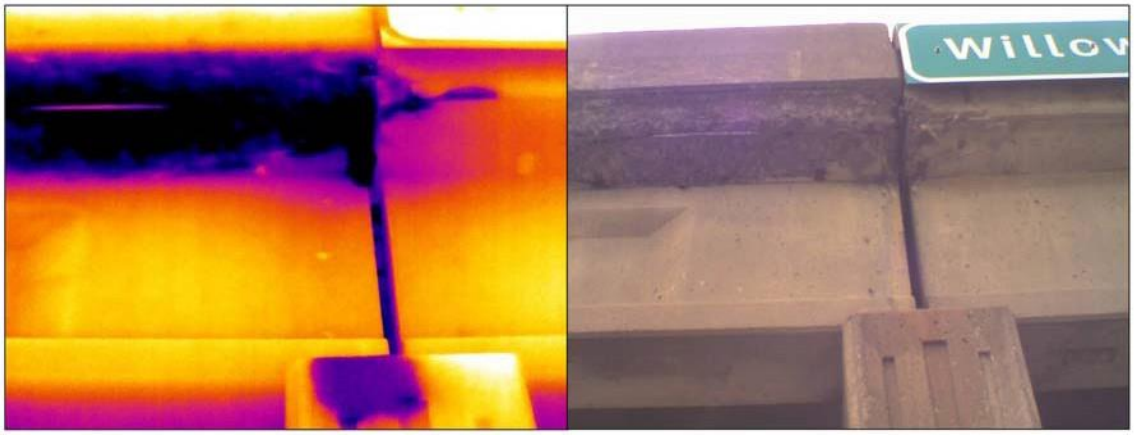

Figure 2-3: Thermal Infrared and Digital Image of Fascia Beam (Willow Rd. bridge August 2011).

Using active infrared thermography for under the deck and fascia beams inspection enables bridge inspectors to determine the location, size and depth of delamination. This condition assessment technique is not dependent on solar radiation to create a temperature difference; therefore, it allows conducting a bridge inspection in a larger time window. Furthermore, active infrared thermography can significantly facilitate inspection of concrete bridge elements that are not exposed to the direct sunlight, such as the underside of a bridge deck.

2.1.4.1.2.2 Limitations

Speed of data collection is one of the main limitations of application of infrared thermography under the bridge deck. It is generally not possible to collect data under bridge decks from a moving vehicle; a data collector has to take the thermal infrared sensing device and point it at areas above them to collect information. Taking thermal infrared images from the shoulders is most common in applying this technology for bridge soffits, however, viewing angle is one of the factors that can affect emissivity and has to be considered in interpreting thermal infrared images, (Washer 2010). In addition, deploying this technology underneath the bridge is dependent on the amount of solar energy that can be absorbed in the bridge deck during the day and may not be as effective for areas closer to the centerline. Therefore, an active heating system may be required for such in-depth inspection. Other factors such as cost and delamination depth may influence the applicability of this method as well. Equipment costs can ranges from $5,000-$50,000, and delamination depths greater than 2 in. can be difficult to identify.

2.1.4.2 Electro-Optical

Electro-optical (EO) sensors are those electronic sensors that are sensitive to electromagnetic radiation in the visible spectrum. The most common EO sensors are Charge-coupled Devices (CCDs) and are used in a typical consumer-grade digital camera. The wide scale availability of digital cameras and low cost make them a good candidate for characterizing condition

information of bridges. Aside from acquiring photo inventories of spalls and other condition information, the photos taken can also be used to extract additional, three-dimensional, information through photogrammetric techniques.

Photogrammetry is "The science or art of deducing the physical dimensions of objects from measurements on photographs of the objects" (Henriksen 1994). This includes measurements made from both film and EO (digital) photography. Digital photogrammetry has been demonstrated as a viable technique for generating 3D models of structures and structural elements (Maas and Hampel 2006). In order to perform 3D photogrammetry, the photos need to be taken with at least a 60% overlap (McGlone et al. 2004). This ensures that a feature on the ground is represented in at least two photos. Figure 2- shows the process of collecting stereoscopic imagery.

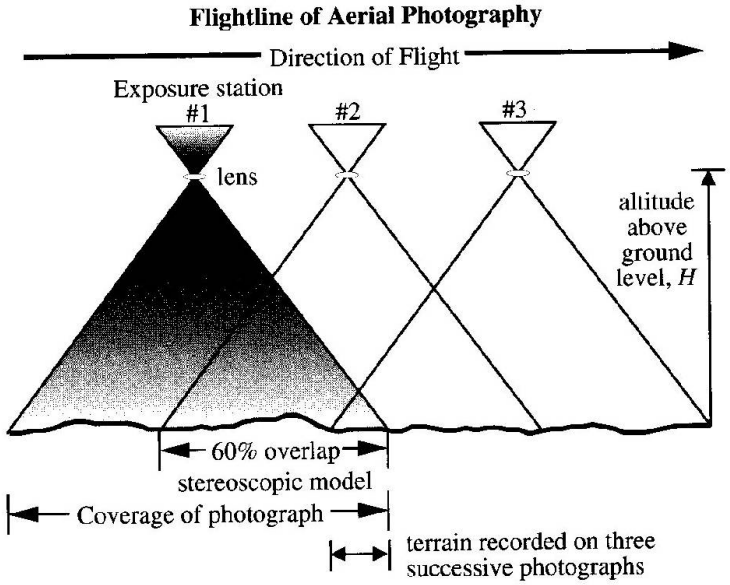

Figure 2-4: An Example of How Stereoscopic Imagery for Generating 3D Models is Collected (Jenson 2007).

Traditionally, photogrammetric techniques have been applied to aerial photography. For the purposes of collecting high resolution imagery of bridges close range photogrammetric techniques would have to be applied. Close range photogrammetry is defined as capturing imagery of an object or the ground from a range of less than 100 m (328 ft) (Jiang et al. 2008). This method can be used to generate 3D models of bridge decks from which condition information is extracted as described by Ahlborn et al. (2012).

2.1.4.2.1 Application to Bridge Decks

This technology can be used to detect spalling on the bridge deck as well as generate a photo inventory and composite image of the deck through a vehicle mounted camera (Ahlborn et al. 2012). Spall detection and a photo inventory are achieved through two different systems. To

create a photo inventory of a bridge deck, a pair of cameras mounted on the front of a vehicle provides sufficient coverage of the vehicle lane. A high resolution composite image of the bridge and a 3D representation of the bridge surface are generated by collecting stereo pair imagery through a camera mounted facing straight down and are used to located and quantify spalls.

Condition information can be extracted from the Digital Elevation Models (DEMs) generated as well as from the raw imagery. However, the condition information is limited to surface features such as spalling and cracks. These features can be detected either through manual interpretation of the imagery or through automated means using a combination of the DEM and imagery. This data can then be integrated with other geospatial data in a GIS or Decision Support System (DSS) to assess broader condition information (Ahlborn et al. 2012).

2.1.4.2.1.1 Advantages

3D Photogrammetry can provide accurate measurements of bridge deck surface condition while minimizing traffic disruptions. By mounting a camera to a vehicle and collecting stereo pair imagery, 3D models are generated to extract condition information such as spalling and cracks. This technology is less expensive than other spatial rendering systems such as the ability to generate high resolution DEMs (Ahlborn et al. 2012). Images collected from this system can also be mosaicked together to form a high resolution composite image of an entire bridge deck to assist with condition rating and visualizing the location of spalls in a GIS (Ahlborn et al. 2012).

This technology can be applied to near highway speeds by using a camera capable of faster frame rates than the first generation 3DOBS system developed in 2011. Higher resolutions can be achieved by choosing a camera with a larger sensor (i.e. more pixels) and a higher quality lens. With the wide availability of cameras and lenses these systems are not limited to a few dedicated and specialized sensor options, which helps to keep cost down.

2.1.4.2.1.2 Limitations

The main speed limiting factor with using close range photogrammetry is with the camera and lens performance. Image quality is directly related to the frame rate, shutter speed and resolution of the camera. Image resolution is a function of the camera sensor, the quality of the lens being used and the shutter speed. The frame rate is determined by the shutter speed and the available lighting. The resolution and rate at which the camera takes pictures limits the size of the distress that can be detected and the speed at which a system can be driven across a bridge deck. An example from Ahlborn et al. is of the Nikon D5000 used that had a sensor that was 12.3 MP (Mega Pixels) with an 18 mm focal length lens. The field of view covered one full road lane and a digital elevation model (DEM) with a resolution of 5 mm was produced. This system was limited by the continuous frame rate of more than 1 frame per second. This limits the speed of the vehicle to 2 mph to achieve the required image overlap. However, faster

cameras should enable collection speeds of at least 45 mph. Logistics and costs of data storage must also be considered.

This system is also limited by lighting and weather conditions. Water or snow on the road surface fills spalls and cracks resulting in incorrect defect detection. Under low light conditions, in order to properly expose an image the shutter speed is lowered to allow for more light to reach the sensor however this would require lower vehicle speeds to reduce motion blur. Testing shows that a Nikon D5000 operating at one frame per second can collect sufficient close range photogrammetry under most natural lighting conditions. (Ahlborn et al.2012).

2.1.4.2.2 Application to Fascia Beams and Underside

EO techniques can also be used to generate photo inventories and 3D models on bridge fascia beams and undersides. Imagery of the underside of the bridge can be collected through a vehicle mounted camera similar to the bridge deck except the camera is mounted facing up, although it is generally not possible to easily drive the entire longitudinal length of a bridge.

2.1.4.2.2.1 Advantages

The current condition of fascia beams and the underside of a bridge can be captured by vehicle mount camera systems. Photo inventories can be collected for both bridge components. Figure 2-5 shows a series of photos taken of the underside of a bridge with the deck bottom and the bottom of the beams clearly visible. These photos could be used as a photo inventory showing the location of a delamination (green square) that has been detected with other technologies (Ahlborn et al. 2012). 3D photogrammetry can also be used to generate 3D models of the fascia beams and portions of the underside from the stereo pair imagery. Figure 2-6 and Figure 2-7 show a model of the Silverbell Rd. box beam that was removed.

Figure 2-5: Photos taken with 3DOBS of the Underside of Willow Rd. Bridge (Ahlborn et al. 2012).

Figure 2-6: A Composite Image of the Silverbell Bridge Box Beam Derived from Stereo Imagery.

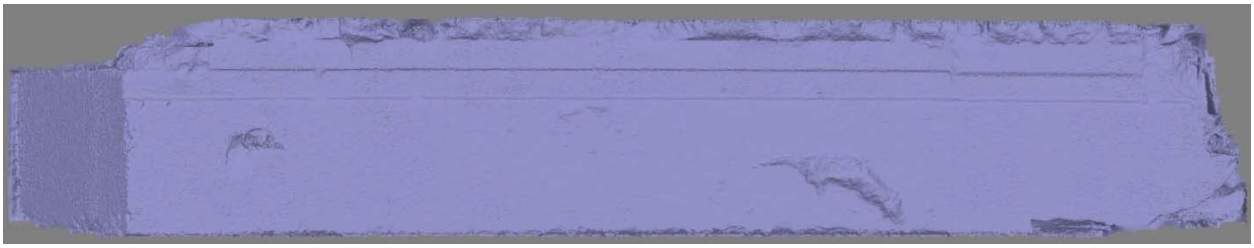

Figure 2-7: 3D Model of the Silverbell Bridge Box Beam Derived from Stereo Imagery.

2.1.4.2.2.2 Limitations

For the collection of imagery of fascia beams, overlapping photos are taken along the length of the beam. This would be difficult for a vehicle mounted system to achieve while driving with traffic. Models can be derived if overlapping imagery is taken along the length of the beam from a stationary camera. As seen in Figure 2-5, the sides of the beams are not visible in the photos taken with a vehicle mounted system.

While an EO system can collect imagery of the underside of a bridge with a vehicle mounted system, a complete model of the beams or underside of a bridge deck could

not be generated (Ahlborn et al. 2012). This is due to the viewing geometry between the cameras and the sides of the beams, how close the beams are to each other and whether at least two overlapping images can be collected. The closer the beams are to each other or the taller they are, the less information can be collected on the sides of the beams. This limitation also applies to the underside of the bridge deck, as the camera needs to be able to collect overlapping images. Due to viewing constraints, models of the underside would be limited to only the bottoms of the beams and parts of the underside of the bridge deck.

2.2 Applications of the Current State of Research and Practice

Applications of remote sensing technologies for bridge condition assessment are limited. This section provides an overview of the current state of research using some remote sensing options most applicable to bridge deck condition assessment. While some technologies are more mature, others have yet to be proven for concrete deck evaluation. Several projects are described below to broaden the reader's knowledge of the current state of remote sensing technology for use in the condition assessment of concrete bridge decks.

2.2.1 USDOT/RITA projects

The Michigan Tech Transportation Institute (MTTI) and Michigan Tech Research Institute (MTRI), in cooperation with the Center for Automotive Research (CAR) and the Michigan Department of Transportation (MDOT), completed a research study exploring the use of remote sensing technologies to assess and monitor the condition of bridge infrastructure and improve the efficiency of inspection, repair, and rehabilitation efforts. This project was sponsored by the United States Department of Transportation (USDOT) Research and Innovative Technology Administration (RITA) Commercial Remote Sensors and Spatial Information Program (Ahlborn et. al, 2012).

3DOBS and passive infrared thermography techniques were studied and deployed on four prestressed concrete I-girder bridges in Michigan in August 2011. Field inspection on these four bridges was conducted at speeds slower than traffic.

The aim of the field demonstration selection process was to identify bridges that had varying degrees of degradation with the potential to be identified and quantified using multiple remote sensing technologies. Four bridges were selected based on their assigned current NBI condition rating. Upon completion of the bridge selection discussion, three field demonstration locations had been established, each fulfilling the selection parameters for the three separate categories. The bridges selected were as follows:

- "Poor" condition; Mannsiding Road over US-127 north bound (NB)
- "Fair" condition; Willow Road over US-23
- "Satisfactory" condition; Freer Road over I-94

2.2.1.1 Mannsiding Rd. Bridge

The selected "Poor" condition bridge, MDOT structure No. 1713 – Mannsiding Road over US-127 north bound, is located in Clare county approximately ten miles north of Clare, Michigan. The structure is 130.92 ft in length and 31.17 ft in width, which translates into 26 ft of riding surface. During 1996, the average daily traffic (ADT) over the structure was found to be 1,000 with 3% being commercial. The condition of the concrete deck surfaces, both top and bottom, were an area of major concern. A 2008 MDOT scoping inspection classified the deck with a NBI rating of "4". The scoping revealed that on the top surface of the concrete deck 176 ft^2 or 4.4% of the deck was delaminated. Additional testing on the bottom surface revealed that 623 ft^2 or 15% of the deck was in distress. False decking was present when visited in 2011. The deck also possessed light scaling throughout and numerous transverse, longitudinal and diagonal cracks were present. Additionally, several high-load hits have resulted in scrapes and spalls of the superstructure underside, but currently there is no sign of exposed reinforcing steel or pre-stressing strands. The bridge is scheduled for complete replacement in 2012/13. Additionally, during the on-site inspection of the selected "Poor" bridge, its complementing twin bridge, Mannsiding Road south bound overpass was also visited. The Mannsiding Road south bound overpass bridge is described in further detail in the "Supplemental" bridge selection section.

3DOBS and infrared thermography results for this bridge were imported in ArcGIS and are shown Figure 2-8 and Figure 2-9, respectively. The total spalled area on Mannsiding Road bridge was 1.73 m^2 (18.62 ft^2) which is 0.47% of the entire bridge deck surface. Chain drag results showed 127.3 ft^2 (3.63% of the total bridge deck area) total delaminated areas on the bridge deck, while the total delaminated area calculated from thermal infrared imagery survey was 136.13 ft^2 (3.88% of the total bridge deck area).

Figure 2-8: A) Mannsiding Road Bridge Digital Elevation Model (DEM) and Spall Map Layer on ArcGIS, B) Mannsiding Road Bridge Spall Map Generated with Spall Detection Algorithm.

Figure 2-9: Combined Results of Thermal IR Imagery Chain Drag Inspection.

2.2.1.2 Willow Rd. Bridge

MDOT structure No.10892 – Willow Road over US-23 was selected for the "Fair" condition field demonstration bridge. The bridge is located in Washtenaw County approximately three miles north of Milan, Michigan. The bridge was constructed in 1962 and is a 4-span prestressed concrete multiple I-beam composite structure. The structure is 209 ft in length and 30.83 ft in width, which translates into 26 ft of drivable surface with no availability for shoulder room. During 1997, the ADT over the structure was found to be 2,220 with 3% being commercial. The current condition of the deck surface is rated as a "5" on the NBI scale. In 2010, the inspection report indicated that open transverse cracks, diagonal cracks and areas of delamination were present throughout the deck. Concrete patching had been completed to help minimize deterioration and prolong the service life of the bridge. Additionally, areas on the bridge superstructure displayed desired sensing deficiencies over both the north and south bound lanes. This is attributed to several high-load hits, which had resulted in scrapes and spalls, but there was no sign of exposed reinforcing steel or prestressing strands.

Figure 2-10 and Figure 2-11 shows the results of 3DOBS and infrared thermography of Willow Rd. bridge, respectively. Total area of spalls on this bridge was 27.3 m^2 (293.7 ft^2) which was 5.15% of the entire bridge deck surface. Hammer sounding results showed 159.5 ft^2 (3.05 % of the total bridge deck area) total delaminated areas on the bridge deck, while the total delaminated area calculated from thermal infrared imagery survey was 157.83 ft^2 (3.02 % of the total bridge deck area).

Figure 2-10: Willow Road Bridge Digital Elevation Model (DEM) and Spall Map Layer on ArcGIS.

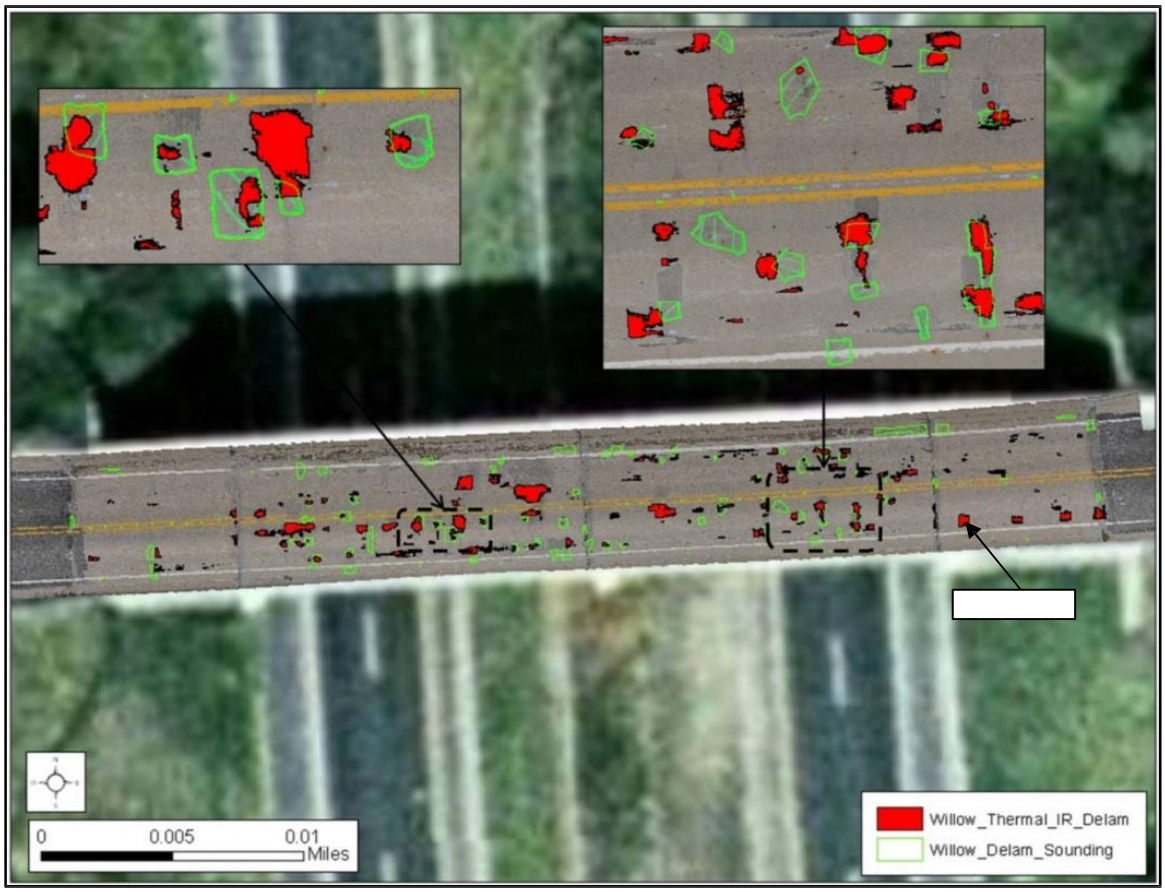

Figure 2-11: Combined Results of Thermal IR Imagery and Hammer Sound Inspection.

2.2.1.2 Freer Rd. Bridge

The "Satisfactory" bridge was chosen to be the MDOT structure No.10940 – Freer Road over I-94, located in Washtenaw County, approximately one mile east of M-52 in Chelsea, Michigan. The bridge was constructed in 1960 and is a 4-span prestressed concrete multiple I-beam composite structure. The structure is 209 ft in length and has a 28'-10" roadway opening including two 11'-0" lanes and two 3'-5" shoulders on each side. During 1997, the ADT over the structure was found to be 150 with 3% being commercial. The NBI rating assigned to the concrete deck surface is a "6". In 2010, the inspection report indicated that there were several areas of concrete patching accompanied by few tight transverse and diagonal cracks present on the deck.

Figure 2-12 and Figure 2-13 shows the results of 3DOBS and infrared thermography of Freer Rd. bridge. Total area of spalls on this bridge was 3.8 m^2 (40.1 ft^2) which is 0.67% of the entire bridge deck surface. Hammer sound results showed 101.74 ft^2 (1.8 % of the total bridge deck area) total delaminated areas on the bridge deck, while the total delaminated area calculated from thermal infrared imagery survey was 29.25 ft^2 (0.52 % of the total bridge deck area). The main cause of variation between the results of the hammer sounding and infrared thermography surveys on the Freer Road bridge is that most of the delaminations on this bridge were around the construction joint and overlapped with the painted centerline on the bridge deck. Reflective paint on the bridge deck has lower emissivity than concrete; therefore, it will appear on the thermal IR image with lower temperature and cause some difficulties in detecting delaminations in those areas.

Figure 2-12: Freer Road Bridge Digital Elevation Model (DEM) and Spall Map Layer on ArcGIS.

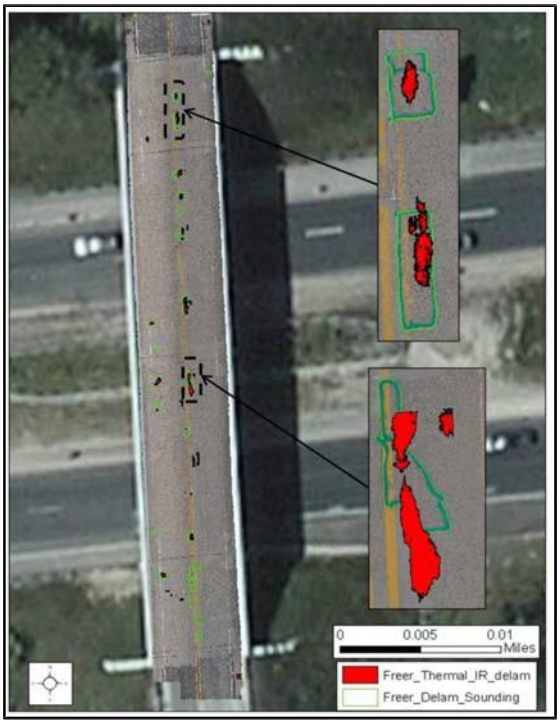

Figure 2-13: Combined Results of Thermal IR Imagery and Hammer Sound Inspection.

2.2.2 BridgeGuard projects

In February 2010, the BridgeGuard framework of passive IR bridge deck image collection and analysis was described in a two-part article in Roads and Bridges magazine (Howard et al. Feb 2010; Howard and Sturos March 2010) The article explored IR technology as a contributing solution to the detection and mapping of concrete bridge deck delaminations. Article 1 re-affirmed previous assertions that (IR) is a valued tool in the application of bridge deck NDE and provided the rationale for the development effort of a dedicated off-the-shelf tool. Article 2 explained how this development proceeded and what capabilities resulted within the BridgeGuard framework. Examples of BridgeGuard case studies are included in this report to show the current stage of the application of infrared thermography on bridges.

2.2.2.1 Oceana County Bridges, Michigan

BridgeGuard, Inc. (formerly Talon Research) conducted infrared thermography surveys on five bridges in Oceana County, MI. The selected bridges were scanned numerous times on several occasions to evaluate and improve calibration of GPS-based imaging frequencies and to improve test protocol in varying weather conditions and collection times. All these five bridges are steel girder bridges with concrete deck.

1) MDOT structural No. 8328 – Webster Rd. Bridge over US-31,
2) MDOT structural No. 8329 – Winston Rd. Bridge over US-31

3) MDOT structural No. 8332 – M20 EXT Bridge over US-31
4) MDOT structural No. 8344 – Hayes Rd. Bridge over US-31 (SB)
5) MDOT structural No. 8345 – Hayes Rd. Bridge over US-31 (NB)

The five bridges evaluated had an average length of 280 feet with an average width of 24 feet. The results of the bridges varied in total delamination percentages as well as total number of delaminations. The highest number of delaminations found in a single bridge was 202, this highlighted obvious visible patches and man-made saw cuts. This bridge registered a total percent of deck delaminations of 14.26%. The lowest number of delaminations found in a single bridge was 24 for a bridge-total percent of 1.77%.

2.2.2.2 Cedar Key Bridge, Florida

BridgeGuard, Inc. conducted an infrared thermography survey on Cedar Key Bridge in Florida, which was built in 1972. The bridge overall length is 952 feet long by 44 feet wide with substructure elements consisting of 20 bents with 7 – 22 inch square piles per bent. As part of the validation and ground truth process, a hammer was used to assist in outlining a targeted sub-surface flaw. A chalk outline was marked on the cap and a visual image was taken showing the chalk outline of this hammer-measurement (Figure 2-14). Also shown is the spatially corresponding IR image taken at 0800 hours on November 7, 2010 (Figure 2-14) illustrating the geometrics of the bridge cap and the outline of the characterized delamination. A qualitative correlation can easily be made by the reader between the IR image and the actual physical measurement shown in the visual image. It is noted that, while not visible in either image, this delamination extended up and around the opposite side vertical surface of the cap.

Figure 2-14: A) Visual Image of Marked Delamination on the Bridge Cap and B) Thermal IR Night Image of Delamination.

3. System Upgrades and Lab Testing

Our pace of technology is advancing rapidly in the past five years. Since completion of the USDOT/RITA study in 2012 (*Bridge Condition Assessment Using Remote Sensors*), commercially available cameras have enhanced performance with increased frame speed for use at near highway speeds, in addition to a lower cost and improved ease of data processing for evaluation of health condition indicators. This chapter describes the equipment and system upgrades used for the evaluation of the top of concrete bridge decks. Chapter 6 presents the system used to evaluate the bottom surface of the deck and field demonstration results.

Passive thermal imaging and a 3-D Optical Bridge-evaluation System (3DOBS, an application of 3-D photogrammetry) were combined for detecting spalls and delaminations on the top deck surface at near-highway speeds (see Chapter 5). Passive thermography is a more mature technology used to locate suspected delaminations and is capable of operating at highway speed. The 3DOBS system, previously used at walking speed, was implemented at near highway speed to detect spalls using a lower resolution camera system. Using a higher resolution system and slower speeds, crack size and location was investigated. In addition, the Bridge Viewer Remote Camera System (BVRCS), also an optical system using Go-Pro cameras, was enhanced to provide a high-resolution photo inventory of the top deck surface while travelling at near-highway speed.

3.1 3DOBS

3.1.1 Near Highway Speed

In order to take the original version of 3DOBS, which was limited to 2mph, to near highway speeds a new camera had to be used. There are two main camera characteristics that limit the collection speed. The first is the maximum sustained frame rate, in frames per second (fps), of the camera. The Nikon D5000 is only capable of 1 fps for continuous shooting which is not sufficient for faster speeds. Frame rate determines how much overlap there will be in the imagery at a given vehicle speed.

The Nikon D5000 used previously was able to capture a full lane width per pass (Ahlborn et. al, 2012). From 9 ft above the bridge deck the field of view (FOV) was approximately 8 ft x 12 ft with an 18 mm focal length lens. In order to achieve at least 60% overlap in the collected imagery at that FOV, an image needs to be collected every 3.2 ft across the bridge deck. For data collection while traveling at 45 mph with a camera with a similar FOV, the camera would have to capture imagery at a frame rate of at least 21 fps (Table 3-1).

Table 3-1: Required Camera Frame Rate for Variable Vehicle Speed.

Speed (mph)	Distance Between Shots (feet)	Frame Rate Needed (fps)
1	3.2	0.46
5	3.2	2.29
10	3.2	4.58
15	3.2	6.88
20	3.2	9.17
25	3.2	11.46
30	3.2	13.75
35	3.2	16.04
40	3.2	18.33
45	3.2	20.63
50	3.2	22.92

The other characteristic is shutter speed. On digital camera this refers to how long the sensor collects light for an image. In typical photography, shutter speed is adjusted to achieve properly exposed images where shutter speed is decreased for low light and increased for bright lighting conditions. For 3DOBS, shutter speed also plays a role in minimizing motion blur. Motion blur typically occurs as the object is moving across the FOV of the camera as the sensor is collecting. This degrades the sharpness of the resulting imagery and therefore reduces the quality of the resulting 3D model. If motion blur is too excessive, 3D modeling software will be unable to process the imagery all together.

In order to minimize motion blur, the shutter speed needs to be increased as the vehicle speed is increased. For the collects with the Nikon D5000 at 2 mph motion blur was not an issues even under overcast conditions. For vehicle speeds up to 45 mph motion blur will become more apparent. Because of this it is important to have a camera that has a fast shutter speed.

Table 3-2: List of Possible Cameras Considered for 3DOBS Upgrades.

Manufacturer	Model	Resolution (Megapixel)	Max FPS (at full resolution)
Nikon	D5000	12.3	4
Nikon	D5100	16.3	4
Nikon	D90	12.3	4.5
Nikon	D7000	16.2	6
Nikon	D300s	12.3	7
Nikon	D700	12.1	5
Nikon	D800	36.3	4
Nikon	D3S	12.1	9
Nikon	D3X	24.5	5
Nikon	D4	16.2	10
Canon	EOS Rebel T3	12.2	3
Canon	EOS Rebel T2i EF-S	18	3.7
Canon	Eos Rebel T3i EF-S	18	3.7
Canon	EOS 60D	18	5.3
Canon	EOS 7D	18	8
Canon	EOS 5D Mark II	21.1	3.9
Canon	EOS-1D Mark IV	16.1	10
Canon	EOS-1Ds Mark III	21.1	5
Canon	EOS-1D X	18.1	12
RED	Scarlet-X	13.8	30
RED	Epic	13.8	60
Sony	F55	8.9	60

Based on research existing DSLR cameras, none of them are capable of the frame rates necessary for a near highway speed version of 3DOBS. The fastest (listed in Table 3-2) are capable of up to 10 fps. Actual sustained frame rates tend to be lower as observed by the project team. The Nikon D5000 is rated at 4 fps but for continuous shooting longer than 30 seconds, it exceeds the buffer capacity and is unable to continue at that speed. Therefore a max frame rate of 1 fps can be achieved without hitting buffer limitations and the camera will continue capturing imagery at 1 fps until the memory card is filled.

Since DSLRs are limited in their frame rate, the project team looked into other, faster camera types. For this, cameras that are traditionally used for the movie industry were investigated. These offer better than HD video quality (> 2 MP per frame), at frame rate exceeding 24 fps. The Sony F55 and the RED Epic cameras were researched as potentially suitable cameras for the near highway speed camera. Since it was necessary to have a resolution of at least that of the Nikon D5000, the RED Epic was chosen to test with a max resolution of 13.8 MP per frame.
A RED Epic was rented at first to test the cameras capabilities and if it would work as a suitable replacement for a near highway speed version of 3DOBS. Since the camera with all of its needed accessories would cost at least $25,000 it was necessary to make sure the camera performed as needed before purchasing. Therefore, a one week trial was conducted in June 2013 to collect

imagery over Freer Rd. The RED Epic was able to collect imagery with minimal motion blur at vehicle speeds of 45 mph (Figure 3-1).

Figure 3-1: An Extracted Frame from the June 2013 RED Epic Test over Freer Rd. This Image Shows very Little Motion Blur and would be Acceptable to run through Agisoft.

During the test runs the weather conditions were mostly sunny which allowed for the maximum shutter speed of 1/8000 sec to be used. With a fast shutter speed, motion blur was reduced to the point that it did not cause an issue with processing. Based on the successful testing of the RED Epic, it was purchased as the 3DOBS near highway speed camera.

3.1.2 High resolution crack detection

In order to detect cracks, frame rates were not as important as resolution of the camera. More pixels allow for greater coverage of the field of view and therefore a high resolution of the surface being imaged. For crack detection, the Nikon D800 was chosen since it had the highest camera resolution of 36.3 MP while other cameras were limited to less than 25 MP (Figure 3-2).

Figure 3-2: Nikon D800.

Lab testing of the Nikon D800 had to be performed in order to determine the actual resolution of the camera. Since different lenses and other factors play a role in actual resolution, these include the lens diffraction coefficient, aperture setting (f-stop), lens distortion, distance to target / focal length, bayer pattern (RGB sensor array that constitutes a single pixel), amount of pixels and JPEG compression. These variables are different for every camera and even between different collects depending upon the lighting. Testing in the lab under controlled conditions had to be performed first to understand these variables.

These tests were conducted using a camera calibration chart to compare the Nikon D800 to the Nikon D5000 which was used previously. Photos were taken from 9 ft away using the same lens set to 18mm focal length. The cameras settings were set the same for both so that the only variable was the number of pixels of each cameras sensor.

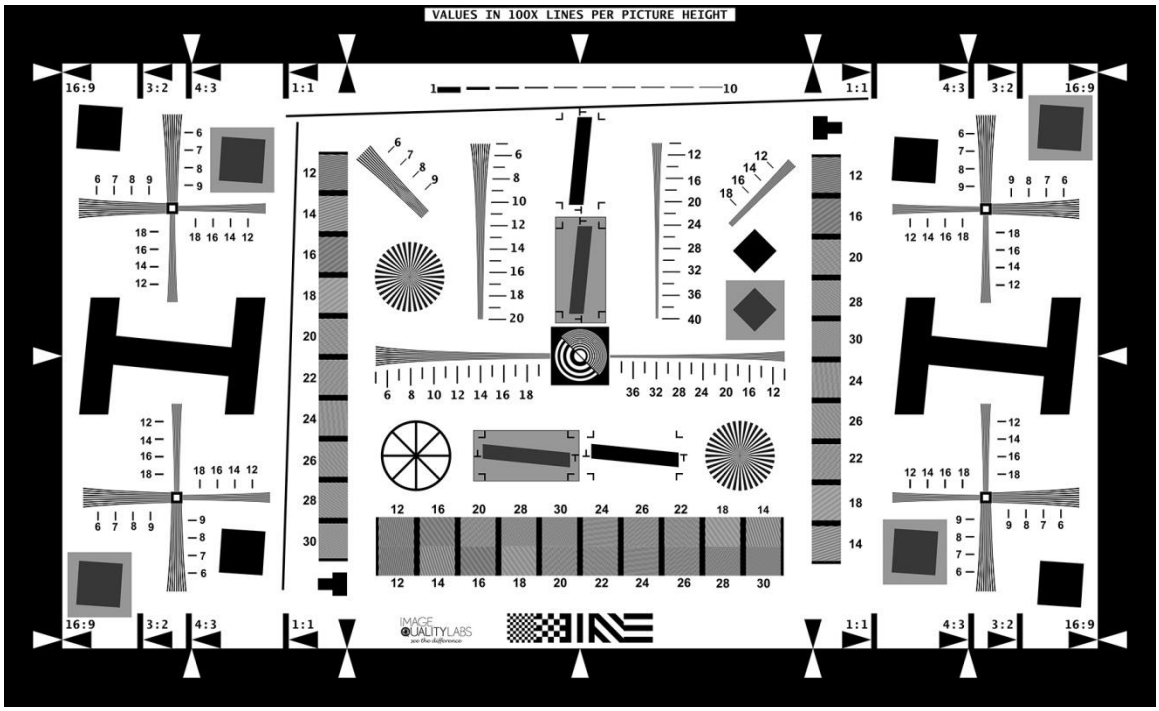

Figure 3-3: Resolution Chart for Testing Camera Resolution.

The images collected by each camera are compared in Figure 3-4. It is shown that the Nikon D800 captures clearer imagery than the Nikon D5000 which was expected. After careful analysis of the limits of each camera to resolve the separation between two lines, it was determined that the resolution of the Nikon D5000 under these conditions was at least 5mm while the Nikon D800 was approximately 1mm (Figure 3-5).

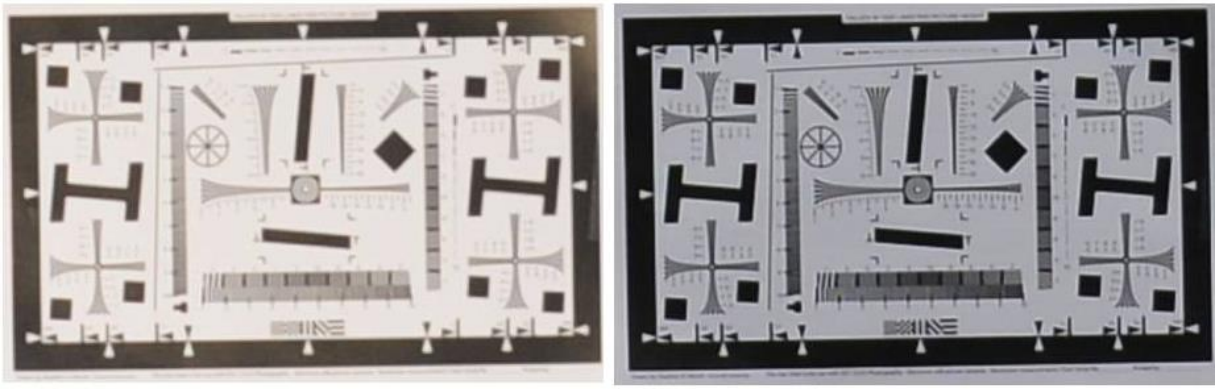

Figure 3-4: Comparison of the Imagery Collected by the Nikon D5000 (left) and the Nikon D800 (right).

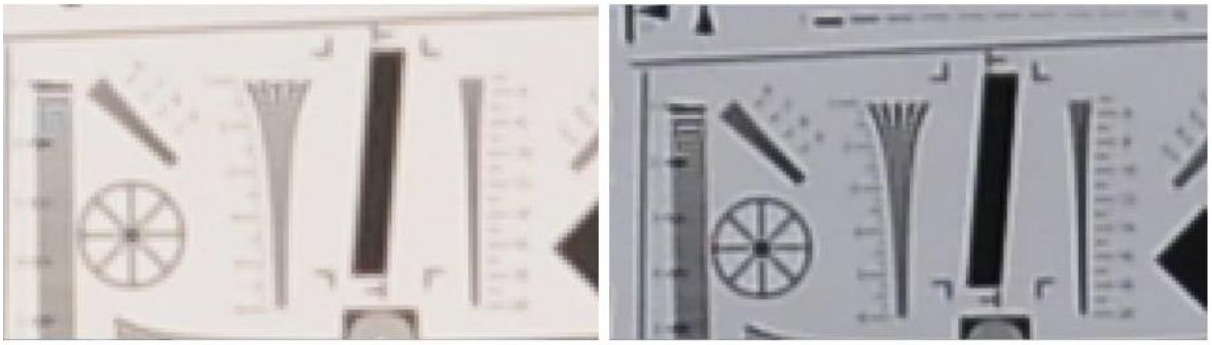

Figure 3-5: Comparison of the Ability of each Camera to Resolve the Separation between Two Lines. The Nikon D5000 is on the Left and the Nikon D800 is on the Right.

Based on this test, it was determined that under optimal conditions should capture imagery with a resolution of approximately 1mm or 1/32nd of an inch. This is higher resolution than the previous Nikon D5000 which had a resolution of about 5mm and is expected to be higher than the RED Epic which has less than a third of the pixels as the Nikon D800.

3.2 BridgeGuard Passive Infrared Thermography

3.2.1 Integration of Advanced GPS Equipment to Facilitate GIS Compatibility

BridgeGuard's fundamental enhancement challenge relative to interfacing with the 3DOBS system was, to begin precisely tagging its imagery to a geographical coordinate system such as Latitude and Longitude, at least with the precision afforded by the state of the art. Interfacing to external data sources such as the data derived from the 3DOBS system requires that BridgeGuard fully enter into and become compatible with the GIS framework. This allows a user of that data to "autonomously" map information coincidentally with external bridge data through any GIS type package.

Independent and external to this contract scope of work, BridgeGuard purchased survey grade GPS equipment that met the needs of this BridgeGuard/3DOBS integration replacing the equipment originally integrated into the BridgeGuard system. Accuracy of coordinates from a commercial grade GPS unit was problematic from several perspectives including:

- Inherent accuracy of standard GPS equipment (approximately 3 meters). This was addressed by using a differential correction process received from a variety of sources. To correct this inaccuracy, integration results using real time correction with the proper equipment is greatly reduced to the order of +/- 4-6 inches (5-15cm).

- Dynamic Response of the Equipment. Commercial GPS equipment that met the needs if this integration, updates position data at a frequency of 1 hertz, which was not adequate. However, post processing methods were developed that mitigated the low resolution GPS update frequency. Using synchronous update time stamps within both data streams, we were able to autonomously identify, within the analysis

process, these update points and then perform a time based interpolation between the points. Beyond this effort, it is the short term goal of BridgeGuard to acquire and integrate a new generation GPS product thus simplifying the process and tightening up location accuracy.

Having solved the accuracy issue within the state of the art, Lat/Lon positions acquired from a GPS unit must be correlated to an image. The most difficult and challenging task, by-far, for BridgeGuard in regards to Lat/Lon positioning is to correlate the collected Lat/Lon position provided by the GPS unit to an actual pixel in an individual image. The camera and the GPS antenna were mounted in such a method that allows the GPS position to be calibrated to the center pixel of each image.

3.2.2 Integration of GPS Positional Data with 3DOBS Data Structure Requirements

BridgeGuard revised its BridgeGuard file systems to accommodate GPS coordinates for each image, as well as each delamination found in that image. This was developed as a set of post-processing software tools that allows BridgeGuard to operate when 3DOBS is not attached and to use all of the current analyses and reporting tools under that scenario. Conversely, when 3 DOBS is attached, the post-processing tools are employed to convert the data set to be compatible with 3DOBS and generic GIS systems.

In this regard, BridgeGuard now can provide geo-reference coordinates for each delamination marked in an image. To accomplish this we calculate and assign a Lat/Lon to each pixel in the image. Algorithms were written to make this conversion based on a known pixel length/width, direction of travel, and a known pixel Lat/Lon location.

Stand-alone tools were developed that will mine the BridgeGuard collection and analysis files and create a specifically formatted output file outlining all the findings on a bridge. This file can be read by the 3DOBS processing software to integrate the thermal results from BridgeGuard with those from 3DOBS. This facilitates both scenarios where BridgeGuard and 3DOBS data are collected coincidentally and where the data sets are collected independently.

3.2.3 BridgeGuard data collection vehicle modifications

Item 3.2.3 employed the necessary effort to mount the two hardware and data systems into a final test and mounting fixture. With an adjustment to the BridgeGuard boom, space and mounting structure was provided to mount the 3DOBS camera side-by-side the BridgeGuard hardware suite. The test set-up simply requires the operator to share the vehicle cab with the BridgeGuard operator and send initiation commands to the 3DOBS camera coincidental with the initiation of the BridgeGuard collection software.

3.3 BridgeViewer Remote Camera System

The BridgeViewer system was upgraded by purchasing two GoPro Hero 3 Black Edition cameras (Figure 3-6) to replace the original Cannon PowerShot SX100 IS that were not rugged, high-speed cameras. In the original version of BridgeViewer the PowerShot was connected to a laptop that ran PSRemote software to run the cameras. Through PSRemote the user adjust the camera settings, control frame rates, and see a live video feed. Altogether the system needed two cameras, a GPS, and a laptop with PSRemote installed.

Figure 3-6: GoPro Camera used to update BridgeViewer.

With the addition of the GoPros, a laptop and additional software were no longer necessary. The GoPro cameras have a time-lapse option that allows for pictures to be taken at rates up to twice a second at 12.3 MP. They can also be controlled by a wifi remote, through a Smartphone or manually on the cameras. The previous PowerShot cameras were only capable of taking 1 fps at 8 MP. Another advantage is that the GoPro's come with a waterproof case, which would allow for it to be mounted to the vehicle in all weather conditions (Figure 3-7).

Figure 3-7: Testing the GoPros Mounted to the Hood of a Vehicle during a 3DOBS High Resolution Collection on 24 Mile Rd. near Marshall, MI.

GeoJot+ is used for geotagging the images after they are collected (http://www.geospatialexperts.com/GeoJot/). This software is designed to simplify the photo-capture to mapping and reporting processes required for many data analyses with close integration with ESRI Desktop ArcMap GIS software. Once imagery is added and the track log from the GPS, GeoJot+ interpolates the location of where the image was captured between the GPS points. A separate water marked image is generated with a date/time stamp and Lat/Lon added. A GIS shapefile is also generated that can be viewed in ArcMap and references the location-tagged and watermarked image for display in a GIS environment.

4. Field Testing and Demonstrations

The objective of the field demonstrations of this research was to evaluate the performance of four non-destructive assessment techniques: BVRCS, 3DOBS, passive infrared thermography, and active infrared thermography. These remote sensing methods were used to assess the condition of selected bridge decks, a major element in a bridge that provides protection from the environment to the superstructure and substructure, indicates overall bridge health, and determines when preservation activities should be performed.

Field deployments of the non-destructive testing methods occurred in three phases, one in the fall of 2013 and then again in the spring and summer of 2014. Fall deployments included testing locations at four highways bridges while three bridges were visited in the spring. Emphasis was taken on the evaluation of the 3DOBS high-resolution system to detect spalls and cracking and passive infrared thermography to detect delaminations during fall deployments. The testing results were used as a basis for comparison for the second deployment phase in the spring. The duration between deployment phases was used to evaluate the remote sensing techniques, make upgrades to the existing systems, and conduct additional lab testing.

The second deployment in the spring of 2014 allowed for further evaluation of the 3DOBS low-resolution system and passive infrared thermography conducted at near highway speeds simultaneously. This phase also allowed for implementation and evaluation of the 3DOBS high-resolution system at slower speeds for more refined crack evaluation. Two highway bridges were selected as data collection sites for the 3DOBS systems and passive infrared thermography testing. The demonstration sites are described in detail in the following sections. An additional demonstration site was visited to perform the active infrared thermography in the summer of 2014 for the bottom deck surface evaluation (see Chapter 6).

For comparison and correlation purposes, an MDOT certified bridge inspector was present for the US-131 and Maryland Ave. field tests to establish ground-truth information. The inspector either conducted an assessment of the entire structure or evaluated only specific areas of interest to produce delamination maps, spall maps, and crack maps. Results from the remote sensing tests were compared to inspector's findings and are included below.

4.1 Bridge Selection

To facilitate the testing and evaluation of the remote sensing techniques, several parameters were established during the bridge selection process. The goal of the selection process was to identify three testing locations for the fall data collection phase and an additional three testing locations for the spring phase within the state of Michigan. The selected bridges were deemed acceptable for both traditional health monitoring techniques, performed by MDOT qualified inspectors such as sounding (hammer or chain-dragging), and for the remote sensing systems.

Preliminary selection was based on the NBI rating scale found from the most recent MDOT assessments. Sites with varying levels of deterioration were preferred in order to evaluate the performance of the several non-destructive techniques on bridges with varying deck conditions. Preference was also given to bridges with all structural components composed of a homogeneous material, however, this was not an essential requirement unless the underside of the bridge was being evaluated. In the case of the active infrared thermography deployment, a selection parameter was established to identify a testing location at which all bridge structural components were composed of concrete. Lab testing had not yet revealed the effects of combining bridge components of different materials on this remote sensing technique and such selection parameter was necessary to ensure accuracy while evaluating the testing method.

Once preliminary selections were made, photographs of each bridge were collected using satellite images. The images were then used to further categorize the selected bridges based on access to the bridge components of interest and surrounding industry and transportation facilities influencing traffic patterns. The average daily traffic (ADT) was also used as a selection parameter. Bridges sites with a relatively low ADT were preferred to minimize lane closures and traffic disruptions and to provide a safe working environment for both MDOT inspectors and remote sensing technicians.

Upon further categorization of the testing sites, upcoming bridge inspection dates were also taken into consideration during the selection process. To establish ground-truth information, selecting bridges that underwent a recent biennial inspection was both beneficial and convenient.

4.2 Fall 2013 Field Test Sites

The following bridges were selected for the fall data collection and testing phase of research. Bridge assessments were made using the 3DOBS high-resolution system and passive infrared thermography and the testing data was evaluated based on ground-truth information obtained by MDOT inspectors.

4.2.1 20 Mile Road Bridge

MDOT structure No. 1279 – 20 Mile Road over I-94 was selected as a demonstration site for the 3DOBS high-resolution deployment and passive infrared thermography and is located approximately 4.5 miles east of I-69 near Battle Creek Michigan in Calhoun County. The structure spans both east and west bound I-94. A satellite aerial view of the structure can be seen in Figure 4-1.

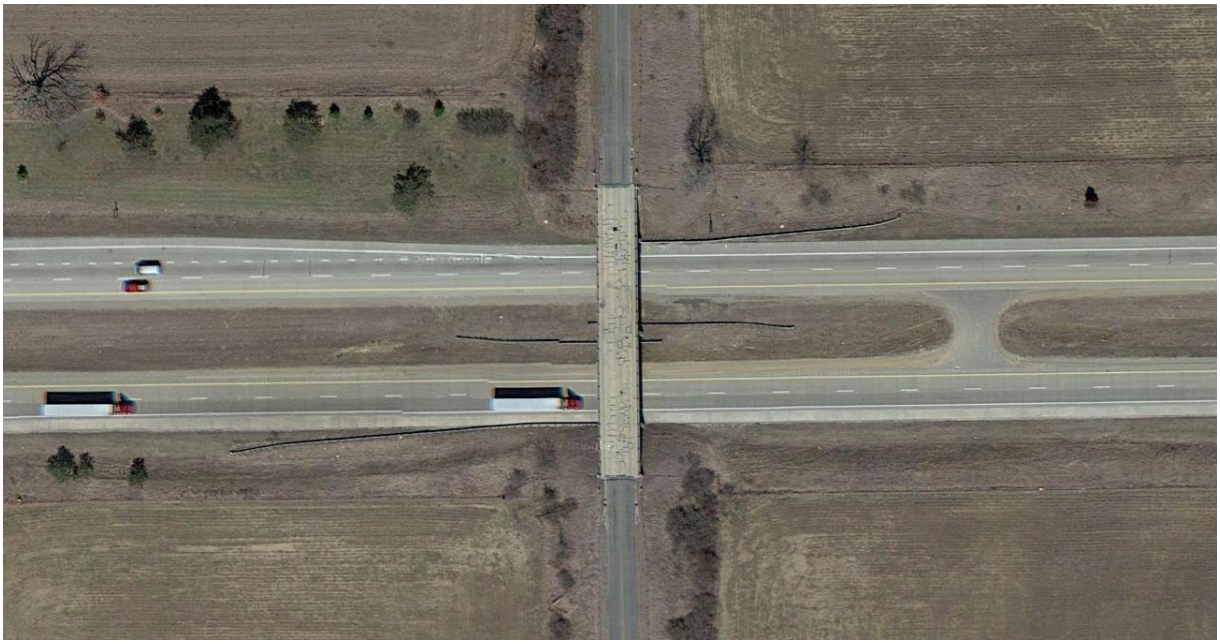

Figure 4-1: 20 Mile Road Bridge over I-94 Located in Calhoun County, Michigan.

Constructed in 1960, the bridge is a 4-span cast-in-place tee beam structure with a total length of 227 ft. The bridge has a total width of 31.2 ft with two 11 ft lanes and 3'-3" shoulders. Measured in 1988, the ADT over the structure was determined to be 1500 vehicles per day with 3% being commercial truck traffic (MDOT). Future ADT predictions for 2000 made at the time of measurement estimated a 36% increase in traffic.

During the most recent bridge inspection on August 8th, 2013, the concrete deck surface was assigned a poor condition NBI rating of 4. A photograph of the current deck surface condition can be seen in Figure 4-2. With the main purpose of this deployment being the assessment of the 3DOBS high-resolution system and passive infrared thermography, the bridge deck was the main bridge component of interest. Only the surface of the bridge deck was evaluated for deficiencies, however, particular interest should be taken to spalling on many of the bridge beams that have left reinforcing steel and stirrups exposed. It was recommended that these areas be patched to preserve the integrity of the structure.

Figure 4-2: Deck Surface for 20 Mile Road Bridge.

Testing on 20 Mile bridge corresponded with the inspection of the bridge by MDOT. A sketch of the deck sounding was georeferenced as a GIS shapefile (Figure 4-3). The sounding determined that there was 1,276 ft^2 of delamination with 32 ft^2 of bit patching and scale which corresponded to 24% of the deck surface.

Figure 4-3: Georeferenced Sketch of the Results of the Deck Sounding Showing the Locations of Delaminations. The Total Area Delaminated is 1,276 ft^2.

4.2.2 24 Mile Road Bridge

MDOT structure No. 1282 – 24 Mile Road over I-94 is located approximately 9 miles east of I-69 near Albion, Michigan in Calhoun County and was selected as a demonstration site for the 3DOBS high-resolution system and passive infrared thermography deployment.

The bridge was constructed in 1959 and is a 4-span cast-in-place variable depth tee beam structure with a total length of 227 ft. The bridge has a total width of 31.2 ft and with a 24 ft roadway and no shoulder. Figure 4- shows the multiple span structure over I-94. The ADT over the structure was determined to be 160 vehicles per day in the year 1988 with 3% being commercial truck traffic (MDOT). At that time, it was estimated that the future ADT in 2000 was to only increase slightly to 218 vehicles per day.

Figure 4-4: 24 Mile Road Bridge Selected as a Fall 2013 Deployment Site.

The concrete deck surface was assigned a poor condition NBI rating of 4 during the last inspection on August 14th 2013. With the assessment of the 3DOBS high-resolution system and passive infrared thermography being the main purpose of this deployment, the bridge deck was the main bridge component of interest. Only the surface of the bridge deck was evaluated for deficiencies, however, it should be noted that numerous spalls have left reinforcing steel exposed on many of the bridge beams reducing the superstructure to a rating of 5. Patching of these areas was recommended prevent further deterioration and extend the service life of the bridge.

The inspection report indicated various transvers and longitudinal cracks across the deck surface, some of which had been sealed with rubber. Various concrete patches were also present over the structure surface. A main area of interest was noted to be the unsealed longitudinal joint where cracking and scaling have contributed to wetness, exposed reinforcement steel from spalling, corrosion, and delaminations on the underside of the deck. To locate and quantify delaminations, the surface of the bridge deck was sounded on October 15th, 2013 revealing that 14% of the deck area contained these defected areas. Upon completion of the two inspections, recommendations

were made to seal construction joins and perform a shallow overlay to preserve the integrity of the bridge. An aerial image of the bridge deck can be seen in Figure 4-5.

Figure 4-5: Satellite Image of 24 Mile Road Bridge Deck in Calhoun County, Michigan.

Like 20 Mile Road, testing on 24 Mile bridge corresponded with the inspection of the bridge by MDOT. A sketch of the deck sounding was georeferenced as a GIS shapefile (Figure 4-6). The sounding determined that there was 762 ft^2 of delamination with 13 ft^2 of bit patching and scale which corresponded to 14% of the deck surface.

Figure 4-6: Georeferenced Sketch of the Results of the Deck Sounding of 24 Mile Rd Showing the Locations of Delaminations. The Total Area Delaminated is 762 ft^2

4.2.3 US-131 NB and SB Bridges

MDOT structures 5002 and 5003 – US-131 over White Creek Ave. are located directly to the east of Cedar Springs Michigan in Kent County and were selected as demonstration sites for the 3DOBS high-resolution and passive infrared thermography deployment. An aerial view of the two structures can be seen in Figure 4-7. Both the north bound (No. 5003) and south bound (No. 5002) bridges of US-131 were inspected for deficiencies. Passive infrared thermal data was also collected by MDOT at these two locations using their agency-owned thermal camera to test the capabilities of their own thermal imaging camera.

Figure 4-7: North and South Bound US-131 Bridges over White Creek Ave. near Cedar Springs, Michigan.

Both bridges, 5002 and 5003, were constructed in 1971 and are 3-span steel beam bridges. Structure No. 5002 has a total length of 176.8 ft while structure No. 5003 spans a slightly larger distance with a total length of 187 ft. Both of the bridges have a 40’-6” roadway with two 12 ft lanes, a 5’-3” shoulder and an 11’-3” shoulder. In 2007, the ADT over structure No. 5002 and No. 5003 was measured to be 13,760 vehicles per day with 10% being commercial truck traffic (MDOT). It was estimated that the ADT over both structures will reach about 20,000 vehicles per day in the year 2018, a significant increase in traffic volume making bridge improvements and preservation activities increasingly more important.

Although these two bridge structures are in close proximity, their levels of degradation are different which raises questions of construction inspection consistency and construction practices. The concrete deck surface of structure No. 5002 was assigned a fair condition NBI rating of 5 while the deck surface of No. 5003 was in poor condition and rated at a 4. The most

recent inspection for both structures occurred on September 10th 2013. The surface of the bridge deck was of particular interest during this deployment because assessments of the 3DOBS high-resolution system and passive infrared thermography were made. It should be noted however that both structures have considerable amounts of rusting and corrosion over many of the steel beams. In order to preserve the structural integrity of the two bridges, it was recommended that the beams, pins, and hangers be cleaned and painted to extend their service lives.

The inspection report for structure No. 5002 indicated considerable amounts of concrete patches, spalling, and delaminated areas across the deck surface. A photograph of the structure can be seen in Figure 4-8. Several transverse cracks were also apparent over the structure. Expansion joints were missing much of their sealer resulting in some cracking and spalling at the deck surface as well as the bottom surface of the deck.

Figure 4-8: MDOT Structure No. 5002 SB US-131 Bridge Deck.

The inspection report for structure No. 5003 indicated that about 26% of the deck surface area was spalled, bit patched or delaminated and about 15% was patched with concrete. Various degrees of cracking were present over the surface of the structure with some occurring around expansion joints where a majority of the sealer was missing. Spalls and cracks on the underside of the bridge deck have originated near joints where water has migrated through the structure. Figure 4-9 shows the north bound structure.

Figure 4-9: MDOT Structure No. 5003 NB US-131 Bridge Deck.

In the case of both bridges, it has been recommended that sealer be applied to expansion joints where deterioration has occurred. Concrete overlay on both bridge decks was also reported for consideration.

US-131 had significantly more vehicle traffic than the previous two bridges. This meant that lanes had to be closed prior to the collection of data by the MDOT inspectors and 3DOBS high-resolution. A sketch of the deck sounding was georeferenced as a GIS shapefile (Figure 4-10 and Figure 4-11). The MDOT sounding determined that there was 2,072 ft^2 of delamination on the north bound lanes (Figure 4-10) and 759 ft^2 of delaminations on the south bound lanes (Figure 4-11).

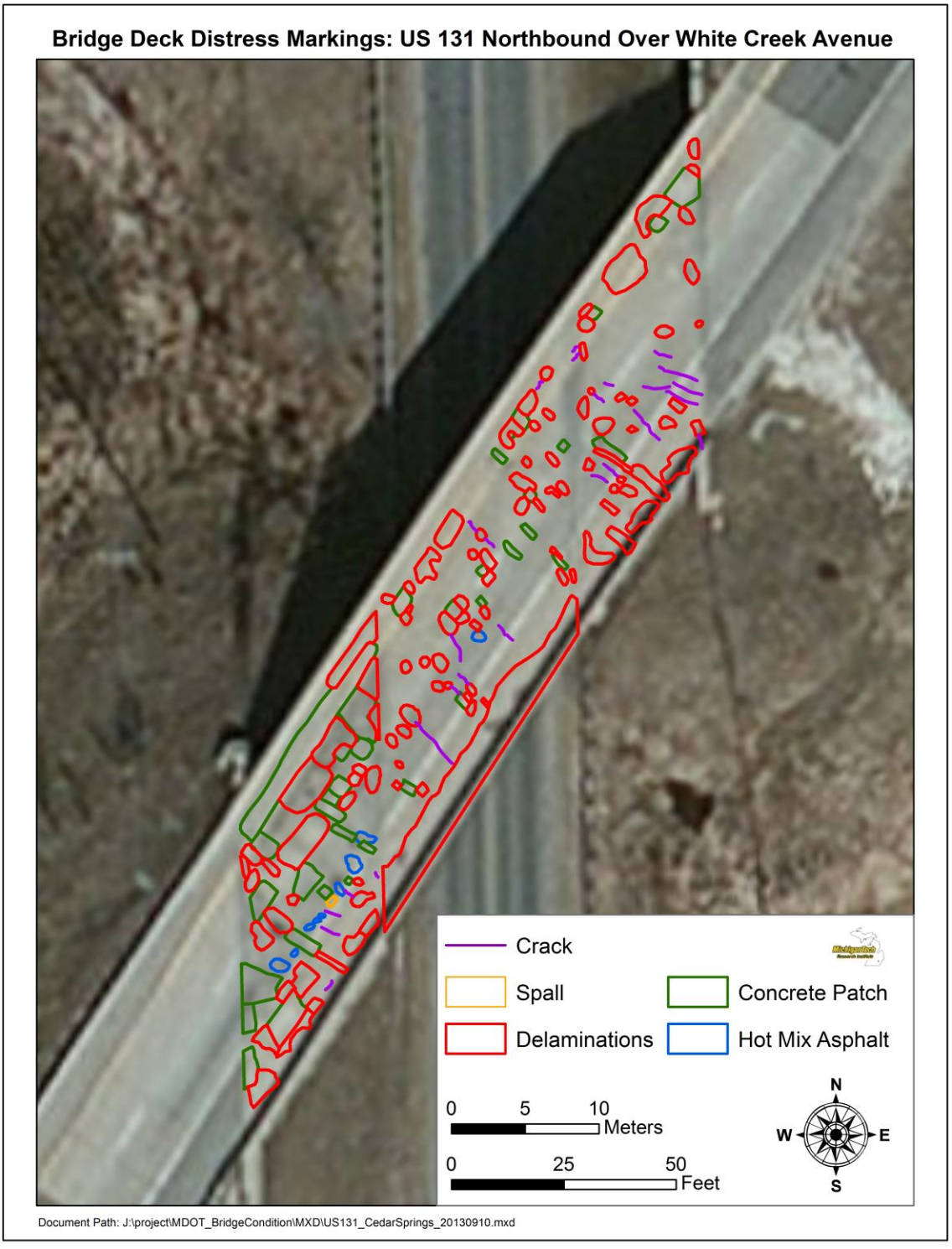

Figure 4-10: Georeferenced Sketch of the Results of the Deck Sounding of the North Bound Bridge of US-131 Showing the Locations of Delaminations, Cracking and Spalls.

Figure 4-11: Georeferenced Sketch of the Results of the Deck Sounding of the South Bound Bridge of US-131 Showing the Locations of Delaminations, Cracking and Spalls.

4.3 Spring and Summer 2014 Demonstration Sites

The following bridges were selected for the spring and summer data collection phases of research. System upgrades for the 3DOBS high-resolution system and passive infrared thermography were implemented, tested, and evaluated. Initial data collection of the 3DOBS low-resolution system at near highways speed and active infrared thermography on the underside of the bridge allowed for the evaluation of these systems in the spring of 2014 at the Maryland Ave. and Freer Rd. bridges. Active thermography was deployed at the Franklin Street Bridge in the summer of 2014.

4.3.1 Maryland Ave. Bridge

MDOT structure No. 4795 – Maryland Avenue over I-196 is located in Kent County approximately 3 miles east of Grand Rapids, Michigan and was selected as one of the two spring demonstration sites for the 3DOBS and passive infrared thermography deployment. The structure spans both east and west bound I-196. A satellite image of the bridge is shown in Figure 4-12.

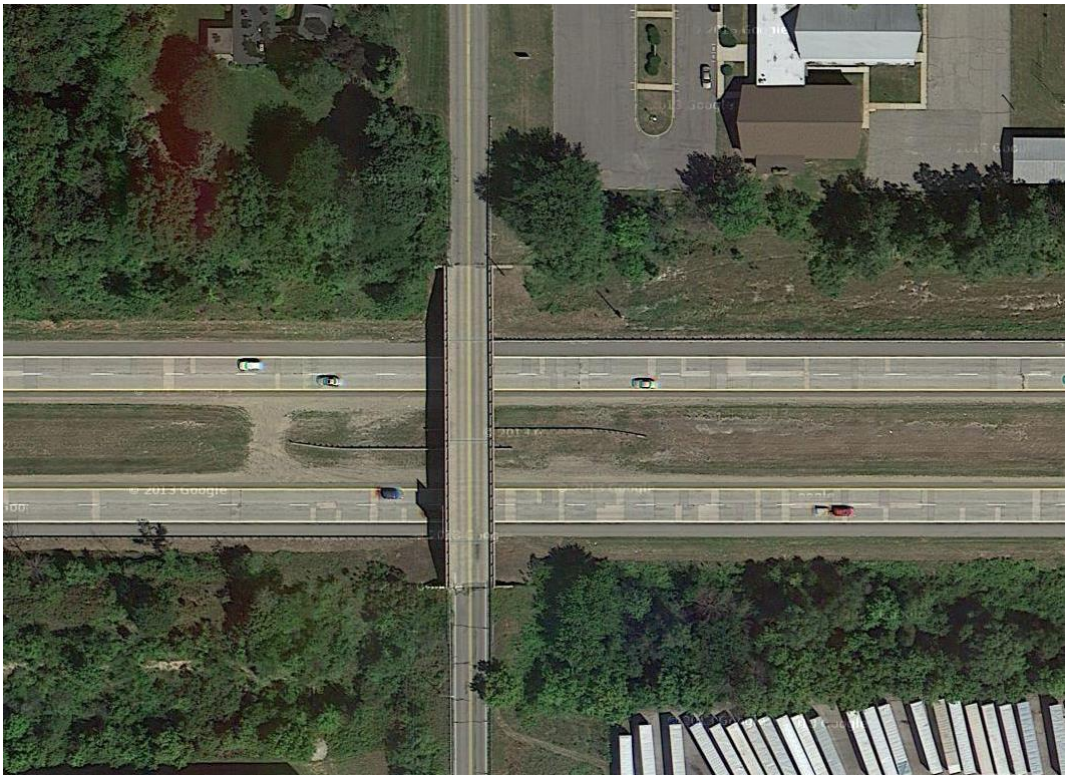

Figure 4-12: Maryland Ave. Bridge over I-196 Located in Kent County, Michigan

The bridge was constructed in 1963 and is a 4-span prestressed concrete composite structure with a total length spanning 230 ft. The bridge has a total width of 35.1 ft with a 28 ft roadway. In the year 1990, the ADT over the structure was measured to be 6,633 vehicles per day with 3% being commercial truck traffic (MDOT). Future ADT predictions for 2010 revealed an expected 15% increase in traffic to 7,628 vehicles per day.

The concrete deck surface was assigned an NBI rating of 6 during the most recent inspection on May 16th 2012. Figure 4-13 shows a photograph of the bridge deck. Because only 3DOBS and the passive infrared thermography testing methods were implemented on this structure, only the condition of the top deck was of interest. Neither the underside of the deck or the superstructure were tested for deficiencies at this location. However, it should be noted that end repairs have been made to fascia beams to prevent further deterioration and extend the service life of the bridge. Shallow spalls that have exposed reinforcing steel on the east fascia beams but still leaves the superstructure in good condition with a rating of 7.

Figure 4-13: Current Condition of the Maryland Avenue Bridge Deck

The inspection report indicated scattered areas of diagonal cracking on the bridge deck, some of which were associated with delaminations. A majority of the identified cracking occurred at the corners of the structure spans. Minor amounts of spalling have left reinforcing steel exposed on the east deck fascia beams but a total of less than 2% of the deck was reported cracked, spalled, or contained delaminations. A majority of the cracking and spalling was reported to occur at joints other than expansion joints.

The Maryland Ave. bridge was inspection of the bridge by MDOT the same day that the combined system deployed. A sketch of the deck sounding was georeferenced as a GIS shapefile (Figure 4-14). The sounding determined that there was 108 ft^2 of delamination with 13 ft^2 of bit patching and scale which corresponded to 14% of the deck surface.

Figure 4-14: Georeferenced Sketch of the Results of the Deck Sounding of Maryland Ave. Showing the Locations of Delaminations.

4.3.2 Freer Rd. Bridge

MDOT structure No. 10940 - Freer Road over I-94 is located in Chelsea, MI approximately one mile east of M-52 and was selected as another spring demonstration site for the 3DOBS systems and passive infrared thermography deployment. The roadway functions as a collector for the area and the bridge structure spans both east and west bound I-94. The structure can be seen in Figure 4-15.

Figure 4-15: Freer Road over I-96 Spring Deployment Location.

Constructed in 1960, the bridge is a 4-span prestressed concrete composite structure with a total length spanning 209 ft. The bridge has a total width of 32.8 ft and has no shoulder. The ADT measured in 1997 over the structure was recorded to be 150 vehicles per day with 3% being commercial truck traffic. ADT predications for the future year of 2017 reveal only a slight increase in traffic volume at 173 vehicles per day.

Upon completion of the most recent inspection on June 5th 2012, the deck surface received an NBI fair rating condition of 6 and can be seen in Figure 4-16. Because the active thermography

inspection method was not implemented at this location, neither the underside of the deck or the superstructure were tested for deficiencies. It should be noted that minor repairs have been made to the superstructure beams due to spalling. Repairs were made to the bottom flanges at the beam ends but the structure components remain in good condition.

Figure 4-16: Bridge Deck of Freer Road Bridge.

The inspection report indicated that concrete patches were present in all spans of the structure. The patches were applied to prohibit further deck deterioration and prolong the service life of the bridge. Transverse and map cracking were also reported to be present in all spans of the structure. An estimated 85 ft^2 of delamination was additionally reported throughout the deck surface of the structure.

4.3.3 Franklin Street Bridge

MDOT structure No. 4947 – Franklin Street over US-131 and CSX railroad line is located in Kent County in Grand Rapids Michigan. The structure spans both the north and south bound US-131 traffic as well as the north and south bound CSX railroad lines. This site was selected for the active infrared thermography deployment because of the ease of access to the bottom surface of the deck. Open land access to the underside of the bridge on the east side of the structure allowed testing to be conducted in a safe environment while minimizing disruptions to traffic flow at road crossings. The structure can be seen in Figure 4-17.

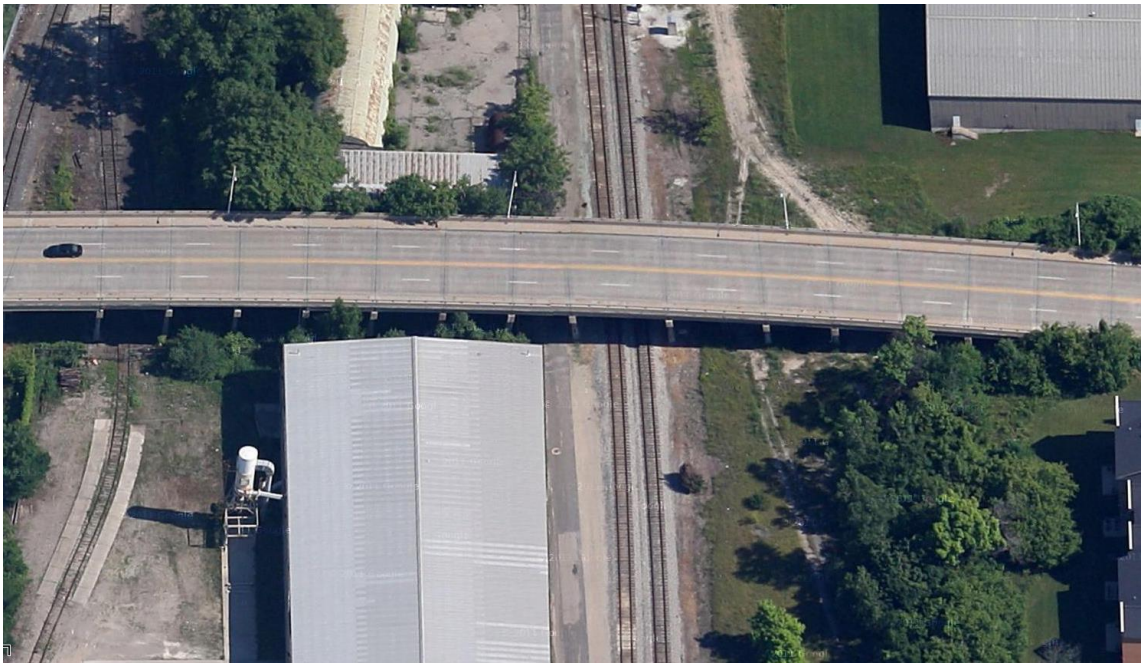

Figure 4-17: East Side of Franklin Street Bridge with Land Access to Underside.

This bridge was constructed in 1960 and is a multiple span structure composed of a combination of both steel and concrete girders. Main spans of the structure over US-131 are composed of steel beams while approach spans were constructed using prestressed concrete beams. The bridge spans a total length of 1,035 ft and is 58.4 ft wide. In the year 2011, the ADT over the structure was measured to be 27,000 vehicles per day with 5% being commercial truck traffic. Figure 4-18 and Figure 4-19 show the east side concrete beam approach structure and condition of the bottom deck surface respectively.

Figure 4-18: Franklin Street Bridge East Side Concrete Beam Approach Structure.

Figure 4-19: Current Condition of Bottom Deck Surface of Franklin Street Bridge.

The bottom concrete deck surface was assigned an NBI fair condition rating of 6 during the last inspection on October 23rd 2012. Because only the active thermography testing method was conducted at this site, the bottom surface of the deck remained the main structural component of interest. It should be noted that seven spans of the structure were replaced while the others were overlaid in 1990.

The inspection report indicated various degrees of deterioration on the bottom deck surface. Replaced deck spans have remained in good condition but other spans contain considerable

amounts of spalling and cracking. In addition, soot buildup from locomotive exhaust was reported directly above the railroad line.

4.4 3DOBS at Near Highway Speed

3DOBS Near Highway Speed System was tested alongside the BridgeGuard thermal camera at both Maryland Ave and Freer Rd bridges. The RED Epic was mounted at the end of the boom next to the thermal camera so that they collect the same section of bride at the same time (Figure 4-20 and Figure 4-21). The Trimble GPS antenna is also mounted above the two cameras so that is collecting GPS data as closely to the center of the cameras position for accurate image referencing.

Figure 4-20: BridgeGuard Thermal Camera and RED Epic Mounted on Vehicle attached Boom.

Multiple runs were collected at speeds ranging from 25 mph to 45 mph under different lighting conditions to test the RED Epic cameras capabilities and to determine if there are limitations due to lighting that would affect the vehicles speed for collection.

Figure 4-21: Combined 3DOBS and BridgeGuard Collecting Imagery over Maryland Ave. in Grand Rapids.

4.5 3DOBS High Resolution System

The Nikon D800 was also mounted to the BridgeGuard vehicle mount to collect high resolution imagery of the bridge decks. Due to a slower maximum frame rate of only 2 fps, the vehicle was limited to speeds less than 5 mph in order to capture imagery with the necessary overlap needed to produce a 3D model of the bridge deck. However, this slower speed enabled high-resolution crack detection. Figure 4- 22 shows an image that was collected from the Nikon D800 over Maryland Ave in Grand Rapids.

Figure 4-22: Imagery Collected from the Nikon D800 of Maryland Ave.

4.6 BridgeGuard Passive Infrared Thermography

BridgeGuard technicians perform weather studies to determine the theoretical ideal scanning times and durations for the bridge site. Bridge identification data and other pertinent information are entered into the collection program prior to or upon arrival at the site. Field delamination control areas are then selected using the infrared cameras and are verified by sounding with a hammer and documented in the field notes. The control areas are used to confirm when conditions are optimal for scanning.

The data collection is carried out using a vehicle-mounted thermal imaging system and high-definition digital imager to record visible and invisible defect data on the bridge deck top (traffic lanes). The camera equipment is set up and scanning begins. In this particular study with the addition of the Nikon D800, travel speeds were limited to only a few miles per hour. Data was collected one lane at a time until the entire deck had been scanned, and the recorded imagery was saved using proprietary software to a laptop computer. The technicians representing Michigan Tech collected their data at the same time as BridgeGuard.

Prior to leaving the bridge, a QA/QC check was done to ensure the data was of good quality and that the bridge measurements were accurate. After scanning was completed, the data was analyzed with the results imported into a CAD file and defects tabulated in spreadsheet form to allow integration into project plan documents.

4.7 BridgeViewer Remote Camera System (BVRCS)

The BridgeViewer Remote Camera System was deployed on the US-131 bridges near Grand Rapids, 20 Mile and 24 Mile Roads near Marshall. In all the deployments the GoPros were capturing 12.3 MP images at 2 fps. The collection setup for US-131 was different than normal as the cameras were mounted to the roof of the truck rather than the hood (Figure 4-23). This was necessary as the hood was not made of steel and the magnets were not effective. This limited the view of the road in front of the truck with the hood taking up a portion of the image (Figure 4-24). The collects form 20 and 24 Mile Roads had a two camera setup with the cameras mounted to the hood the truck (Figure 4-25).

Figure 4-23: The Collection Setup for US-131 with a Single GoPro Mounted on the Roof of the Collection Vehicle.

Figure 4-24: Example Image Collected from a Single GoPro Mounted to the Roof of the Collection Vehicle.

Figure 4-25: Example Image Captured on 24 Mile Road with a GoPro Mounted on the Hood of the Collection Vehicle.

The GPS for all collects was mounted on the dash of the collection vehicle. Prior to each collect a picture was taken with the GoPro of the GPS screen showing the time (Figure 4-26). This

allowed for the researcher to add the correct time difference between the camera and the GPS within GeoJot+. The image locations are interpolated based on the time adjustment calculated in GeoJot+.

Figure 4-26: Detailed Image Showing the GPS Time in a Photo used to adjust the Time Difference between the Camera and the GPS Unit.

5. Top of Deck Evaluation using Photogrammetry and Thermography

5.1 3DOBS at Near Highway Speed

3DOBS Near Highway Speed collected imagery at both demonstration bridges alongside the BridgeGuard thermal camera on the new mount. An image processing issue arose in the lab even though the imagery collected met all of the 3DOBS collection criteria (capture one lane per pass, correctly exposed and minimal motion blur). Agisoft software seemed to have issues correctly aligning the imagery and building the model. Even after adding in ground control points the resulting 3D model was warped and staggered.

The RED Epic camera was further tested under different conditions. These included both roadway and non-road features such as slopes. After successful reconstruction of other features, the demonstration bridges were reevaluated. Both Freer Rd and Maryland Ave were recently resurfaced and as a result they had very little variation in elevation on the surface. Tests conducted with slopes and other features which contained a significant variation in depth lead to successful reconstructions.

It was then determined that the reason for the inability to reconstruct the demonstration bridges was due to a lack of angular diversity between images because of the high quality (excellent condition) of deck surface. The Nikon D800 did not have this issue due to its higher resolution and ability to resolve smaller features. To prove this concept, another collection on Freer Rd. was made with the RED Epic. This time instead of driving one pass per lane, a third run was done down the middle of the bridge.

This third run down the middle was conducted to increase the overlap between all of the imagery. The effect would be that instead of a single feature only represented in at least five images in a single "flight line" (i.e., a driver over the bridge), it would also be represented in another flight line with at least five more images. The result is that there is greater than 100% overlap in the imagery, which would increase the chances of the software to correctly align the images and calculate depth (Figure 5-1 and Figure 5-2).

Using the new imagery from the Freer Road structure, Agisoft was able to correctly align the photos and create a DEM of the bridge deck. It confirmed that under situations where the bridge deck is in good conditions and contains very little or no distresses it is difficult to reconstruct 3DOBS outputs without additional imagery overlap. For bridges with significant spalls or other features, only a single pass per lane is needed, as there would be enough 3D information in the imagery for accurate reconstruction. Table 5-1 below is a table displaying the minimum distress sizes that 3DOBS Near Highway Speed can resolve.

Table 5-1: Minimum Resolvable Distresses for 3DOBS Near Highway Speed.

System	*Bridge Health Indicator*	*Minimum Size Resolved*	*Data Output Needed*	*Technique Used*
3DOBS Near Highway Speed	Spalls	1/8" depth and 1/2" wide	DEM	Visual or Automated Detection
	Cracking	1/8" wide	Orthoimagery	Visual
	Map Cracking	Spacing of 1/4"	Orthoimagery	Visual

Figure 5-1: Orthoimage of Freer Rd Generated from Imagery Collected from the RED Epic.

Figure 5-2: DEM of Freer Rd Generated from Imagery Collected from the RED Epic.

5.2 3DOBS High Resolution

The imagery collected from 3DOBS high-res was processed through Agisoft to generate an orthoimage, DEM and hillshade of Maryland Ave (Figure 5-3) and Freer Rd (Figure 5-5). The resulting x,y resolution of the Agisoft output is 0.5 mm and is shown in detail in Figure 5-4 and Figure 5-6.

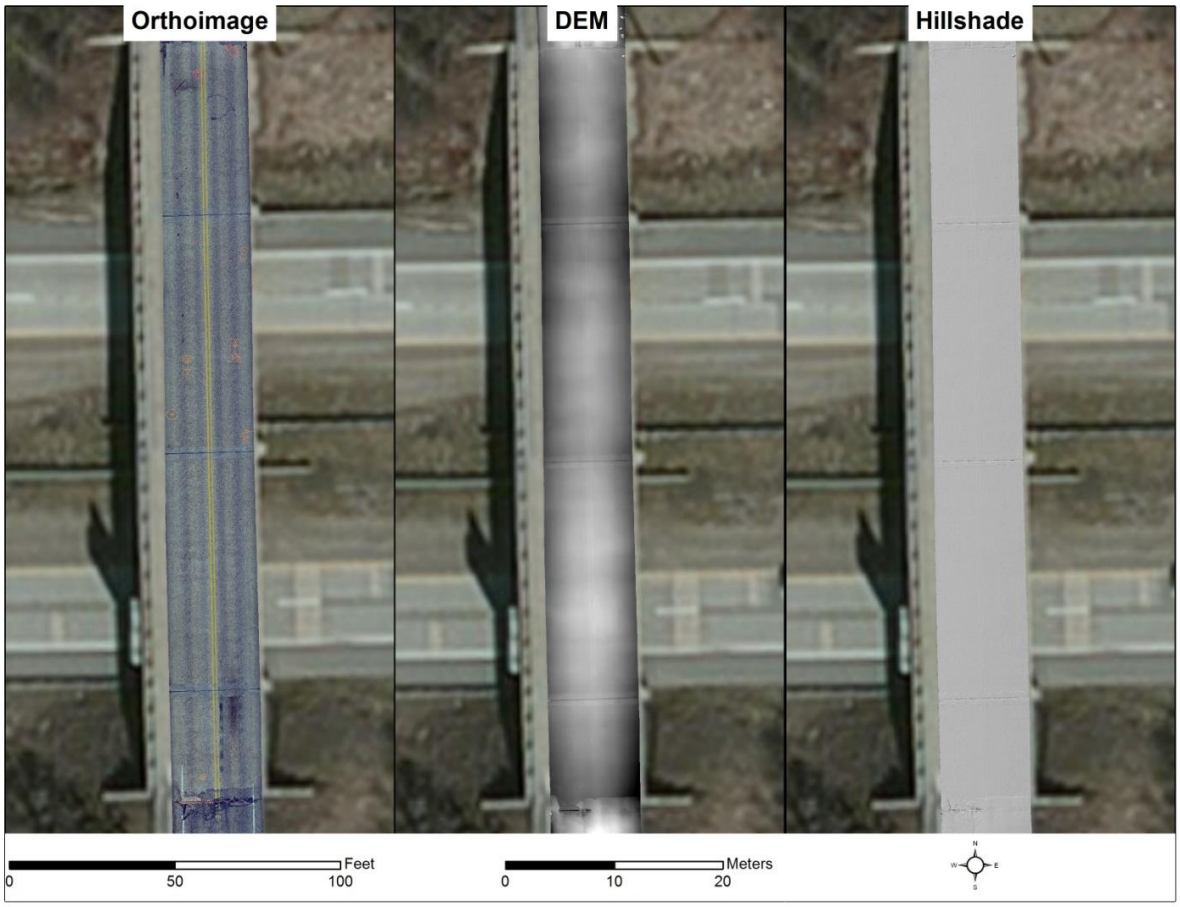

Figure 5-3: Overview of the Orthoimage, DEM and Hillshade Layers Generated from 3DOBS High Resolution over Maryland Ave.

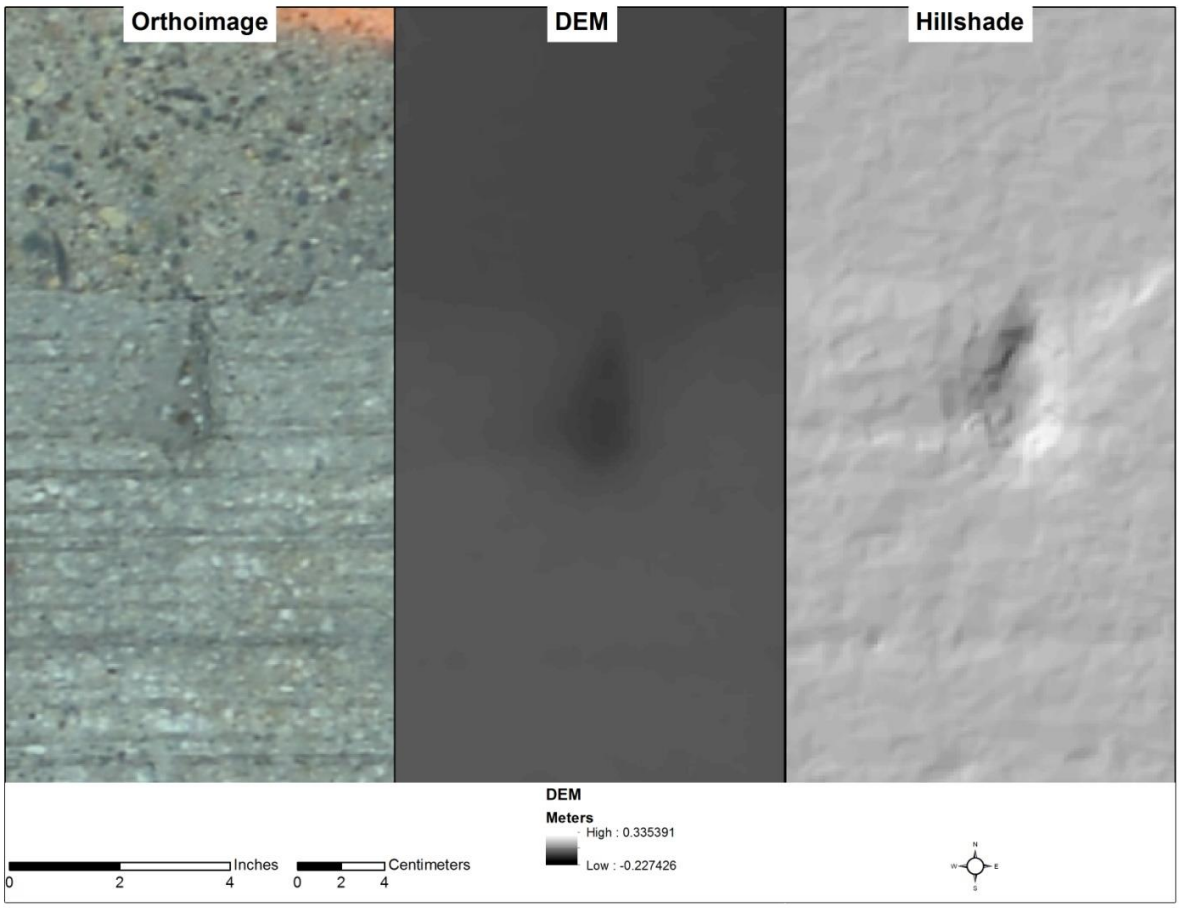

Figure 5-4: Zoomed In View of the Orthoimage, DEM and Hillshade Layers Generated from 3DOBS High Resolution over Maryland Showing 0.5 mm Resolution of the Outputs.

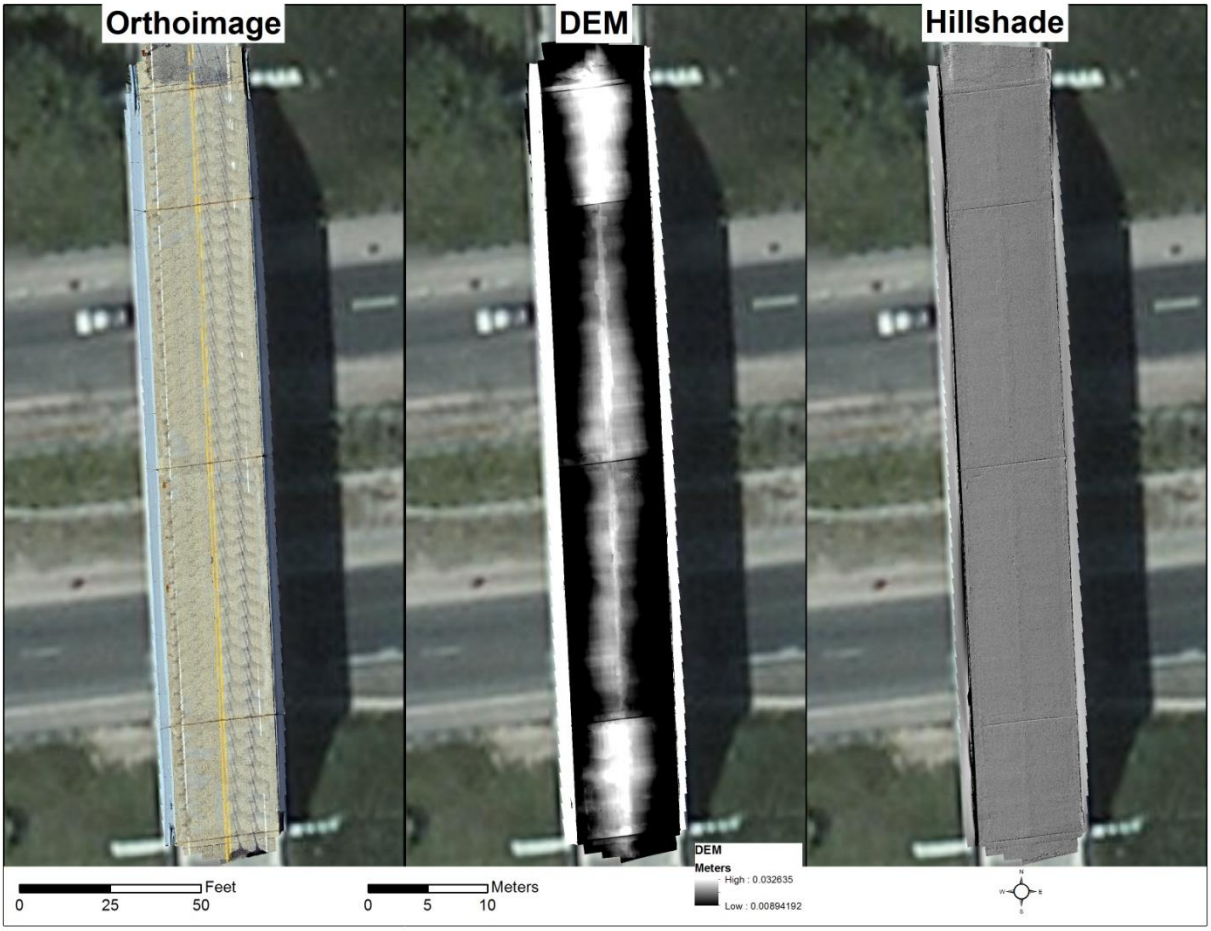

Figure 5-5: Overview of the Orthoimage, DEM and Hillshade Layers Generated from 3DOBS High Resolution over Freer Road.

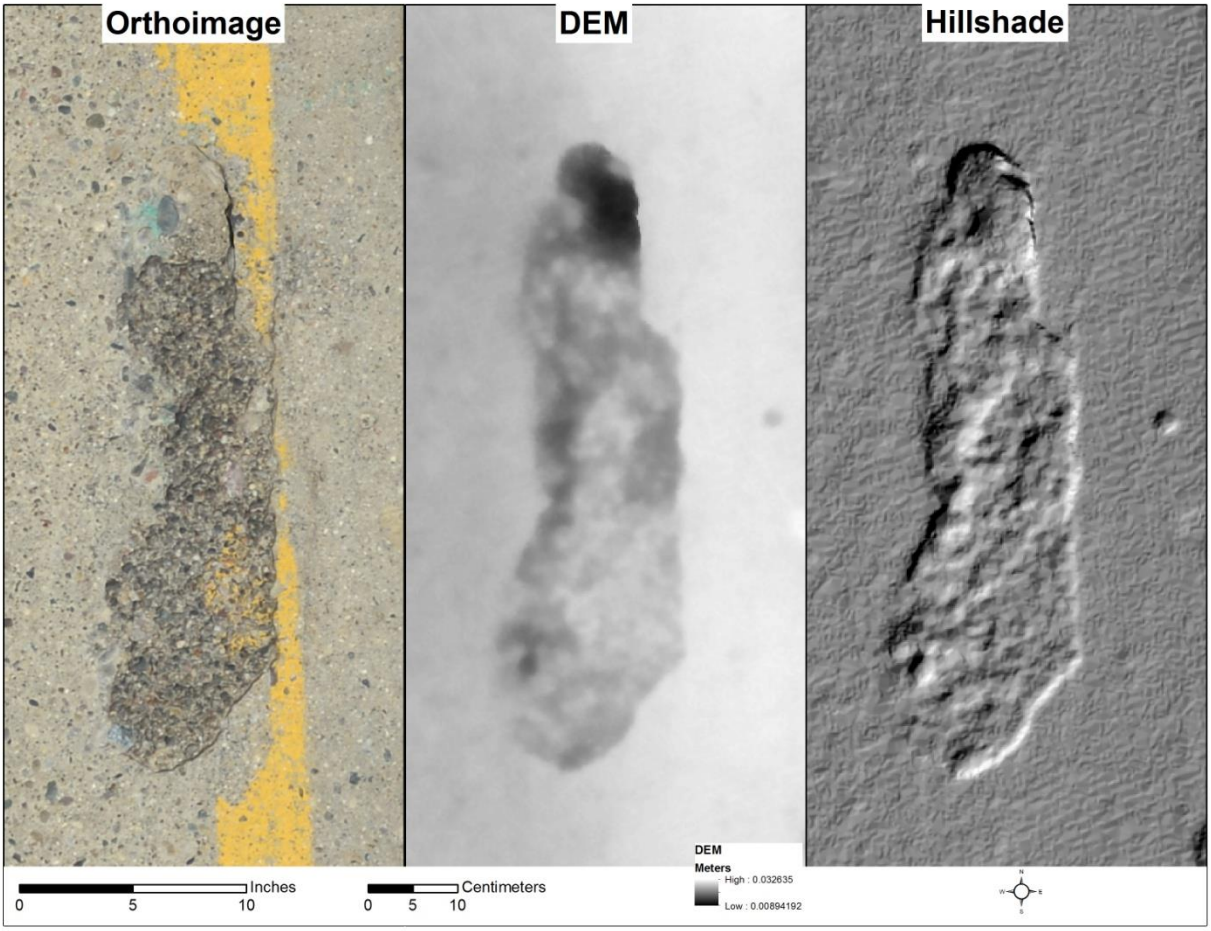

Figure 5-6: Zoomed in View of the Orthoimage, DEM and Hillshade Layers Generated from 3DOBS High Resolution over Freer Rd. showing 0.5 mm Resolution of the Outputs.

Crack detection was performed through visual inspection of the orthoimagery. With a resolution of 0.5 mm the smallest crack that could be seen is at least 1 mm or just over 1/32nd of an inch. Smaller cracks are not detectable since there needs to be at least two pixels over the crack in order for the crack to show in the imagery. For Maryland Ave (Figure 5-7) where MDOT marked some of the cracking, a visual inspection of the orthoimage located more cracking. Freer Rd also had some cracking but it was not marked by MDOT prior to the field data collection (Figure 5-8). Table 5-2 below is a table displaying the minimum distress sizes that 3DOBS High Resolution can resolve.

Table 5-2: Minimum Resolvable Distresses for 3DOBS High Resolution.

System	*Bridge Health Indicator*	*Minimum Size Resolved*	*Data Output Needed*	*Technique Used*
3DOBS High Resolution	Spalls	1/32" depth and 1/8" wide	DEM	Visual or Automated Detection
	Cracking	1/32" wide	Orthoimagery	Visual
	Map Cracking	Spacing of 1/16"	Orthoimagery	Visual

Figure 5-7: Detected Cracks on Maryland Ave.

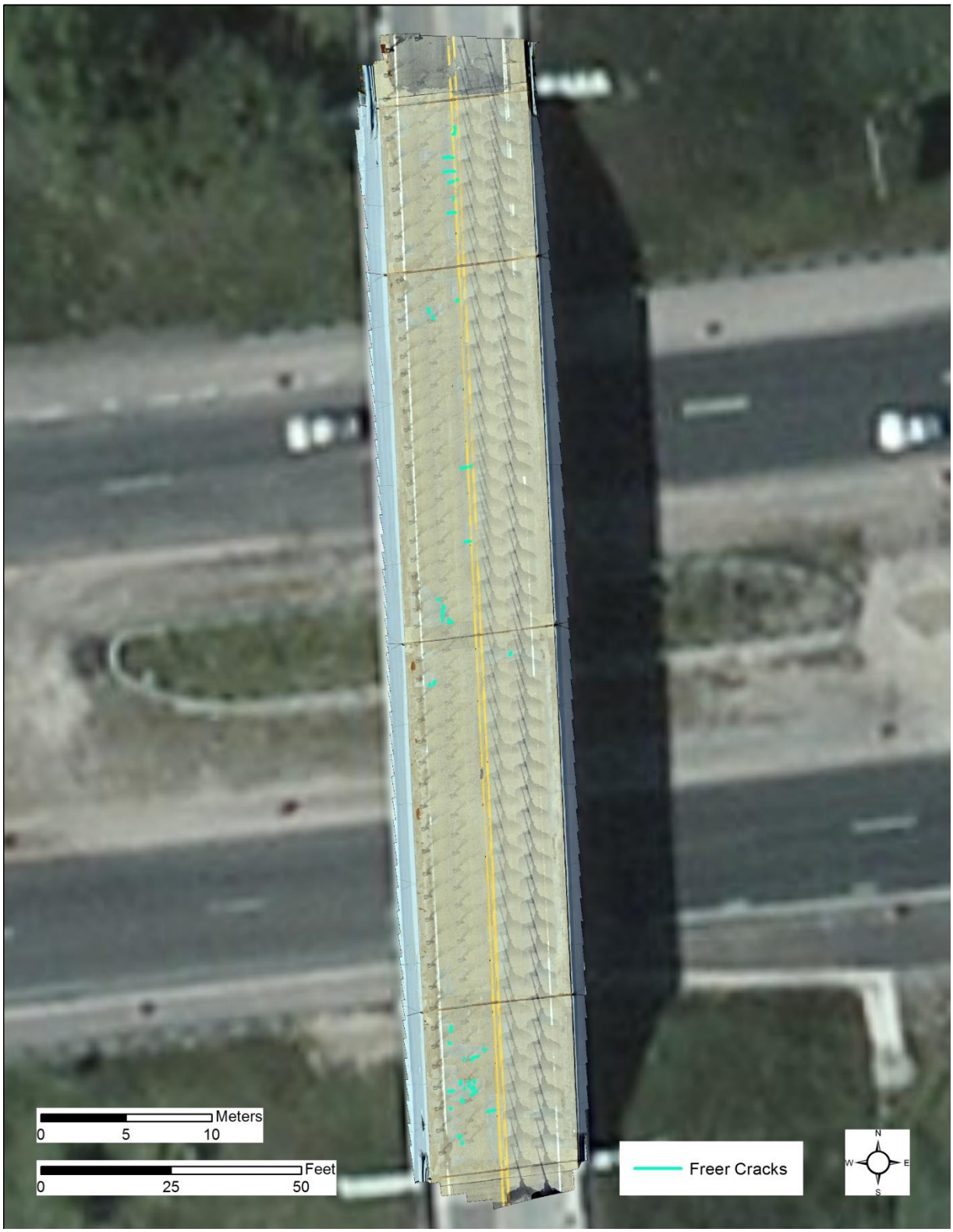

Figure 5-8: Detected Cracks on Freer Rd.

5.3 BridgeGuard Passive Infrared Thermography

During the analysis phase, the delaminations and spalls were identified, quantified and percentages obtained, based on total square foot area. The results are comprehensive and assembled in a manner that can be easily incorporated into Inspection Reports, Pontis, work recommendations, and/or detailed scoping documents. Appendix B-F includes the individual reports for the bridge decks evaluated in this study.

All reports and deliverables are designed to meet the needs, requirements, and expectations of the client and can be submitted in MicroStation or AutoCAD native files with MS Excel spreadsheets summarily detailing the locations and sizes of defects, and are subject to QA/QC reviews prior to being submitted.

During the field testing phase, BridgeGuard assessed bridge decks separately from 3DOBS. Figure 5-9 shows BridgeGuard results from 20 Mile Rd. and it was determined that there was was 1,767 ft^2 of potential delaminations on the bridge deck. This was almost 500 ft^2 more than was recorded by MDOT. For 24 Mile Rd. BridgeGuard determined that there was 1,765 ft^2 of potential delaminations on the bridge deck (Figure 10). Compared to MDOT, this was approximately 1,000 ft^2 more than MDOT's estimate.

US-131 consists of two bridges, each with its own report. For the north bound lanes the BridgeGuard assessment determined there was 1,609 ft^2 of potential delaminations (Figure 11). The south bound lanes contained 989 ft^2 of potential delaminations according to BridgeGuard's analysis (Figure 12). By comparison MDOT reported there was 2,072 ft^2 for the north bound lanes and 759 ft^2 for the south bound lanes.

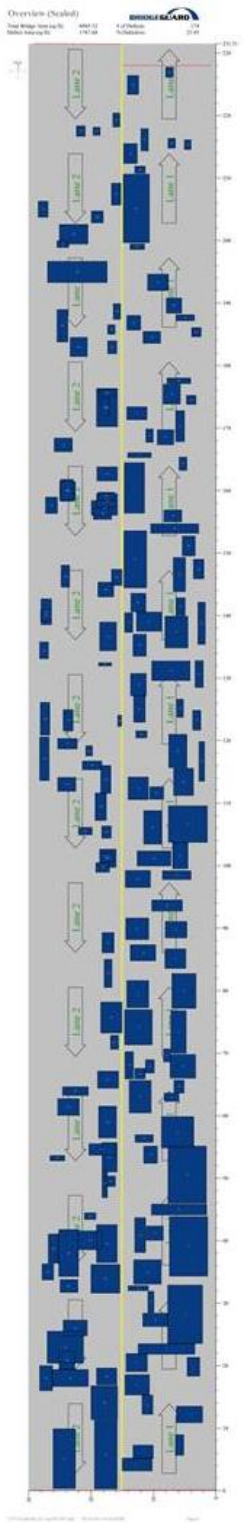

Figure 5-9: Location of Potential Delaminations as Determined by BridgeGuards Thermal Survey on 20 Mile Rd.

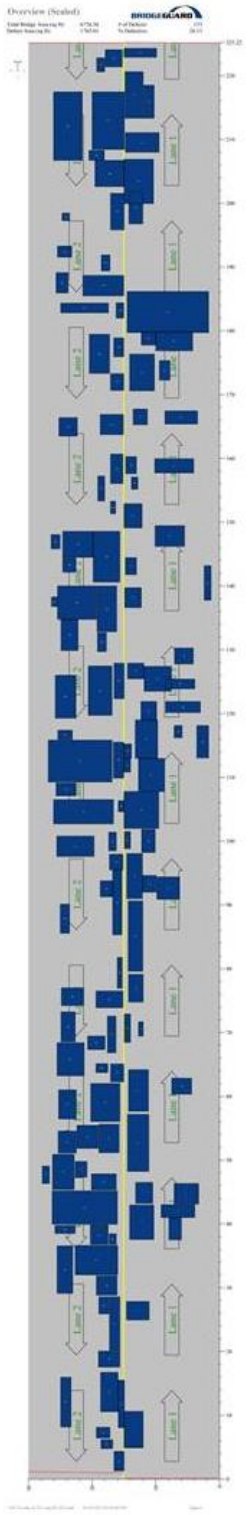

Figure 5-10: Location of Potential Delaminations as Determined by BridgeGuards Thermal Survey on 24 Mile Rd.

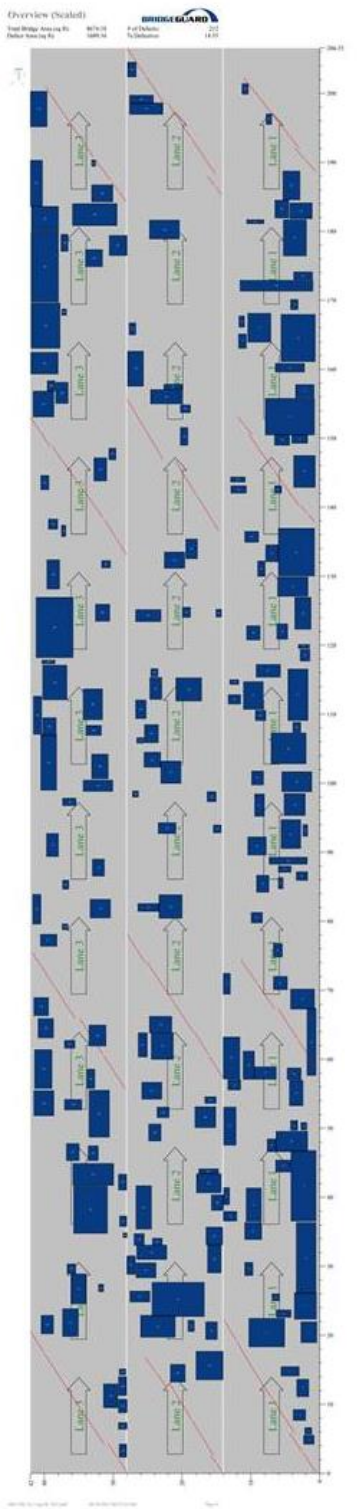

Figure 5-11: North Bound Lanes of US-131 Showing Potential Delaminations from the BridgeGuard Survey.

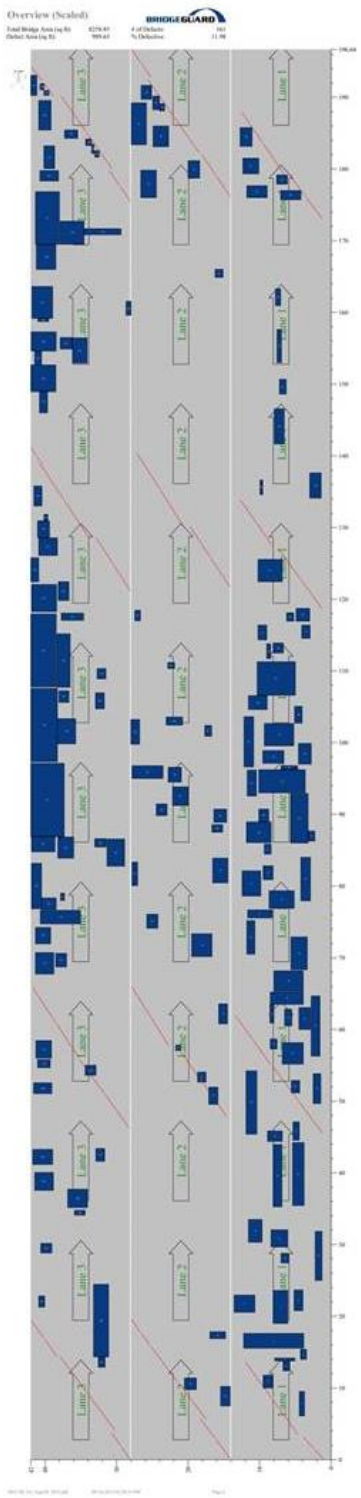

Figure 5-12: South Bound Lanes of US-131 Showing Potential Delaminations from the BridgeGuard Survey.

5.4 BridgeViewer

Imagery collected with BridgeViewer wes geotagged using the track log from the GPS used in the vehicle. The geotagging process produces a shapefile of the picture locations as well as watermarked pictures that include the Lat/Lon and date/time (Figure 5-13). The imagery from the two cameras was also separated into right and left as they were mounted (Figure 5-14). Because there was only one GPS, the photos were tagged to the center of each lane. The shapefile is then edited to separate the right and left cameras to represent the offset as they were collected.

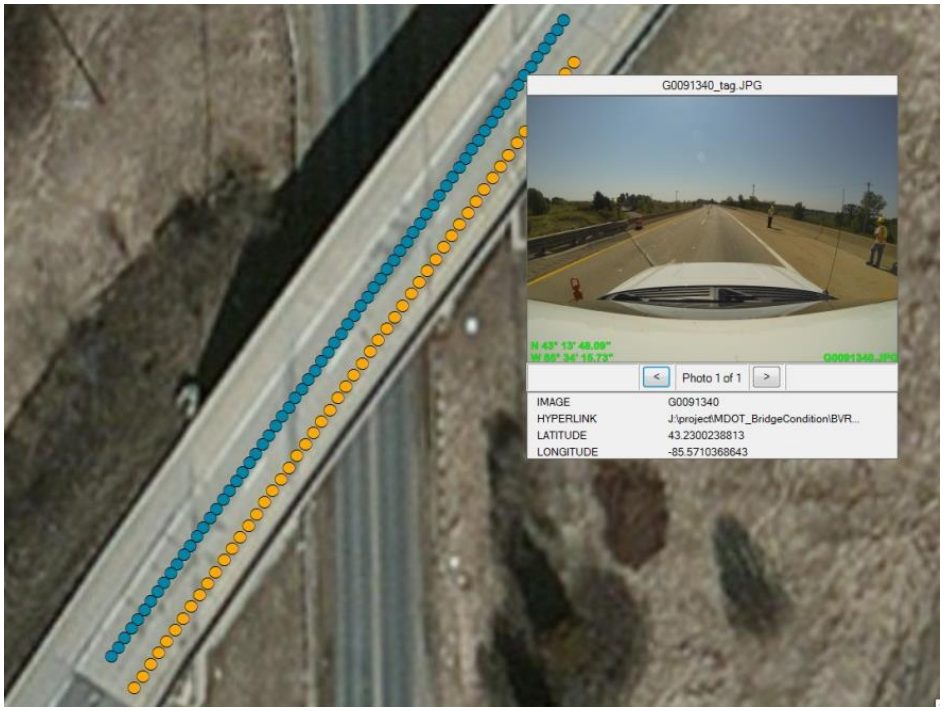

Figure 5-13: BridgeViewer Collect on US-131 near Grand Rapids, MI. For this Collect the Cameras were Mounted to the Roof of the Vehicle since the Hood was not Steel.

Figure 5-14: BridgeViewer collect of 24 Mile Rd near Marshall, MI.

5.5 System Integration Results

After the data are collected, a spall detection analysis is run for 3DOBS, a delamination detection is performed by BridgeGuard for the thermal the imagery, and results are combined within ArcMap GIS software. 3DOBS data and results are already generated as GIS layers and shapefiles with a geographic reference. BridgeGuard data is not referenced in a standard GIS format but it is locally referenced to the bridge.

The thermal images collected by BridgeGuard are individually georeferenced to the orthoimage created by 3DOBS. This is done using the georeferencing tool in ArcMap. Once georeferenced they are mosaicked (using the ArcGIS "mosaic to new raster" tool) to form a single image (tif) layer that can be easily displayed in any GIS. The detected delaminations are then traced in ArcMap to create a separate shapefile (Figure 5-15).

The final GIS output for a bridge includes six layers: an orthoimage, DEM, Hillshade, thermal layer, detected spalls shapefile, and delaminations shapefile. As noted by MDOT Survey Support staff, another useful geospatial layer can be created – a 3D point cloud in standard LAS format that can be analyzed and visualized using image processing software. The shapefile of detected cracks is also spatially referenced similar to the spalls layer except it is only produced from the high-res version of 3DOBS. All of these data sets overlay in a GIS, which makes it easy to

analyze spalls and delaminations simultaneously (Figure 5-16). Spalls and delaminations can easily be visualized while overlaid on the orthoimage or the thermal layers (Figure 5-17).

Figure 5-15: BridgeGuard Imagery as Georeferenced Layers with Delaminations Shapefile.

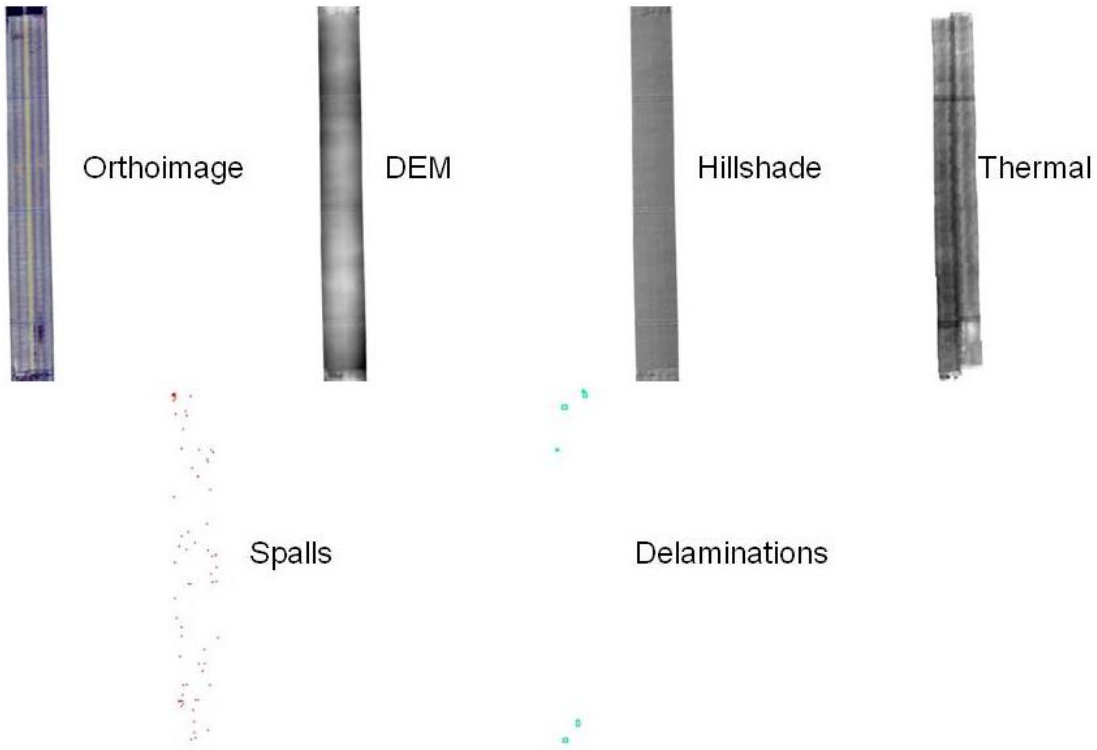

Figure 5-16: All of the Data Sets Created from the Combined System.

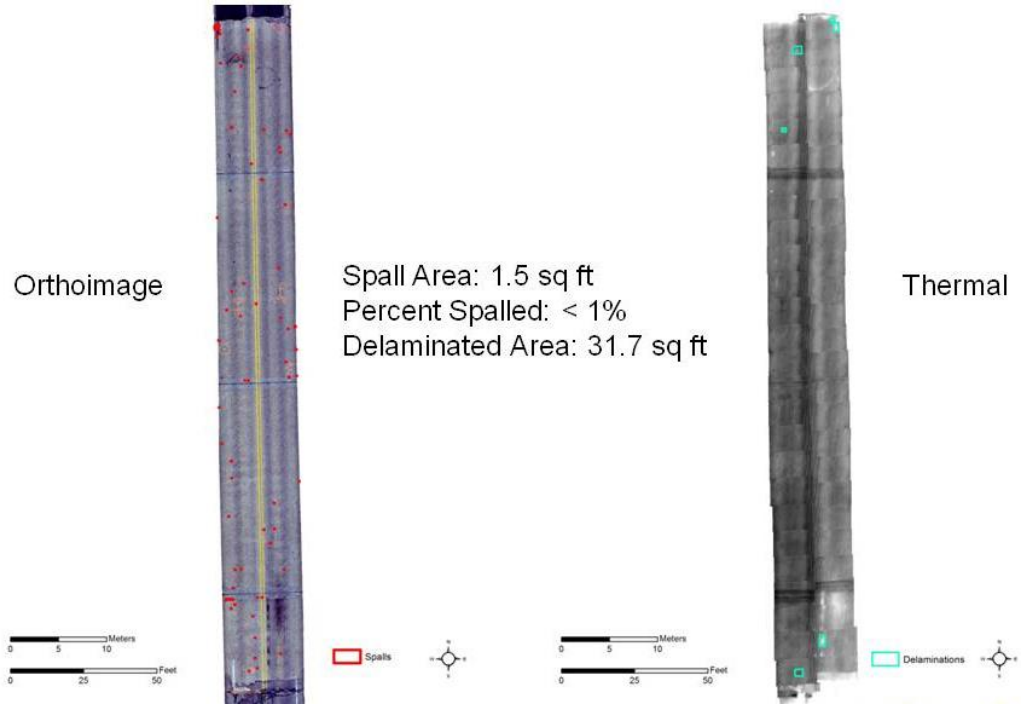

Figure 5-17: Comparison of the Results Generated from 3DOBS High Speed and the BridgeGuard Thermal Cameras as a Combined System over Maryland Ave.

Through the combination of these technologies, bridge inspectors are able to visualize and objectively assess the surface and subsurface condition of concrete bridge decks. All of the output generated is in the form of GIS layers and shapefiles that can be viewed in any GIS. Once in a GIS, these files can be processed using a variety of tools to extract more information out of the optical and thermal data collected. One example would be if multiple collects are done over a period of time, a change detection analysis can be performed and deterioration rates can be calculated.

6. Underside of Deck Evaluation using Active Infrared Thermography

Non-destructive testing (NDT) techniques have shown potential in accurately assessing the deterioration condition of concrete bridge elements but few have the capabilities needed to quantify subsurface defects such as delaminations. However, these technologies are not readily deployable during routine bridge inspections. Infrared thermography is one remote sensing NDE technique that is gaining popularity among bridge inspectors due to its potential in detecting delaminations within concrete structural elements and its simplistic method of data acquisition and analysis. Infrared thermography can be conducted in either a passive or active test set-up. Active infrared (IR) thermography can overcome some obstacles associated with passive infrared thermography due to the use of an external heating source, rather than relying on solar energy and the presence of the sun. Although more focus in the bridge inspection field is given to passive infrared thermography inspection (ASTM 2007), active infrared thermography also has capabilities for detecting delaminations specifically on structural elements found on the underside of bridges that are not exposed to direct sunlight (Vaghefi 2001).

A primary objective was to determine the feasibility of using active IR thermography for detecting delaminations on the deck underside and fascia beams. Through a series of laboratory tests, the active heating method was investigated to include variable depth delaminations and heating time. A proof of concept field demonstration confirmed the feasibility of using active IR thermography for concrete delamination detection on an in-service bridge in areas not exposed to passive solar heating. Testing was conducted on a bridge located in downtown Grand Rapids, Michigan and provided valuable information regarding the current condition of the underside of the bridge deck and side of a pier cap. A simple method to quantify suspected delamination area is defined to evaluate performance of the active IR method. This chapter provides a comprehensive evaluation of active thermal IR for deck inspection including laboratory and field demonstration results leading to recommendations for further development prior to implementation.

6.1 Active Thermography for Concrete Bridge Element Evaluation

Unlike passive infrared thermography, active IR thermography involves a transient heat transfer phenomena using an external heater other than the sun or thermal properties of the object itself. In this case, electromagnetic energy is transmitted to the specimen by an external heater and radiant energy emitted from the object can be recorded using a thermal infrared camera. This testing procedure requires that the specimen be intentionally heated to create a gradient temperature difference between the object's interior and surface. As infrared radiation from the heater propagates through dry concrete, delaminations restrict the heat transfer and the concrete near the surface retains more heat than surrounding areas of sound concrete. Thermal IR images are collected during either the heating or cooling period.

A variety of controllable heating sources, including hot air guns, quartz lamps and heat blankets can be used to produce thermal excitation on the test specimen. Active IR thermography techniques are commonly named based on the source of the external heater. Examples of active methods include: Pulsed (Flash) thermography, Pulsed phase thermography, Lock-in thermography, Vibrothermography, Inductive thermography, Laser spot thermography and Step heating (Maldague 1993). This study specifically focused on pulsed thermography with pulse heating times of 5 and 15 minutes.

6.1.1 Advantages of Bridge Inspection Using Active Infrared Thermography

Similar to passive infrared thermography, the capability of detecting subsurface defects and delaminations, commercial availability, remote sensing, ease of data collection and image interpretation are some of the benefits of using the active IR thermography technique for bridge inspection. Remote data collection of active IR thermography is an outstanding advantage of this technology, which helps in reducing traffic disruption and lane closures during the testing period. With the ability to store data for monitoring the damage growth process during the service life of a structure, condition assessments using active IR thermography also allow for better allocation of bridge maintenance funds.

Determination of delamination depth, as well as the location and size, is an important feature in active infrared thermography (Maldague 1993). This approach is not dependent on the weather condition and clear sky; therefore, it allows conducting a bridge inspection in a larger time window during the day. Furthermore, this method can be applied on the concrete bridge elements which are not exposed to the direct sunlight, such as girders and the underside of the bridge deck.

6.1.2 Limitations of Bridge Inspection Using Active Infrared Thermography

Although active IR thermography allows for a wider inspection time window and does not have to be conducted at a certain time of day, environmental conditions can impact the data collection process, such as moisture on the test surface from precipitation or condensation.

Materials with different emissivity on the surface (for example patched areas surrounded by existing concrete) provide challenges in detecting subsurface flaws due to the perturbing contrast in thermal infrared images. As with passive IR thermography, optical (visual) images are recommended (Vaghefi and Ahlborn 2013).

6.2 Laboratory Experiment Methodology

To investigate the feasibility of using active IR thermography to detect and quantify delaminations in concrete test specimens, a laboratory test set-up was developed following an in-depth literature review of this non-destructive remote sensing condition assessment technique.

Several laboratory experiments were conducted using the concrete test specimens, equipment, procedure, and analysis methods described in the following sections.

6.2.1 Concrete Test Specimens

As layers of concrete separate and delaminations form, pockets of air become present within the concrete. Due to the difference in thermal conductivity of concrete and air, these subsurface defects can be detected using a thermal infrared camera when exposed to a thermal impulse. To simulate the presence of delaminations in concrete, a material with similar thermal properties to air was selected and embedded into several concrete specimens. Due to the similarity of the thermal conductivity between air and Styrofoam with respect to concrete, 3/8 in. thick Styrofoam blocks were selected to simulate delaminations (Vaghefi 2013). The thermal conductivity of air was determined to be 0.024 W/(m^oK) or 0.116 (Btu x in)/(hr x ft^2 x ^oF) while the conductivity of Styrofoam was determined to be 0.03 W/(m^oK) or 0.229 (Btu x in)/(hr x ft^2 x ^oF) (Maldague 1993; Engineering ToolBox 2012). With the thermal conductivity of dry concrete being between 0.4 and 1.8 W/(m^oK) or 2.8 and 12.5 (Btu x in)/(hr x ft^2 x ^oF), Styrofoam can be considered representative of delminations within concrete elements (Lamond and Pielert 2006).

6.2.1.1 Laboratory Test Slabs I-VI

A total of six concrete slabs containing simulated delaminations were constructed for active IR thermography experiments in the laboratory, one of which was used for a parametric study to investigate several testing variables. Test Slabs I-V include a repurposed slab with dimension of 45 in. x 45 in. x 5.5 in. constructed in April 2010 (Slab V) and four 2.5 ft x 2 ft x 5.5 in. slabs that were built between November 2012 and June 2013 (Slabs I- IV). The specimen size for slabs I-IV was selected based on the field of view of the thermal infrared camera used during testing which has the capability to capture a majority of the specimen at a relatively close range (6 ft.). Specific concrete information used for constructing test slabs I-VI is summarized in Table 6-1. Because Slab V was repurposed from previous laboratory tests conducted at Michigan Technological University that were not concerned with mix design or properties, mix proportions for this test slab are unknown.

Table 6-1: Concrete Mix Design and Wet Properties for Test Slabs I-V.

Properties	***Slab I***	***Slab II***	***Slab III***	***Slab IV***	***Slab V****	***Slab VI***
Cement (lb/cy)	737.5	737.5	737.5	567	-	565.8
Water (lb/cy)	312.8	312.8	312.8	270	-	216.5
Coarse Aggregate (lb/cy)	1794.4	1794.4	1794.4	1869.75	-	1865.3
Fine Aggregate (lb/cy)	765	765	765	1269	-	1366.3
Air Entrainer (oz/cy)	14.75	7.5	9.8	0	-	3.47
Slump (in.)	8.5	0	2.5	0.5	2.75	8.75
Air (%)	8.1	2.4	3.3	1.6	5	8
Date of Construction	11/15/2012	04/30/2013	05/16/2013	06/06/2013	April 2010	9/13/2013

Concrete delivered via Ready mix truck based on Michigan Department of Transportation (MDOT) grade D mix (MDOT 2003).

The plan layout for Slabs I-VI are shown in Figure 6-1. All simulated delaminations shown in Figure 6-1 (A) are 3 in. x 3 in. x 3/8 in. Styrofoam blocks. The selected defect size allowed for the placement of six delaminations in the concrete slab with sufficient distance to the edges of the specimen. Simulated delaminations in Slabs I-IV were placed at varying depths inside the concrete slabs. The Styrofoam was positioned at these various depths using fishing line and concrete was cast around the blocks. Care was taken when placing concrete to ensure the simulated delaminations remained level to the surface of the specimen and at the planned height.

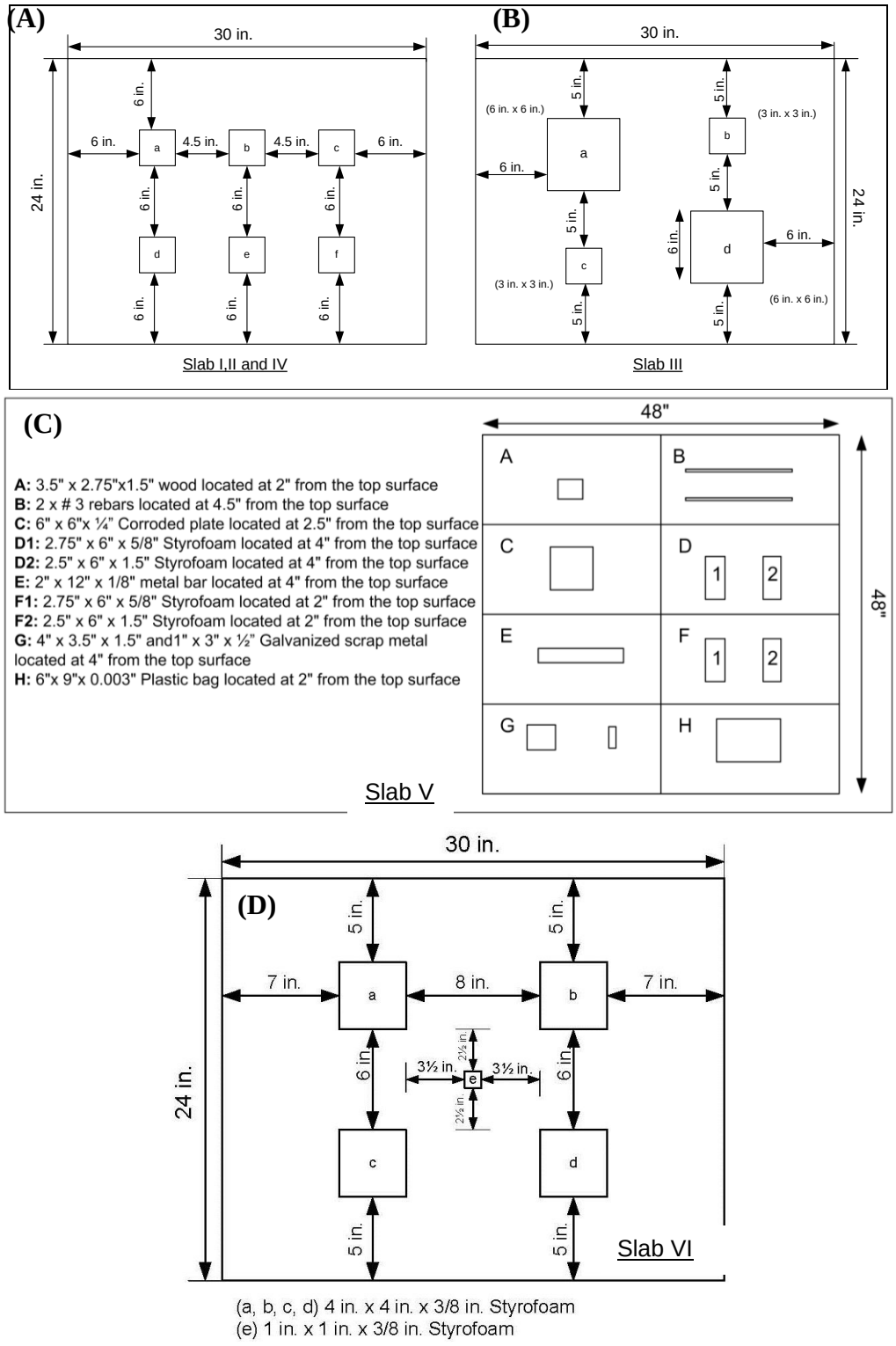

Figure 6-1: Plan Layout of Simulated Delaminations for (A) Test Slabs I, II, and IV (B) Test Slab III (C) Test Slab V and (D) Test Slab VI.

Test specimen III was constructed using Styrofoam blocks of different sizes. Simulated delaminations (a) and (d) in the plan layout for Slab III (Figure 6-1 (B)) have dimensions of 6 in. x 6 in. x 3/8 in. while delaminations (b) and (c) have dimension of 3 in. x 3 in. x 3/8 in. These sizes were selected to investigate the effects of delamination size and depth on defect detection using active IR thermography.

Slab V (shown in Figure 6-1 (C)) has larger dimensions than other test slabs. Simulated delaminations of different materials were placed in this slab for previously conducted passive infrared thermography studies (Vaghefi et al. 2011). In the current study, delaminations F1 and F2, composed of Styrofoam, were considered for investigation using active IR thermography. The impact of several test parameters including heat impulse duration, heater distance, and heater element type on the thermal contrast between delaminations and sound concrete in thermal images were investigated using Test Slab VI. This test slab is 24 in. by 30 in. by 5.5 in. and contains four 4 in. x 4 in. x 3/8 in. Styrofoam blocks and one 1 in. x 1 in. x 3/8 in. block. The blocks were positioned in the specimens using the same procedure as described for test slabs I-V at a depth of 1.5 in. from the concrete surface.

6.2.2 FLIR SC640 Thermal Imaging Camera

A FLIR ThermaCAM SC640 thermal infrared camera was used during laboratory experiments to capture temperature data on the surface of concrete specimens. This camera has a 640 x 480 pixel display with a 24^o x 18^o field of view and a temperature resolution of 0.1 ^oF. An external visual display allows for a real time image display and the alignment of test subjects. The camera was operated using ThermaCAM Researcher Professional software from a laptop computer. Several parameters, including ambient temperature, relative humidity, and emissivity, were used as inputs to the camera software prior to each test to compensate for the material properties of concrete as well as the amount of radiation reflected by the concrete surface and absorbed into the atmosphere. Images were recorded every 30 seconds to ensure that small, incremental changes in thermal contrast between delaminated areas and sound concrete were captured.

6.2.3 Heat Source

A 1500W electric Solaira infrared patio heater was selected as a viable heat source for laboratory tests based on a literature review of heat sources for active IR thermography testing on concrete elements (Vaghefi and Ahlborn 2013). Selecting a heating source is highly dependent on the thermal output desired and the depth of flaws including delaminations. In general, heat sources with a lower thermal output are effective for detecting subsurface flaws closer to the surface. Deeper defects require a higher thermal output heat source for detection. Selecting the heat source for an active IR thermography test also depends on the heating method selected for testing. Table 6-2 summarizes heating parameters and applications in previous literature.

Table 6-2: Heating Methods and Parameters for Different Applications in Civil Engineering.

Heater	*Power (W)*	*Power (Btu/hr)*	*Distance*	*Heating Duration (sec)*	*Application*	*Area*	*Source*
Six halogen flood lights	3200	11000	NA	NA	Voids in Concrete Slab	4 ft x 4 ft (1.2 m x 1.2 m)	(Abdel-Qader et al. 2008)
Three infrared radiator (moving along the surface)	3x2400	3x8200	6 in. (15 cm)	300, 900 , 2700	Voids in Concrete Slab	60 in. x 60 in. (1.5 m x 1.5 m)	(Maierhofer et al. 2002)
Two 250 W infrared heating lamps (200mm)	500	1710	13 in. (33 cm) 2 in. (50 mm)	10	CFRP laminates	24 in. x 9.84 in. x 1.77 in. (610 mm x 250 mm x 45 mm)	(Starnes et al. 2003)
Quartz lamp (laminate FRP)	500	1710	6 in. (152 mm)	NA	FRP laminates	3 ft^2 (0.29 m2)	(Levar and Hamilton 2003)
Kerosene heater (larger area - Fabric FRP)	22000	75000	6 in. (152 mm)	NA	FRP laminates	3 ft^2 (0.29 m2)	(Levar and Hamilton 2003)
Quartz heater	1500	5200	NA	NA	Existing RC bridge pier	NA	(Halabe et al. 2012)
Fan heater	2000	6800	NA	<300	Voids in Concrete Slab	<10.76 ft^2 (<1 m^2)	(Arndt 2010)
Halogen lamp	2x650	2x2200	NA	3	FRP delaminations	6.73 ft^2 (0.625 m^2)	(Arndt 2010)
Flash light	2x1500	2x5200	NA	0.10	FRP delaminations	6.73 ft^2 (0.625 m^2)	(Arndt 2010)
Xenon arc lamp	6000	21000	18.7 ft (5.7 m)	950	Elevated concrete bridge FRP delamination	90.4 ft^2 (8.4 m^2)	(Kurita et al. 2009)
Flash light	2 x 500	2 x 1710	7.9 in. (20 cm)	50ms	FRP composite system	72 in^2 (464.5 cm^2)	(Brown and Hamilton 2007)
Scan (line heating)	2 x 500	2x 1710	3 in. (7.6 cm)	12	FRP composite system	288 in^2 (1858 cm^2)	(Brown and Hamilton 2007)
Long pulse (flash lights)	2 x 500	2x 1710	7.25 in. (18 cm)	30	FRP composite system	432 in^2 (2787 cm^2)	(Brown and Hamilton 2007)
Long pulse (flash lights)	2 x 500	2x 1710	7.25 in. (18 cm)	60	FRP composite system	432 in^2 (2787 cm^2)	(Brown and Hamilton 2007)

NA – Information is not available in the literature.

Providing a relatively uniform heat across the concrete specimen surface and a heat impulse capable of creating visible contrast between subsurface defects and sound concrete in thermal images, the Solaira heater is compact in size, portable, and lightweight. Measuring 9 in. x 16 in. x 6 in. and weighing 7.5 lbs., this heater can be easily repositioned for testing concrete specimens in the laboratory. With the ability to heat relatively large areas of concrete at once compared to other heating techniques, this heater has the potential to be used for field applications of active IR thermography on structural concrete bridge elements.

6.2.4 Laboratory Test Set-Up and Data Collection

All laboratory testing of concrete specimens was conducted indoors at the Cement and Concrete Research Laboratory on the campus of Michigan Technological University in Houghton, Michigan. Each of the test specimens were specifically designed and constructed with simulated delaminations to investigate the feasibility of using active IR thermography to detect delaminations at different depths and sizes. The specimens were positioned horizontally on wooden shipping pallets level to the ground for testing. Before testing began, several environmental variables including the ambient temperature and humidity were measured using a handheld thermo-hygrometer, recorded for future reference, and used as input parameters to the ThermaCAM Researcher computer software used to record data throughout experiments. Because all objects absorb and emit different amounts of radiation, another important input parameter to the ThermaCAM software that accounts for material properties of concrete and allows for acquisition of accurate surface temperature data is emissivity. Emissivity describes the effectiveness of an object to emit energy as radiant temperature and can vary over the concrete surface due to the type and distribution of aggregate or the amount of moisture present from precipitation and condensation. A value of 0.95 was estimated for this material property and was considered sufficient for the purpose of detecting subsurface anomalies as the relative temperature difference between delaminations and sound concrete is most important for delamination detection and analysis methods in this study (Vaghefi 2013).

Providing a heat impulse to the surface of the concrete specimens, the infrared heater was positioned above the concrete specimens at a distance of 3.5 ft. This distance was selected to ensure that the heat impulse delivered to the test specimens was capable of producing detectable contrast between delaminations and sound concrete in thermal infrared images over a short period of time (Vaghefi 2013). The heater was positioned parallel to the concrete surface to achieve uniform heating of the test specimens and was suspended from two support arms by means of bungee cords. The support arms were clamped to two tripods positioned on either side of the slab specimens. Counter weights were used on the support arms to balance the weight of the heater over the center of the tripod.

To record changes in the surface temperature of the concrete test specimens, the FLIR was positioned at a distance of 6 ft. above the same surface of the test specimen as the heater. The camera was tripod mounted and adjusted to best capture the entire area of the specimen surface. The tripod supporting the FLIR SC640 was secured to a wood support structure constructed on

top of a wheeled cart to allow for camera repositioning. A camera angle of approximately 20^{o} to 30^{o} from vertical was used to ensure the image of the heater was not captured. This relatively small angle was necessary to analyze the relative shapes, locations, and depths of the simulated delaminations. Figure 6-2 shows the laboratory experimental set-up.

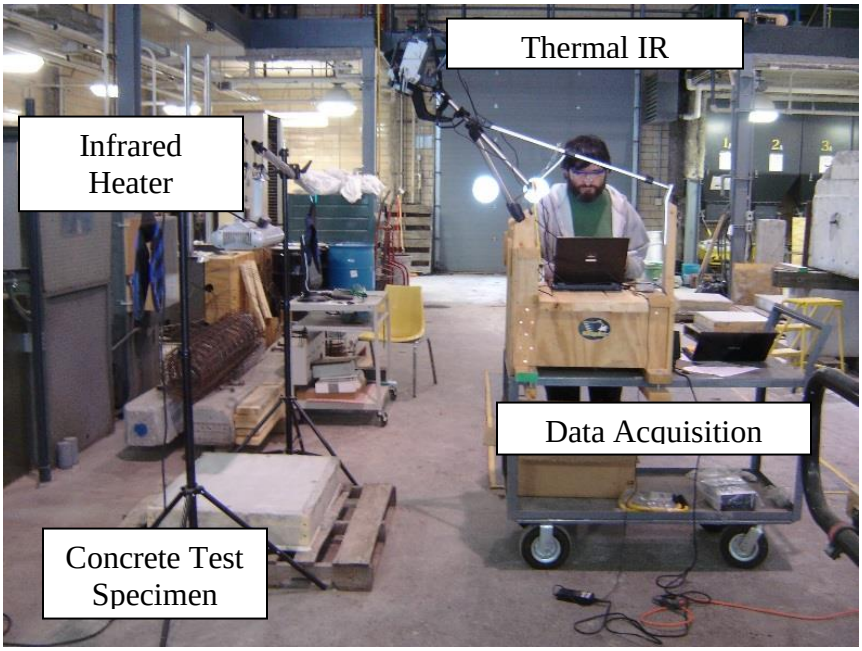

Figure 6-2: Experimental Laboratory Set-Up.

For each experimental test, data collection began immediately as the heater was turned on. After the heating period, the heater was turned off and remained in position over the specimen surface. Data collection continued for an additional period of time to ensure a majority of the heat impulse had dissipated throughout the concrete specimen and little to no thermal contrast between simulated delaminations and sound concrete could be seen in the external display of the FLIR SC640 thermal camera.

6.2.5 Thermal Imaging Analysis

Upon completion of laboratory experiments, thermal images from the test specimens were compiled and analyzed. Based on the visible temperature contrast between subsurface defects and surrounding areas of sound concrete in thermal images throughout the temporal sequence, the simulated delaminations were subjectively located. The following sections describe the analysis process to predict the depth of delaminations using estimated observation times from absolute contrast graphs.

6.2.5.1 Absolute Contrast

The absolute contrast of a defected area at a particular time ($\Delta T(t)$) is defined as the relative temperature change between the surface temperature above a suspected defected area ($T_{def}(t)$) and the surface temperature of a reference background area ($T_s(t)$) on a thermal IR image (Maldague 2001).

$$\Delta T(t) = T_{def}(t) - T_s(t) \qquad \text{Equation 6-1}$$

Two different methods can be used to calculate the absolute contrast in a single infrared image: (1) consider the surface temperature difference of a single pixel above the suspected delamination and a single pixel above the background area or (2) consider the average surface temperature within the boundaries of an area above the suspected defect and above a selected background reference area close to the suspected defect (Vaghefi 2013). The second method has been proven to be more effective as it diminishes the variability in selecting only one point in the background (Brown and Hamilton 2007). Therefore, the average temperatures within the suspected defective area and the reference background area were considered for monitoring the absolute contrast of areas of delaminations (Vaghefi 2013).

The representative area above a simulated defect was selected throughout all laboratory experiments using subjective interpretation based on the size and shape of the simulated delaminations and on the visible areas of temperature contrast between suspected delamination and areas of sound concrete in the thermal infrared images (Vaghefi and Ahlborn 2013). It should be noted that the intention of the bounded area above the defect is to calculate absolute contrast with respect to the reference background area and is not necessarily an accurate representation of the actual size of the subsurface defect. The background reference area for each individual delamination can also be located subjectively, however, for this study, the reference area was defined as a rectangular box-shape around each delaminated area with a thickness of 5 pixels. This shape was chosen to account for non-uniform heating patterns across the concrete surface. Once the delaminated area and background reference area were selected, Equation 1 was used to construct an absolute contrast graph. Figure 6-3 shows the background reference area configuration on a thermal infrared image taken 6.5 minutes after the heater was turned off during one of the laboratory tests. The figure was produced in Matlab using data obtained from the ThermaCAM software. “Ref” indicates the background reference area (sound concrete) close to the delamination that was considered for determining the temperature of the background and the absolute contrast of each delamination.

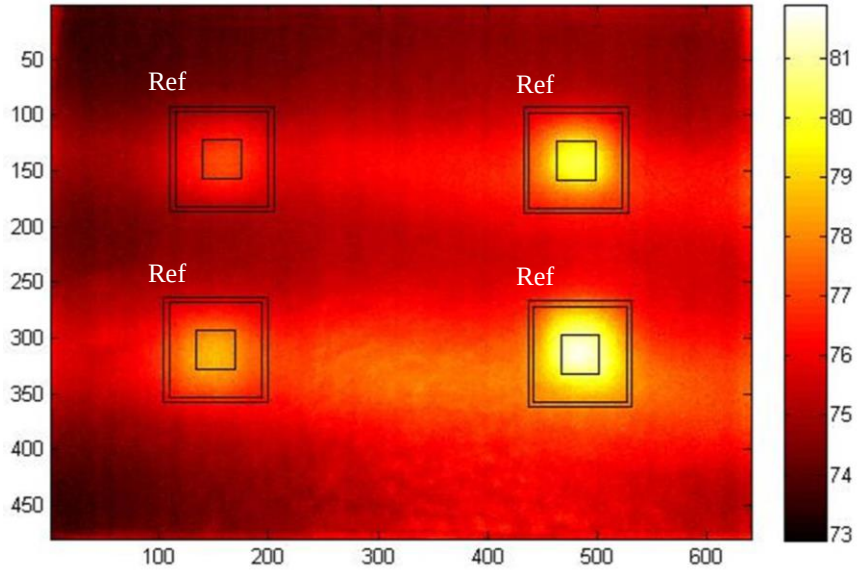

Figure 6-3: Selected Delamination Area and Background Reference Area for Slab VI used to Calculate Absolute Contrast.

Figure 6-4 shows the absolute contrast variation of delaminations for one of the laboratory experiments using a reference background. Absolute contrast graphs are obtained to determine the observation time of each simulated delamination and to estimate the depth of delaminations relative to one another based on the values of maximum absolute contrast. For example, from the graphs presented in Figure 6-4, it can be seen that delaminations (c) and (f) appeared with higher absolute contrast values than delaminations (a) and (d) and can therefore be estimated as deeper defects.

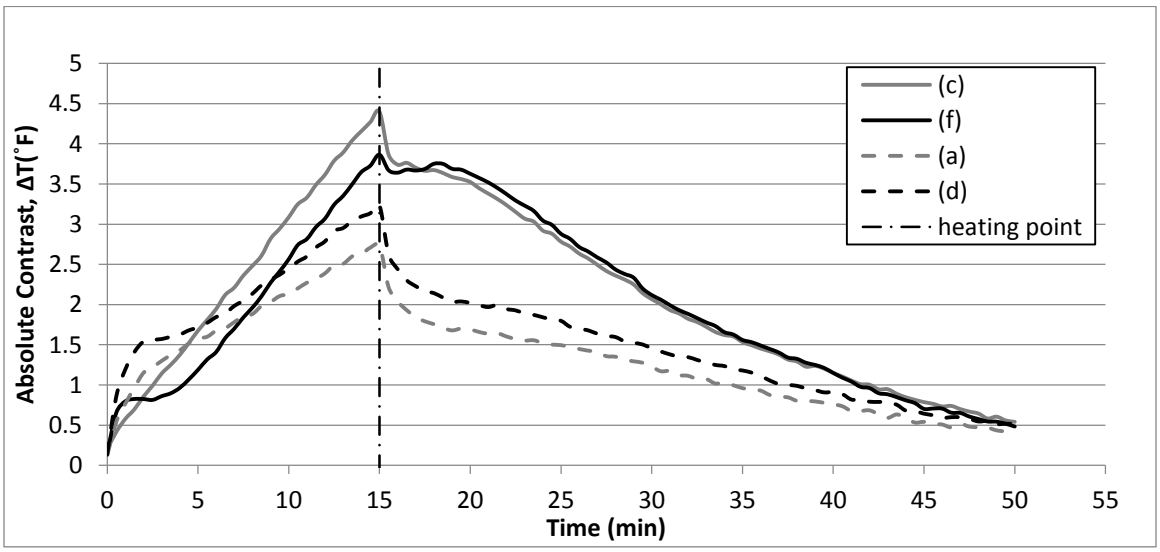

Figure 6-4: Absolute Contrast Variation above Simulated Delaminations for one of the Conducted Laboratory Tests.

6.2.5.2 Observation Time

Observation time is defined as the time at which delaminated areas appear on a thermal infrared image with the maximum absolute contrast after the heating period of active IR thermography or at the vertex of negative convexity of the absolute contrast variation graphs (Vaghefi 2013). Observation time is determined by monitoring the absolute contrast of each suspected delamination during both the heating and cooling periods of active IR testing. Because observation time is dependent on the interpretation of the absolute contrast graphs, the method of calculating absolute contrast and the subjective selection of defect areas and sound concrete background reference areas will have an effect on estimating this time step value (Vaghefi 2013). Figure 6-5 shows a diagram depicting the process of determining the observation time using an absolute contrast graph.

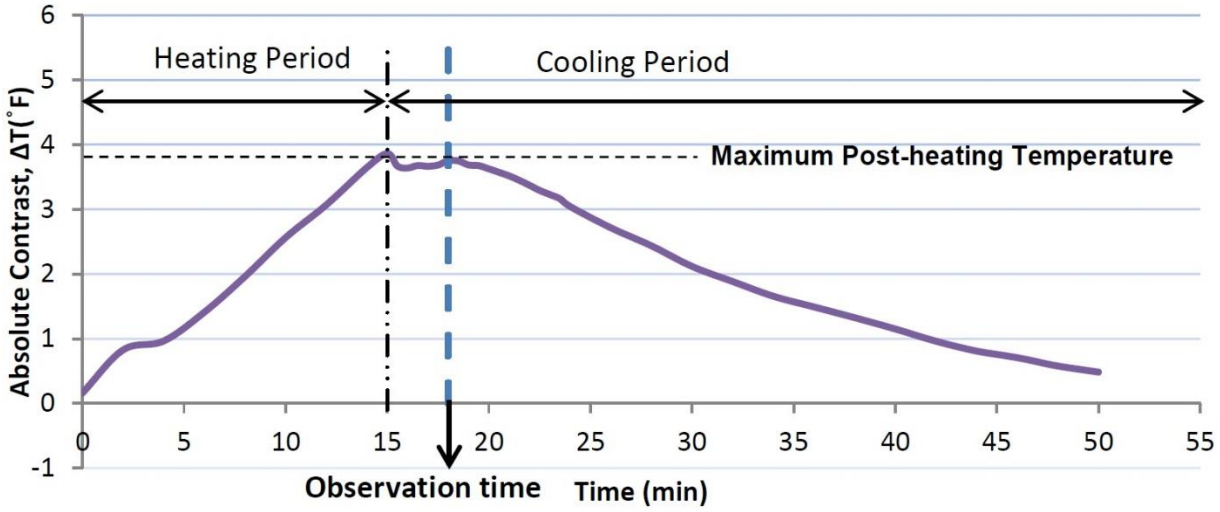

Figure 6-5: Definition of Observation Time Shown on an Absolute Contrast versus Time Graph Obtained from an Active IR Thermography Test.

6.2.5.3 Delamination Depth Computation

The theory of active IR thermography testing suggests that the depth of flaws and delaminations can be estimated using results obtained from monitoring the temperature change on the test specimen surface and determining the observation time of each delaminated layer (Maldague 1993). In general, during infrared thermography testing, deeper delaminations appear on the thermal infrared images with less contrast to surrounding sound concrete than shallower delaminations. The relationship between observation time and depth is shown in Equation 6-2 and was proven previously to be valid for estimating the depth of the delaminations in concrete slabs (Vaghefi 2013).

$$t \approx \frac{z^2}{\delta} \qquad \text{Equation 6-2}$$

where, t is the observation time, z is the defect depth, and δ is thermal diffusivity of the material as defined by Equation 6-3.

$$\delta = \frac{K}{\rho C} \quad \text{Equation 6-3}$$

where K is thermal conductivity, ρ is material density and C is thermal capacity or material specific heat (Maldague 1993; Ghosh and Karbhari 2006). Thermal diffusivity of concrete depends on the type of the coarse aggregate used in concrete. The general range of thermal diffusivity of concrete is between 0.016 ft^2/h (for expanded shale aggregate) and 0.085 ft^2/h (for quartz aggregate) (Lamond and Pielert 2006).

6.2.5.4 Relationship between the observation time and the depth of delamination

According to Equation 2, observation time (t) has a quadratic relationship with the depth of the defect (z). To discuss and prove the relationship between the observation time and the depth of the defect, the observation time for each delamination was plotted against the square of the delamination depth obtained from ground truth information. A linear regression line was then drawn to obtain the accuracy of the relationship between t and z^2 and estimate the thermal diffusivity for the concrete laboratory test specimens.

6.3 Results of Laboratory Experiments

Laboratory experiments were conducted for this study to prove the concept of active IR thermography applied to concrete specimens prior to field applications of this non-destructive remote sensing technology. Thermal contrast between subsurface anomalies and sound concrete in thermal images was used to investigate the accuracy of Equation 2 for test slabs I-V. The relationship between delamination size and depth to absolute contrast was also investigated for these test slabs. In addition, a parametric study was conducted on test specimen VI to investigate the effects of the heat impulse duration, heater distance, and heater element type on the thermal contrast between delaminations and sound concrete in thermal images. The concrete test specimens and results from each laboratory experiment are described in the following sections. For a more in-depth discussion regarding delamination depth estimation using absolute contrast please reference Khatera Vaghefi's dissertation work (Vaghefi 2013).

6.3.1 Delamination Depth and Delamination Width to Depth Ratio

Laboratory tests conducted on concrete specimens I-V emphasized delamination depth analysis procedures using absolute contrast graphs constructed from thermal IR data. In addition, the ratio of the delamination depth to the delamination radius (width) was observed to determine the dimensions and depth at which delaminations are no longer detectable using the described analysis methods.

6.3.1.1 Measured Depth of Delaminations

To validate the testing results and obtain the relationship between the depth of delaminations and observation times, 4 in. diameter cores were extracted at the locations of simulated delaminations upon completion of active IR thermography testing on concrete Slabs I-V. A summary of the measured depths of the Styrofoam blocks and the width-to-depth ratios for each simulated delamination in test slabs I-V are provided in Table 6-2. Depth of the Styrofoam block was measured from the top surface of the core (concrete slab) to the top surface of the Styrofoam layer using a micrometer with a 0.01 in. resolution.

Table 6-2: Measured Depth of Simulated Delaminations and Width-to-Depth Ratio Obtained from the Extracted Cores of Test Slabs I-V.

Core No.	*Measured Depth Determined by coring (in.)*	*Width-to-Depth Ratio*	*Core No.*	*Measured Depth Determined by coring (in.)*	*Width-to-Depth Ratio*
Slab I-a	1.04 *	2.89 **	Slab III-a	1.92*	3.12**
Slab I-b	2.20	1.36	Slab III-b	2.96	1.01
Slab I-c	0.72 *	4.16**	Slab III-c	1.37*	2.19**
Slab I-d	1.14*	2.64**	Slab III-d	3.18	1.89
Slab I-e	2.13	1.41	Slab IV-a	1.81*	1.66
Slab I-f	0.75*	3.98**	Slab IV-b	1.03*	2.91**
Slab II-a	2.72	1.10	Slab IV-c	1.46*	2.06**
Slab II-b	3.34	0.90	Slab IV-d	2.36	1.27
Slab II-c	2.95	1.02	Slab IV-e	2.15	1.39
Slab II-d	1.27*	2.36**	Slab IV-f	1.92*	1.57
Slab II-e	2.37	1.27	Slab V-F2	0.33*	7.66**
Slab II-f	2.43	1.24	Slab V-F1	0.89*	3.10**

*depth (z) < 2 in.
** width/depth (R) > 2

6.3.1.2 Data Collection and Procedure

Thermal infrared images were collected from test Slabs I-V using the surface heating method during a 50 minute test period which included a 15 minute heat time and a 35 minute cooling period. Table 6-3 summarizes the environmental conditions that were used as inputs in the ThermaCAM computer software for data collection.

Table 6-3: Environmental Conditions for Active IR Testing on Concrete Slabs I-V.

Test Specimen	*Humidity (%)*	*Ambient Temperature (˚F)*
Slab I	14.1%	72.3˚F
Slab II	37%	73˚F
Slab III	32%	75˚F
Slab IV	51%	76.2˚F
Slab V	19.2%	67.8˚F

6.3.1.3 Results and Analysis

Upon completion of active IR thermography testing on test slabs I-V, areas of suspected delamination and background reference areas were identified. Figure 6-6 shows the selected delamination areas and background reference areas for test slabs V and III. The dimensions, given in pixels, of the selected areas are also shown on the figure.

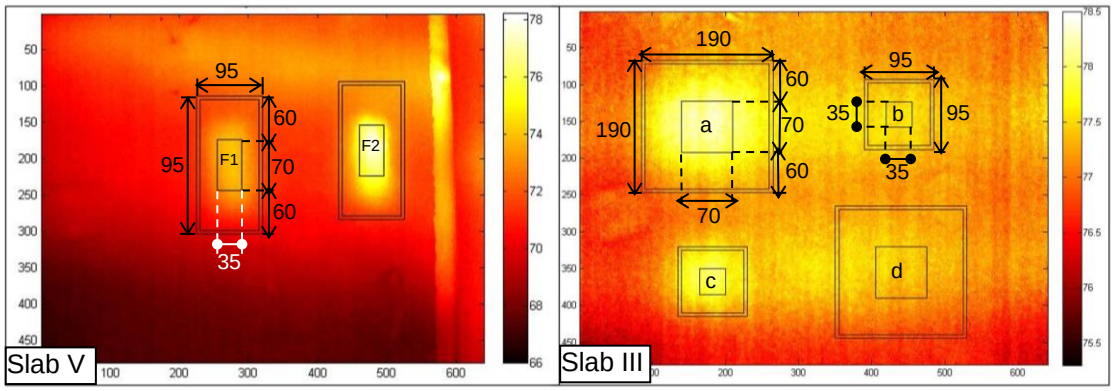

Figure 6-6: Boundaries Selected for Areas of Delamination and the Associated Background Reference Areas for Concrete Test Slabs V and III.

Average temperature within the selected areas was monitored over both the heating and cooling periods at 30 second intervals, and absolute contrast between the suspected delaminated area and reference background was determined and plotted. Figure 6-7 shows the absolute contrast of delaminated areas that were apparent on thermal infrared images collected from each slab. The depth of the delamination presented on the plots indicates the measured depth of the delaminations obtained by coring. From the absolute contrast graphs in Figure 6-7, observation time was estimated for the eleven simulated delaminations that were apparent in the recorded thermal images. The estimated observation times are presented in Table 6-4.

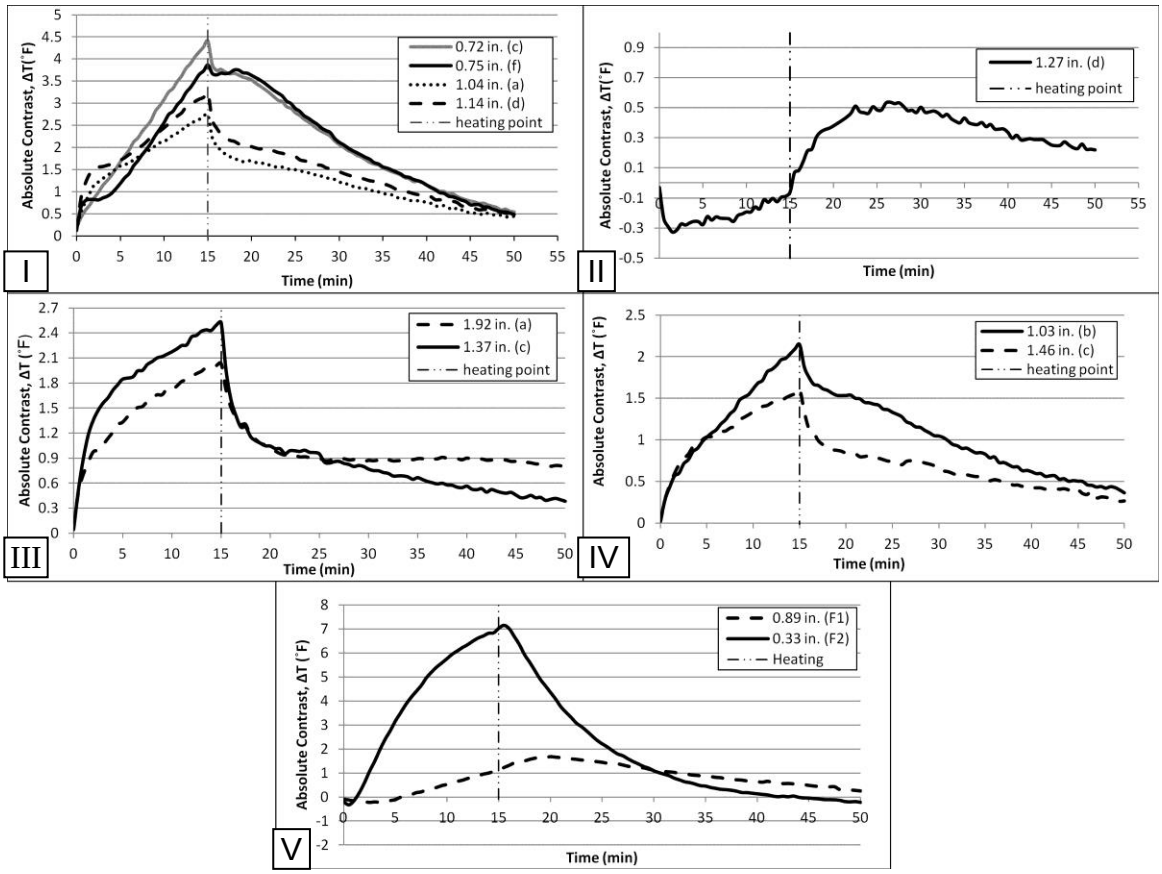

Figure 6-7: Absolute Contrast Variation above each Simulated Delamination during Active IR Thermography Testing on Test Slabs I-V.

Table 6-4: Observation Time and Corresponding Absolute Contrast for each Suspected Area of Delamination, Obtained from the Absolute Contrast Variation Plots.

Delamination No. (Depth)	*Observation time (min)*	*Corresponding Absolute Contrast (˚F)*
I-a (1.04 in)	4.5	1.7
I-c (0.72 in)	1.0	3.74
I-d (1.14 in.)	6.5	2.03
I-f (0.75 in.)	3.0	3.75
II-d (1.27 in.)	7.5	0.51
III-a (1.92 in.)	12.5	0.89
III-c (1.37 in.)	8.5	0.99
IV-b (1.03 in.)	5.5	1.54
IV-c (1.46 in.)	12.0	0.75
V-F2 (0.33 in.)	0.5	7.16
V-F1 (0.89 in.)	5.0	1.68

6.3.1.4 Discussion

To develop the relationship between the depth and the observation time of each simulated delamination, observation time for each simulated delamination was plotted against the square of the measured depth. The linear regression line was drawn to confirm the linear relationship between t and z^2 and the square of the correlation coefficient (R^2) was determined to be 0.896 (Figure 6-8).

Although, different mixes were used for the construction of the five slabs, the aggregate type for all these slabs were similar and were according to the Michigan Department of Transportation (MDOT) Standard Specification for Construction (MDOT 2003). Thus, an approximate value for the thermal diffusivity was estimated based on the results of the active IR thermography test on the concrete test slabs. From the linear regression equation, thermal diffusivity can be estimated as 0.2219 in^2/min (0.092 ft^2/h), which is approximately the thermal diffusivity for concrete containing quartz aggregate (0.085 ft^2/h).

The linear regression equation obtained from the data set presented in Figure 6-8 proves that observation time is a function of the square of the depth in the first approximation. Thus, the relationship defined in Equation 2 is a valid relationship for concrete material, and the depth of delaminations can be estimated based on the observation time of each delaminated area. One unexpected variable within the presented experiment was the air content of each test slab which is reported in Table 6-1 and again in Figure 6-8. Further investigations were conducted regarding the effect of concrete air content on delamination observation time which are beyond the scope of this study. For more information about concrete air content considerations for determining observation time, please reference Khatereh Vaghefi's thesis work entitled "Infrared Thermography Enhancements for Concrete Bridge Evaluation" (Vaghefi 2013).

From the results of the active IR thermography testing, it can be seen that the observation time for delaminations appeared between 0 and 12.5 minutes after the heat source was turned off. This observed time period can help in identifying the time at which thermal infrared images should be captured to obtain the vertex of negative convexity on the thermal infrared images, specifically in situations where location and size of the delamination are of interest rather than the depth of the delamination. Note that the time period determined from the results of this study is specific to the heat source and the selected distance between the concrete slab surface and the heat source (3.5 ft). Additional studies must be conducted to generalized the relationship between the observation time period, heater, heater distance, and diffusivity of the concrete.

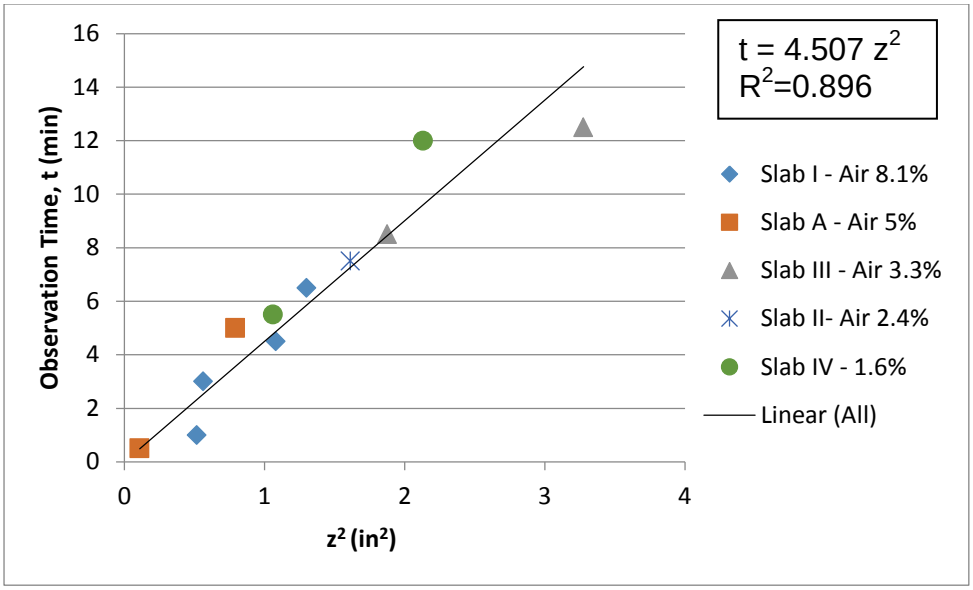

Figure 6-8: Observation Time Versus the Square of the Depth of each Detected in Active IR Thermography Testing of Test Slabs I-V.

Another important observation from the results of active IR thermography testing on concrete slabs I-V is that only delaminations with a depth less than or equal to 2 in. and with a width-to-depth ratio greater than 2 were detected using the current test method, equipment and analysis method. Delaminations with a depth of less than 2 in. are shown with one asterisk in Table 6-2 and delaminations with a width-to-depth ratio (*R*) value greater than 2 are shown with two asterisks. Results show that delaminations can only be detected when both limits are satisfied. For example, delamination "a" in Slab IV was located 1.81 in. from the top concrete surface but had a width to depth ratio of less than 2, thus it was not detected during the active IR thermography testing. The effects of delamination size and width-to-depth ratio on detecting subsurface defects in concrete is in agreement with the previously discussed empirical rule for infrared thermography (Maldague 1993). Further investigations regarding heater output and distance from the concrete specimen of interest should be conducted to determine the possibility of detecting delaminations at greater depths.

6.3.1.5 Conclusions

Results from laboratory testing on concrete test Slabs I-V provide evidence to verify the capabilities of pulsed (active) infrared thermography to predict the location and estimate the depth of delaminations in concrete bridge elements. Data confirms the linear relationship between the square of the depth and observation time for subsurface defects suggesting that the observation time is generally between 0 and 5 minutes for delaminations with a depth less than 1 in. and between 5 and 20 minutes for delaminations with a depth between 1 and 2 in. In addition, results from active IR thermography testing contribute additional evidence supporting the capabilities of this remote sensing technology to detect delaminations shallower than 2 in. deep and with a width-to-depth ratio greater than 2. Further study is required to investigate the

maximum depth and the minimum width-to-depth ratio at which delaminations can be detected using active IR thermography. The methodology of estimating depth from the results of an active IR test on concrete specimens and the discussion about the effects of the width-to-depth ratio in detecting delamination has introduced a method of infrared thermography data interpretation that serves as a base for future studies.

The laboratory study conducted on test specimens I-V was limited by the specific distances between the camera, the test specimen and the heat source. Heating sources with higher heating output and various distances between the heat source and the concrete test specimens should be further investigated to identify the most suitable heat source for field applications, and the practical distance between the heat source and concrete surface for accurate delamination detection.

Recognizing that all laboratory tests were conducted indoors, one of the major concerns for applying active IR thermography in the field is the possible conflicts between ambient temperature change caused by heating effects of the sun and the use of an external heating source to create the necessary temperature gradient for active IR thermography testing. Depth prediction and size determination of subsurface defects should be further investigated while exploring the influence of environmental conditions.

6.3.2 Parametric Study 1: Heat Impulse Duration

The objective of parametric study 1 conducted on concrete specimen VI was to investigate the effects of shortening the thermal impulse duration on the thermal contrast of simulated delaminations and determine the feasibility of shorter inspection times on the bridge deck underside and fascia beams. Heat times of 5 minutes and 10 minutes were investigated and compared to the results of a control test using a 15 minute heat time. All other testing variables remained constant throughout the experiment. However, for the purpose of improving equipment positioning capabilities, reducing experimental set-up time and the ease of equipment transport for future field applications, two mounting systems were custom fabricated for the FLIR SC640 thermal camera and infrared heater. The mounting systems were constructed using aluminum square tubing and were supported by collapsible tripods. Counter weights were used to balance the weight of the test equipment. The new mounting systems allowed for greater versatility in positioning the equipment for testing concrete elements in different orientations.

Two laboratory tests were conducted on concrete specimen VI using the aforementioned methodology and heat impulse durations less than 15 minutes. For each test, data collection began immediately as the heater was turned on and continued for a total of 60 minutes to ensure that a majority of the heat impulse dissipated through the concrete specimen and little to no thermal contrast could be seen between delaminated areas and areas of sound concrete in thermal images. The environmental conditions measured prior to testing and included as inputs to the ThermaCAM computer software are summarized in Table 6-5.

Table 6-5: Environmental Conditions for Active IR Testing on Concrete Slab VI for Heat Time Investigation.

Heat Impulse Duration (min)	*Humidity (%)*	*Ambient Temperature (^{o}F)*
5	5.9	72.3
10	25.5	65.6
15	6.6	72.5

6.3.2.1 Results and Analysis

Areas of suspected delamination and sound concrete background reference areas were selected upon completion of active IR thermography testing on test slab VI using shortened heat times. These areas were monitored throughout the testing period and absolute contrast graphs were constructed. Results from the 5 minute and 10 minute tests were then compared to the 15 minute control test. Thermal images obtained from laboratory testing and the analysis areas selected for Delamination 4 can be seen in Figure 6-9. The absolute contrast graphs for each of the four simulated delaminations are shown in Figure 6-10 for the 5 minute, 10 minute and 15 minute tests. After construction of the absolute contrast figures, observation times were estimated for each delamination. The estimated observation times are reported in Table 6-6.

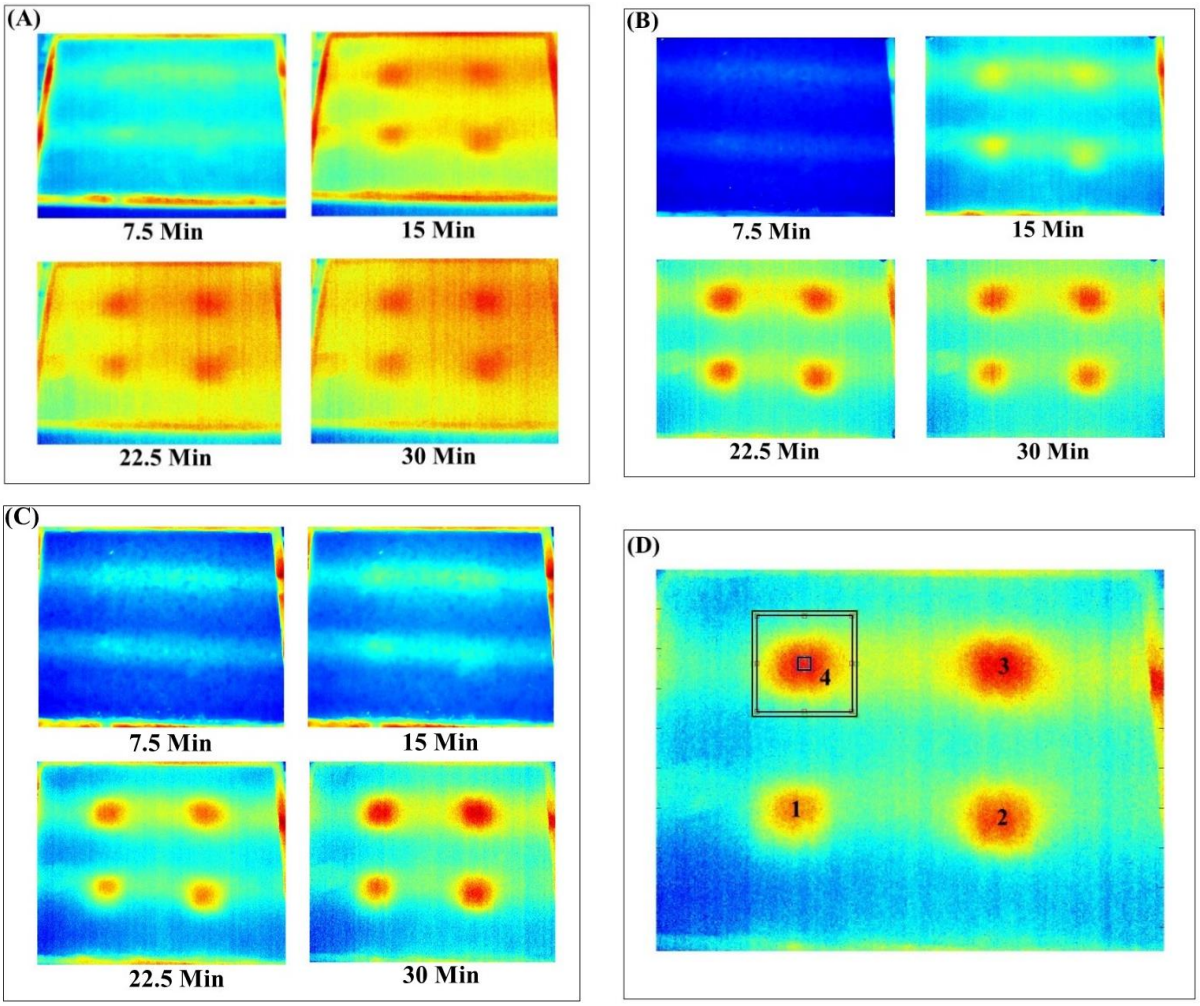

Figure 6-9: Thermal Images Captured during Parametric Experiment 1 (A) 5 Min. Heat Impulse (B) 10 Min. Heat Impulse (C) 15 Min. Heat Impulse Control Test (D) Delamination Numbering System and Selected Areas for Analysis for Delamination 4.

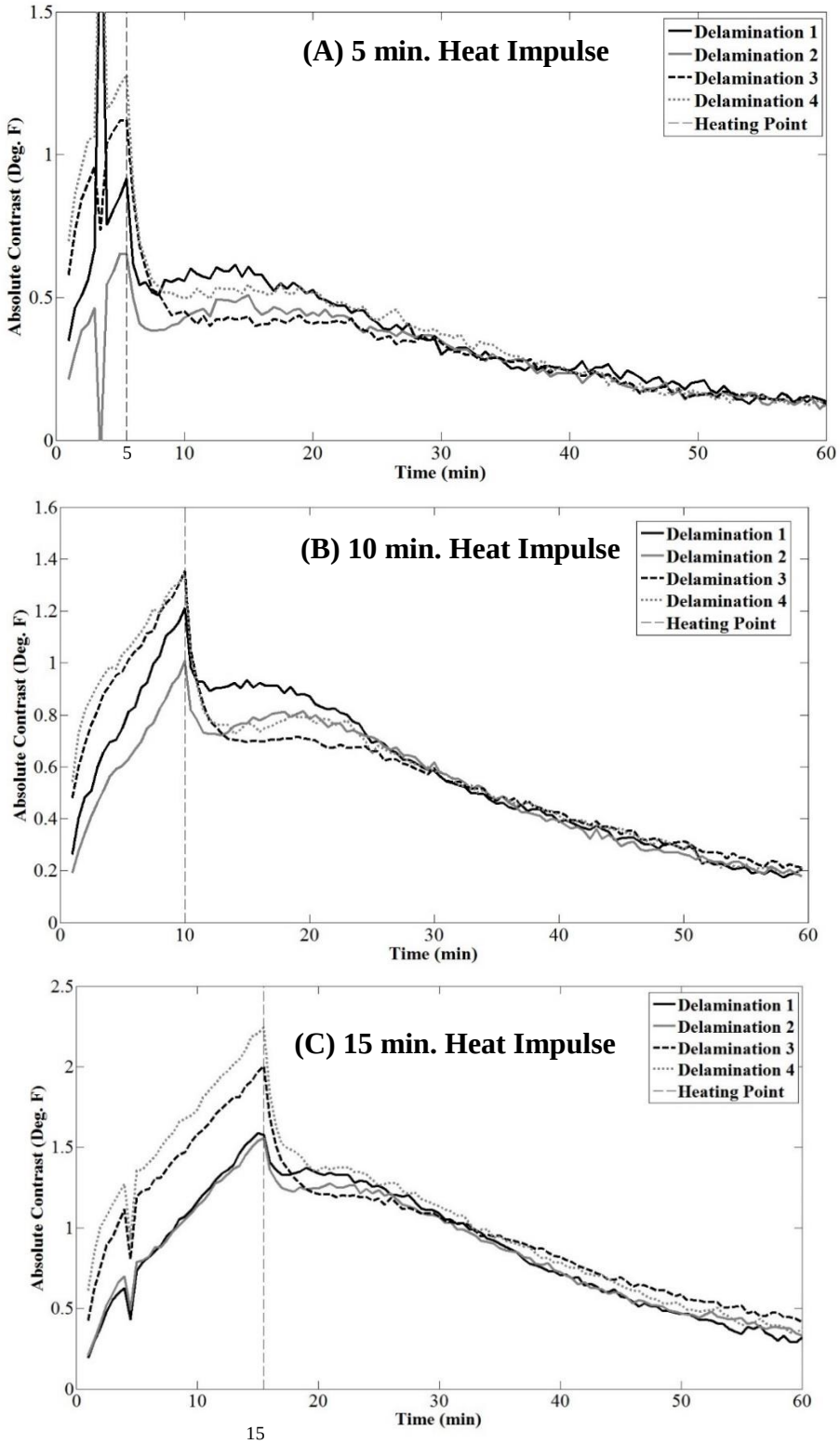

15

Figure 6-10: Absolute Contrast Graphs Constructed from Heat Impulse Durations of (A) 5 Minutes (B) 10 Minutes and (C) 15 Minutes

Table 6-6: Estimated Observation Times and Corresponding Absolute Contrast for Simulated Delaminations in Concrete Test Slab VI Tested with Different Heat Impulse Durations.

Heat Impulse Duration (min)	*Delamination Number*	*Observation Time (min)*	*Corresponding Absolute Contrast (^{o}F)*
5	1	9.0	0.6
	2	10.0	0.5
	3	18.0	0.4
	4	19.0	0.5
10	1	10.0	0.9
	2	9.5	0.8
	3	14.5	0.7
	4	8.5	0.8
15	1	4.0	1.4
	2	7.0	1.3
	3	11.0	1.2
	4	8.5	1.3

6.3.2.2 Discussion and Conclusions

Results from active IR tests conducted on concrete specimen VI show that changing the duration of the thermal impulse directly affects the thermal contrast between areas of suspected delamination and areas of sound concrete. Decreasing the heat impulse duration from a control test of 15 minutes to 5 minutes and 10 minutes resulted in less thermal contrast between simulated delaminations and surrounding areas of intact concrete. The acquired thermal images and absolute contrast graphs also show that delaminations appear sooner in the thermal temporal sequence when exposed to shortened impulse durations than longer heat times. During active IR testing, delaminations do not become visible in thermal images until after the heating phase when the heater is turned off or removed from the vicinity of the test area. Therefore, changing the duration of the heat impulse also changes the observation time period at which delaminations appear with maximum contrast to surrounding areas of concrete.

It should be noted that the 1 in. x 1 in. simulated delamination located in the center of test slab VI did not appear in any of the active IR thermography tests conducted to investigate heat impulse duration. With a width-to-depth ratio of less than two, it was expected that this Styrofoam block would not be detected using current analysis procedures based on the findings of previous laboratory tests. Additional width-to-depth delamination studies are recommended using test slab VI, specifically with a focus on the 1 in. x 1 in. simulated delamination, for improvements in testing procedures to detect delaminations with a width-to-depth ratio less than two. It should also be noticed that thermal images collected in this experiment show a heat concentrated boarder around the test specimen. Test specimen VI was constructed using 2 x 4

wood framework which remains attached to the test slab. Due to the difference in emissivity between wood and concrete, the wood frame around this test slab appears at a different temperature in thermal images compared to concrete. These areas were avoided during the construction of absolute contrast graphs and illustrates the importance of understanding the correlation between emissivity and objects seen in thermal infrared images. For this reason, optical images are strongly recommended for field demonstrations to explain thermal anomalies.

Absolute contrast graphs in Figure 6-11 reveal absolute contrast spikes during the heating phase of the 15 minute and 5 minute tests. Although the interest of these graphs lies in the cooling phase and the distinct rise or vertex in absolute contrast to estimate observation time of delaminations, these temperature spikes must be addressed to explain experimental outlier data. The FLIR SC640 thermal camera contains an internal calibration shutter that triggers automatically to ensure accurate temperature readings based on initial calibrations from environmental conditions. As the camera captured images at a rate of two images per minute, the calibration shutter continued to trigger throughout the testing period and was captured in one of the thermal images. The shutter caused thermal distortion in the image and resulted in erroneous temperature readings. It is recommended that operators conducting active IR thermography testing in field applications be familiar with their thermal camera functions to explain unexpected variations in temperature readings.

Laboratory experiments investigating the effects of changing the thermal impulse duration on thermal contrast between areas of delamination and sound concrete areas has also led to the consideration of heater specifications and their influence on the selection of an appropriate thermal impulse duration. When selecting an impulse duration, one should consider both the power output of the heater as well as the time it takes for heater elements to reach maximum operating temperature. If a short impulse duration is selected for experimentation, the maximum power output of the heater may not contribute to the thermal contrast between delaminations and areas of sound concrete if the heater is not capable of reaching maximum operating temperature in that time period.

6.3.3 Parametric Study 2: Effect of Heating Elements on Thermal Banding

The objective of parametric study 2 conducted on concrete specimen VI was to confirm that thermal banding present in thermal images acquired from previous laboratory tests is a function of the selected heat source used for experimentation. In addition, results from this test were used to investigate the effects of thermal banding on analysis procedures used in the lab and to consider the impact of this phenomenon on analysis procedures used in the field. All testing variables described in section 6.3.2 remained constant throughout experimentation, including the 15 min. heating time, except the orientation of the infrared heater was rotated 90^{o} compared to the heater position of previous laboratory tests. Data collection began immediately as the heater was turned on and continued for a total of 30 minutes. The environmental conditions measured prior to testing and included as inputs to the ThermaCAM computer software are summarized in Table 6-7.

Table 6-7: Environmental Conditions for Active IR Testing on Concrete Slab VI for Thermal Banding Investigation.

Heat Orientation	*Humidity (%)*	*Ambient Temperature (^oF)*
Original Position	5.9	72.3
Rotate 90^o	24.6	66.9

6.3.3.1 Analysis and Results

To determine the effects of rotating the heater on thermal concentrations and banding on the specimen surface, visual analysis procedures were used upon completion of active IR thermography testing on concrete test Slab VI. Results were compared to the 15 min. heat time control test with the heater in its original test set-up position. Four thermal images captured from both the control test and rotated heater test are shown in Figure 6-11.

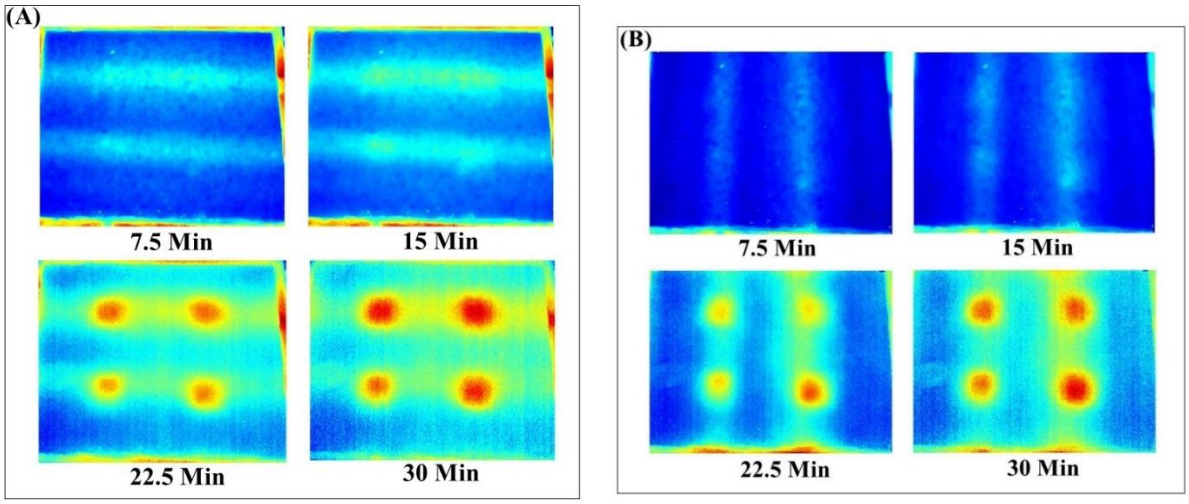

Figure 6-11: Thermal Images Captured during Parametric Study 2 (A) Control Test with Original Heater Position (B) Test with Rotated Heater Position.

6.3.3.2 Discussion and Conclusions

Rotating the infrared heat source 90^o and conducting an active IR test on concrete specimen VI confirms that thermal banding shown in thermal images is a function of the heater. The Solaira infrared patio heater used to deliver the heat impulse for laboratory experiments contains a single tube element and a curved reflective heater backing. The angled construction of the heater backing causes a concentration of infrared energy on either side of the heating element and results in two distinct thermal bands on the concrete surface after the heating period. Depending on the orientation of the heater, thermal bands appear differently in successive tests. Due to this

non-uniform heating phenomenon and the subjectivity of selecting representative areas of delamination and areas of sound concrete for analysis procedures, thermal banding has a direct impact on the absolute contrast between delaminations and sound concrete. However, delaminations are still identifiable.

A more uniform heating of the concrete surface may be achieved by using a different heat source. Heaters with multiple heating elements may provide a more distributed thermal impulse making areas of delamination and areas of sound concrete more distinguishable from each other in thermal images. In addition, increasing the distance of the heater from the concrete surface may decrease the effects of thermal banding and provide a more uniformly heated area. However, increasing the heater distance will likely decrease the absolute contrast between areas of delamination and areas of sound concrete for the same heating duration. Further investigations regarding the effects of heater distance on thermal banding and absolute contrast are recommended before field applications of active IR thermography using the presented test method. It should also be noted that heaters of different types will have different heating effects on the surface of the test area. It is especially important for operators conducting active IR thermography tests to understand the heating behavior of their specific heater and how it will effect analysis procedures.

6.3.4 Parametric Study 3: Heater Distance

The objective of parametric experiment 3 conducted on concrete specimen VI was to determine the effects of changing the distance between the infrared heat source and concrete specimen on the thermal contrast between areas of delamination and sound concrete to select an appropriate distance for field applications. A distance of 2 ft. between the infrared heater and concrete specimen surface was chosen and results were compared to a control test using a distance of 3.5 ft. All other testing variables remained constant as previously discussed in the test set-up section 6.3.2, including the 15 min. heating time. Data collection began immediately as the heater was turned on and continued for a total of 60 minutes to ensure that a majority of the heat impulse dissipated through the concrete specimen and little to no thermal contrast could be seen between delaminated areas and areas of sound concrete in thermal images. The environmental conditions measured prior to testing and included as inputs to the ThermaCAM computer software are summarized in Table 6-8.

Table 6-8: Environmental Conditions for Active IR Testing on Concrete Slab VI for Heat Distance Investigation.

Heat Distance from Specimen Surface **(ft)**	***Humidity*** **(%)**	***Ambient Temperature*** **(^{0}F)**
3.5	5.9	72.3
2	11.8	71.7

6.3.4.1 Analysis and Results

Upon completion of active IR thermography testing, areas of suspected delamination and sound concrete background reference areas were selected. These areas were monitored throughout the testing period and absolute contrast graphs were constructed. Results from the test were then compared to the control test with the heater positioned 3.5 ft. from the concrete surface. Thermal images obtained from laboratory testing and the representative areas selected for analysis are shown in Figure 6-12 and Figure 6-13 respectively. The absolute contrast graphs for each simulated delamination in concrete slab VI are shown in Figure 6-14 for the heater positioned 3.5 ft. and 2 ft from the specimen surface. After construction of the absolute contrast figures, observation times were estimated for each delamination and are reported in Table 6-9.

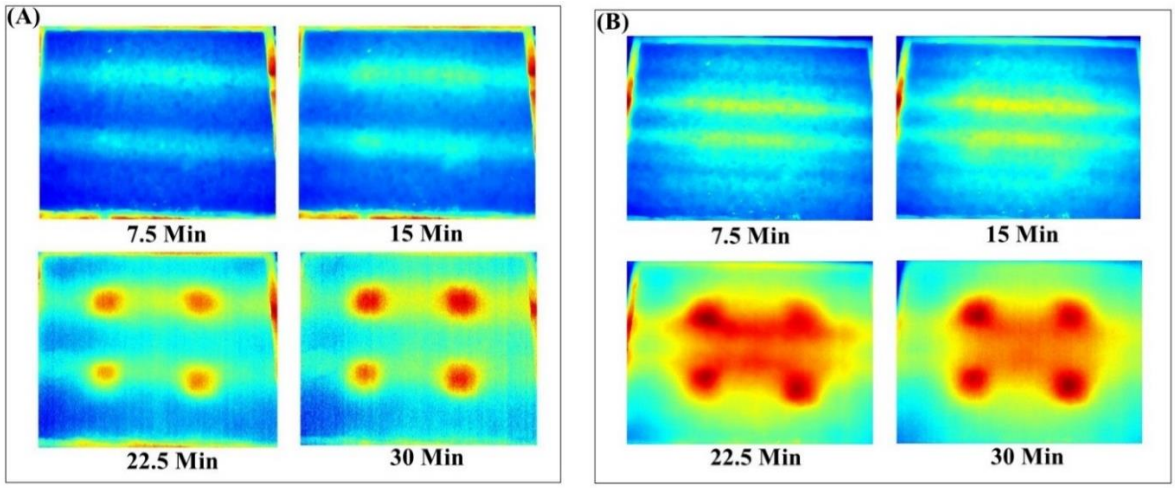

Figure 6-12: Thermal Images Captured During Parametric Experiment 3 (A) Control Test with Heater Placed 3.5 ft. from Test Specimen Surface (B) Heater Placed 2 ft. from Test Specimen Surface.

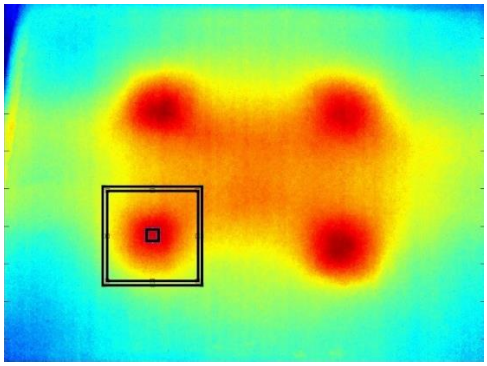

Figure 6-13: Selected Area of Suspected Delamination and Sound Concrete Area for the Active IR Test Conducted on Test Slab VI Using a 2 ft. Heater Distance from the Specimen Surface.

(A) Heat 3.5 ft. from Concrete Surface

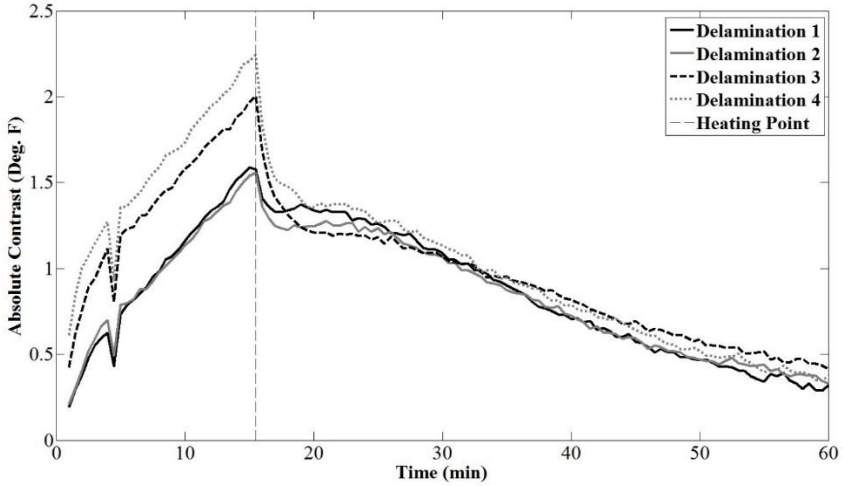

(B) Heat 2 ft. from Concrete Surface

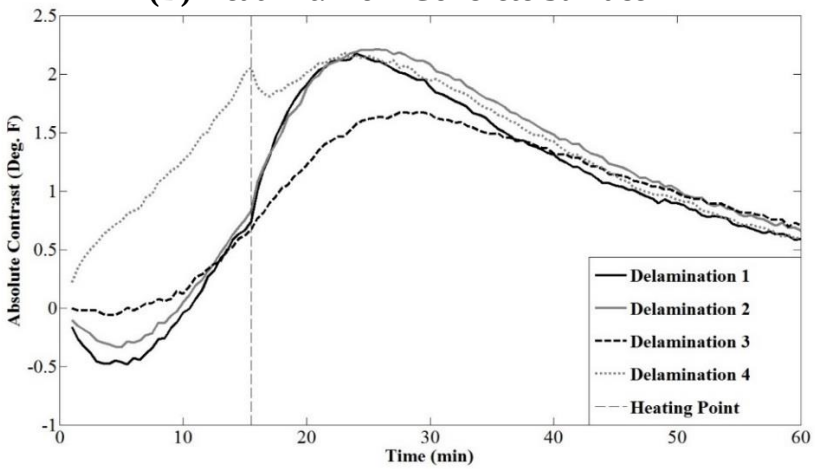

Figure 6-14: Absolute contrast graphs constructed from heater distances of (A) 3.5 ft and (B) 2 ft.

Table 6-9: Estimated Observation Times and Corresponding Absolute Contrast for Simulated Delaminations in Concrete Test Slab VI Tested with Different Heater Distances.

Heater Distance from Specimen Surface (ft)	*Delamination Number*	*Observation Time (min)*	*Corresponding Absolute Contrast (^{o}F)*
3.5	1	9.0	0.6
	2	10.0	0.5
	3	18.0	0.4
	4	19.0	0.5
2	1	9.0	2.2
	2	9.5	2.2
	3	14.0	1.7
	4	8.0	2.2

6.3.4.2 Discussion and Conclusions

Results from the laboratory test conducted on concrete specimen VI suggest that changing the distance between the heat source and the surface of the concrete specimen changes the uniformity of heating. Thermal banding originating from the heater's reflective backing is more prominent during the heating phase of testing for the test conducted with the heater positioned 2 ft. from the specimen surface than the control test with the heater positioned above the specimen surface at 3.5 ft. Thermal images also show a heat concentration in the middle of concrete specimen VI directly below the infrared heater for the 2 ft. test but not in the control test (Figure 6-13). This heat concentration resulted in higher surface temperatures above the center of the test slab compared to previous laboratory tests and may make detecting delaminations by visual inspection more challenging. With the basic understanding of heat transfer and the fact that relative depths of delaminations can be estimated directly from thermal images based on thermal contrast to areas of sound concrete, the subjective analysis procedures used to locate delaminations in this study may lead to false positive results. For example, sound concrete appearing at higher temperatures due to heat concentrations may be misidentified as delaminations.

In addition to the challenges presented to visual delamination detection from non-uniform heating, heat concentrations are also shown to have a direct impact on the absolute contrast of delaminations. From Figure 6-14 it can be concluded that observation time is more easily defined from the results of the test conducted with the heater positioned at 2 ft from the specimen surface. Although this may be the case for the selected analysis areas as shown in Figure 6-14, it may not be true in all testing cases. As previously mentioned, one of the main challenges in active IR thermography analysis is selecting appropriate areas representing delaminated areas and sound concrete areas. These areas ultimately define the absolute contrast graph and observation time. Due to the bias of this experiment and knowing the locations of the simulated delaminations, heat concentrations were not misidentified as areas of delamination and were included in the background reference area. The resulting absolute contrast graph shown in Figure 6-14 will differ from a graph constructed with a background reference area not including areas of concentrated heat.

Furthermore, the results of this test provide insight on selecting an appropriate heater distance for active IR thermography testing. For the Solaira infrared heater used in this study, it can be advised that a heating distance greater than two feet from the surface of the concrete specimen should be used to ensure uniform heating and prevent thermal concentrations and banding. Further investigations are recommended to explore the relationship between heater distance and the duration of the heat impulse to ensure significant thermal contrast between areas of delamination and areas of sound concrete for the estimation of observation time.

6.4 Active IR Field Application Spring 2014

Using the test set-up and methodology developed through the laboratory testing, active IR thermography was applied to an in-service concrete bridge for condition assessment. One objective of the field application included the confirmation of active IR thermography capabilities to detect delaminations on the bridge deck underside not exposed to passive solar heating and fascia beams. Another objective was to determine the influence of heating times (5 min. versus 15 min.) in the field. In addition, the capability of using this non-destructive, remote sensing technique to estimate subsurface defect depth was also investigated.

6.4.1 Demonstration Site

MDOT structure No. 4947 – Franklin Street over US-131 and CSX railroad line is located in Kent County in Grand Rapids, Michigan. The structure spans both the north and south bound US-131 traffic lanes as well as the north and south bound CSX railroad lines. This site was selected for the application of active IR thermography due to the accessibility to the underside to the bridge. Open land access to the underside of the bridge on the east side of the structure allowed testing to be conducted in a safe environment without disruptions to traffic flow at road intersections.

Constructed in 1960, this bridge is a multiple span structure. Main spans of the structure over US-131 are composed of steel beams while approach spans were constructed using prestressed concrete beams. The bridge spans a total length of 1,035 ft and is 58.4 ft wide (MDOT 2012). Figure 6-15 shows the east side concrete beam approach structure and current condition of Pier 22.

Figure 6-15: Precast Concrete Approach Spans under Franklin Street Bridge.

The bottom concrete deck surface was assigned an overall NBI fair condition rating of 6 during the last inspection on October 23, 2012, however, the degree of deterioration varied between spans and ratings ranged from 5 to 9. These assessment results reflect the overlay of sections in 1990 and, more recently, the replacement of seven concrete deck spans. Replaced deck spans have remained in good condition but other spans contain considerable amounts of spalling and cracking. In addition, soot buildup from locomotive exhaust was reported directly above the railroad line.

6.4.1.1 Ground Truth Information

Prior to the active IR thermography testing, MDOT inspectors used hammer sounding to locate areas of suspected delamination on the underside of the bridge deck on span 22W. The inspectors used spray paint to outline the defect areas. These marked areas were later used to calculate the percentage of deficiency within the test areas and were compared to results of the active IR thermography testing.

6.4.2 Test Locations

From the results of the ground truth testing, three test locations on span 22W of the Franklin Street bridge were selected for the application of active IR thermography to the underside of a concrete bridge deck and pier cap. The lack of surface moisture was used as a primary criteria during the selection process. The selected test locations are described in the following sections and are shown in Figure 6-16.

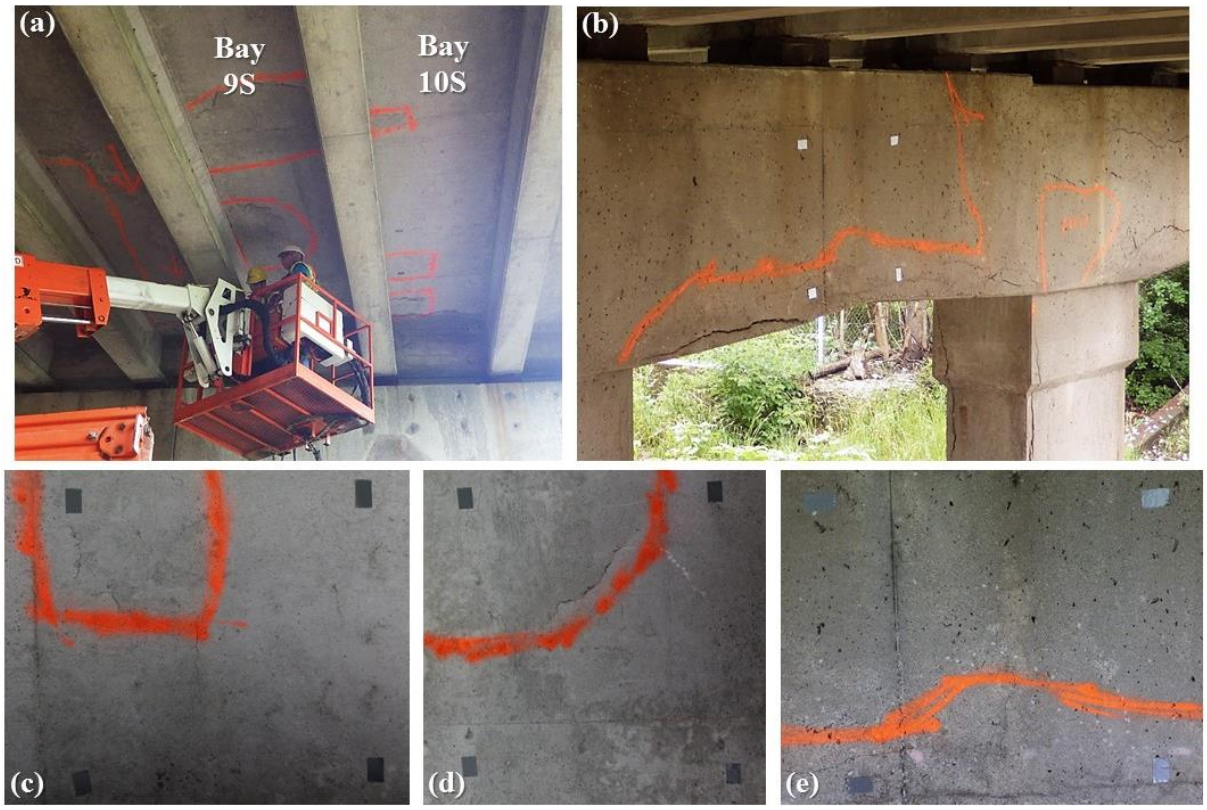

Figure 6-16: (a) Underside of the Franklin Street Bridge Deck. (b) Delamination on Pier 22. (c) Test Location A: Underside of Bridge Deck in Bay 10S. (d) Test Location B: Underside of Bridge Deck in Bay 9S. (e) Test Location C: Pier Cap of Pier 22.

On the scheduled testing day, scattered rain showers and high humidity in the morning had left several areas of the underside of the bridge deck wet due to cracks extending to the top bridge deck and the effects of condensation. These areas were avoided when selecting test locations, as the effects of surface moisture and moisture within concrete can negatively affect results from active IR thermography test methods. Emmisivity is an essential parameter for thermography and can differ for dry concrete and wet concrete. Because of this change in material property, dry concrete may appear at a different temperature in thermal IR images than wet concrete, even if the two areas have the same temperature. Therefore, detecting delaminated areas is more difficult due to the different appearance of wet and dry concrete areas in thermal infrared images.

Rectangular test locations were selected based on the field of view of the thermal infrared cameras used for testing. The corners of all test locations were marked with pieces of tape to visually define the area. The tape aided in aligning the heater, optical image and thermal image prior to data acquisition. The tape marks were also used to correlate and precisely align the optical images with thermal images during analysis procedures. The markers defined an area of approximately 3 ft by 3 ft at each of the test locations.

6.4.2.1 Location A

Test location A was selected for two active IR thermography tests to compare the effects of the duration of the heat impulse on the thermal contrast between areas of delamination and sound concrete and detection of subsurface defects. The first test at this location was conducted using a 15 minute heat time and was identified as test A1. After the heating period, data collection continued for an additional 35 minutes to ensure a majority of the heat impulse had dissipated throughout the concrete and little to no contrast between delamination and sound concrete could be seen in the thermal IR images. A second test was conducted at this location, test A2, using a 5 minute heat time and 25 minute post-heat monitoring time. Laboratory studies have shown that a smaller heat impulse provides less thermal contrast in thermal infrared images. Therefore, data acquisition was terminated sooner than tests conducted with a longer heat pulse because the thermal contrast between delamination and sound concrete diminished sooner. Prior to conducting a test at location A with a 5 minutes heating period, data was acquired at test location B to allow the concrete at location A to reach thermal equilibrium with the ambient environment.

Test location A was located on the far west end of Bay 10S. Ground truth information had revealed that the southwest corner of the selected area contained a suspected delamination. Several surface cracks were observed with a majority located near the suspected delamination. These surface defects were used to align the optical and thermal IR images for analysis.

6.4.2.2 Location B

Test location B was selected for additional active IR thermography testing on the underside of the bridge deck using a heat time of 15 minutes and was identified as test B1. Similar to test A1 conducted at location A, a 35 minute post-heat monitoring time was used to ensure a majority of the heat impulse had dissipated throughout the concrete and little to no contrast between delamination and sound concrete could be seen in the thermal IR images.

Test location B was located on the far west end of Bay 9S. Ground truth information had revealed that the southeast corner of the selected area contained suspected delamination. Several surface cracks were noticed with a majority located near the boundary of the suspected delamination.

6.4.2.3 Location C

One of the objectives of this study was to investigate the feasibility of active IR thermography applied to bridge fascia. Due to the inclement weather on the scheduled testing day, the criteria for selecting a testing location on the bridge fascia beam was not met, however, a testing location on one of the bridge piers was selected instead. The similarity between the test setup for the bridge pier and fascia beam allowed for the evaluation of the active IR thermography testing system on vertically oriented bridge element surfaces.

Test location C was located on the west side of the most southern end of the pier cap at Pier 22. Unlike testing conducted at test location A or B, the heater was positioned vertically to provide the required heat impulse.

6.5 Active Infrared Thermography Field Demonstration Equipment

Two thermal cameras, the high resolution FLIR SC640 used in laboratory studies and a compact lower resolution camera, were used to conduct the tests on the underside of a bridge deck and pier cap. The results from each camera were compared to the ground truth information provided by the Michigan Department of Transportation (MDOT) and the findings were used to make recommendations on the future implementation of active IR thermography for detecting delaminations on bridge superstructure elements not exposed to sunlight. To provide the necessary heat impulse to the selected concrete test areas, the Solaira infrared heater was utilized as the heating effects of this heater were well understood from laboratory investigations. Both the thermal cameras and heater were mounted to the portable support arms fabricated for lab tests. The test equipment and mounting system are shown in Figure 6-17.

(A) **(B)**

Figure 6-17: (A) FLIR SC640 and FLIR Tau 2 Thermal Infrared Cameras (B) Tripod Mounted Solaira Infrared Heater and Thermal Infrared Cameras.

6.5.1 FLIR Tau 2

A FLIR Tau 2 thermal imaging camera was used to investigate the feasibility of using compact, low cost thermal imaging equipment for non-destructive bridge condition assessments. The FLIR Tau 2 is significantly less expensive and smaller than the FLIR SC640 making it more attractive to bridge inspectors and owners. Due to its small size (fitting in the palm of a hand), this camera was mounted directly to the top of the FLIR SC640 in a way to capture a similar test area without obstructing the view of the companion camera.

The FLIR Tau 2 had a 13mm lens and a 336 x 256 pixel display with a 25^o x 19^o field of view. The camera recorded images to an external memory source where images were later transferred to a computer for analysis procedures. One of the limitations of this thermal camera is that it does not have an external visual display making it difficult to align and determine the appropriate field of view for the test area of interest.

The FLIR Tau 2 was used to record thermal IR images from the time the heater was turned off until termination of the FLIR SC640 data acquisition when a majority of the heat impulse had dissipated throughout the concrete and little to no contrast between delamination and sound concrete could be seen in the thermal IR images shown on the FLIR SC640 visual display. Because analysis procedures used in this study focus on the cooling phase of testing to estimate observation time, the FLIR Tau 2 start time of acquisition was appropriate. The frame rate of the FLIR Tau 2 was correlated to the images acquired from the FLIR SC640 based on the number of images recorded during the duration of the cooling phase of testing.

6.6 Field Demonstration Methodology

To investigate the feasibility of using active IR thermography to detect and quantify delaminations on concrete structural elements of highway bridges, the field test set-up was similar to the developed laboratory test set-up and was used to conduct four tests which are described in detail in the following sections. Using a simplistic area analysis technique and the previously explained absolute contrast analysis method, delaminations were quantified from the results of active IR testing.

6.6.1 Field Application: Test Set-up and Procedure

Several factors dictated the test setup for the active IR thermography field demonstration including the heater size and heater distance. Because the Solaira heater used for testing was relatively small, the test area was limited in size. In addition, the distance from the heater to the concrete surface was established at a distance of 3.5 ft (1.07 m). This distance was used in laboratory studies and was selected to ensure that the heat impulse is capable of producing detectable contrast between delaminations and sound concrete in thermal infrared images over a short period of time (Vaghefi 2013). Increasing the heater distance provides a larger test area and a more uniform heat across the concrete surface for the specific heater used in this test. On the other hand, increasing the heater distance may increase the heat duration needed to obtain the same thermal contrast as closer heater distances. To ensure the thermal infrared cameras captured the heated area on the test location, cameras were positioned 6 ft (1.83 m) from the surface of the test location at an angle of approximately 10^o to 20^o from normal. This angle was used to get the best perspective of the test area without capturing the image of the heater and was necessary to analyze the relative shapes, locations and depths of delaminations.

To access the underside of the bridge deck and pier cap, MDOT provided a scissor lift truck on the scheduled test date. The hydraulically powered lift platform provided ample space for the tripod mounted heater and cameras as well as a 2000 W generator used to power test equipment. The positioning of the heater and thermal infrared cameras for the pier cap test, as well as the lift truck used to provide access to test locations, can be seen in Figure 6-18.

(A) **(B)**

Figure 6-18: (A) Platform Lift Truck (B) Active IR Thermography Test Set-Up for a Franklin Street Bridge Pier Cap.

Prior to active IR thermography testing at each selected location, environmental conditions were measured and used to calibrate the FLIR SC640 thermal imaging camera. A summary of the test numbers and corresponding heat and data acquisition times are shown in Table 6-10. Environmental conditions used for thermal camera calibrations for each test are also summarized in this table.

Table 6-10: Environmental Conditions and Testing Procedure Summary for Field Demonstration Testing.

Test Number	*Humidity (%)*	*Ambient Temperature (^{o}F)*	*Heat Time (min)*	*Total Acquisition Time (min)*
A1	78.5	75.2	5	30
A2	85.4	71.4	15	50
B1	86.0	71.5	15	50
C1	73.0	76.1	15	50

6.6.2 Data Processing

Two objectives were established for the analysis of data collected during the active IR field demonstration: to estimate the percentage of delamination from thermal images and compare findings to MDOT ground truth information and to investigate the feasibility of estimating delamination depth using a known active IR thermography estimation technique. The following

sections describe the data processing used to complete these objectives and provide an analysis base for future studies.

6.6.2.1 Percent Area of Delamination

To determine the percentage of suspected delaminated concrete area at the three selected test locations on the Franklin Street bridge, and to ensure accurate comparison of ground truth data and the acquired thermal data, the field of view of both the FLIR SC640 and FLIR Tau 2 thermal imaging cameras was correlated to an optical image of the test locations taken from the same perspective as the thermal cameras. Images were aligned using surface features and anomalies such as cracks and spalls, both of which appeared within the thermal images during the heating phase of testing with noticeable contrast from surrounding concrete. This correlation technique was used because the tape markers placed on the concrete surface for image alignment were not consistent with the field of view of the thermal cameras. After correlation, the field of view of the thermal cameras was projected to the optical image generating a total area boundary for comparison.

All processing of the optical images and thermal images was conducted in MATLAB. A simple polygon method was used to determine the percent of delamination on the bridge deck underside and pier cap. No specific polygonal shape was used during analysis, instead, a polygon most similar to the shape of the delamination was constructed. The thermal IR image and optical image correlation of the FLIR SC640 data collected during test B1 as well as the polygon method for determining percent of delamination based on ground truth information can be seen in Figure 6-19. The paint marks placed by MDOT inspectors is seen in Figure 6-19 (B).

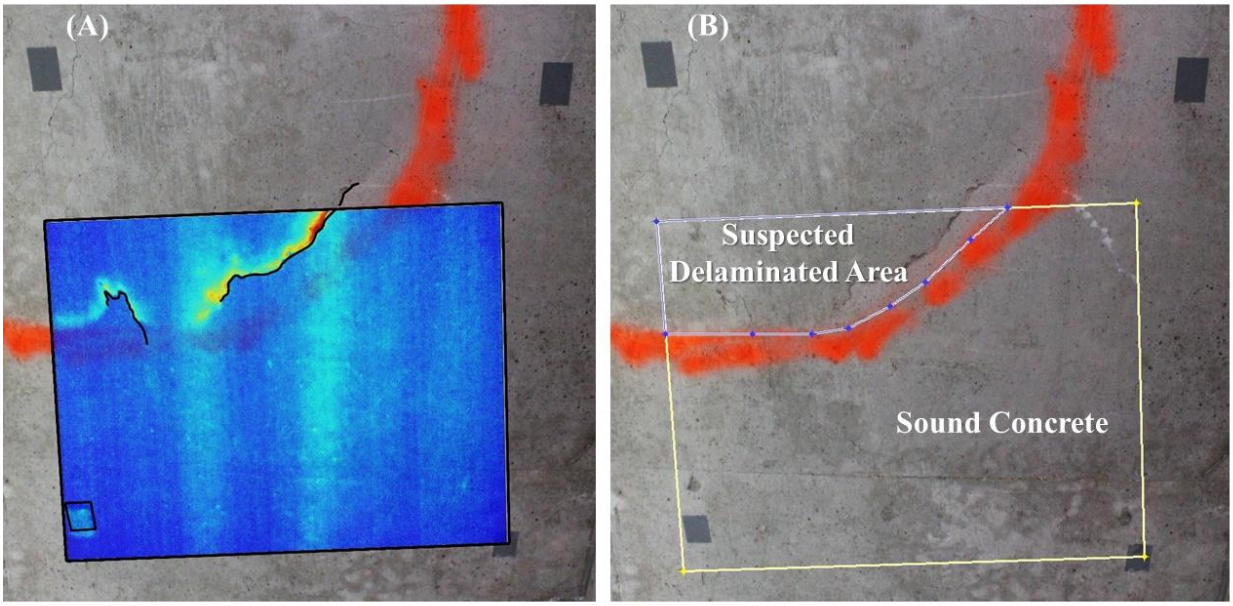

Figure 6-19: (A) Thermal and Optical Image Correlation of FLIR SC640 Using Surface Cracking at Test Location B. (B) Polygon Method for Determining Delamination Percent Based on Ground Truth Information.

The percentage of delaminated area was calculated from the thermal images and optical images using Equation 6-3. The total area of the thermal IR images was taken as the field of view of the corresponding thermal IR camera.

$$\text{Delaminated Area (\%)} = \frac{\text{Number of Pixels of Delaminated Area}}{\text{Number of Pixels of Test Area}} \times 100 \qquad \text{Equation 6-3}$$

Within the acquired thermal IR images, delaminations appeared as hotspots compared to surrounding sound concrete. The thermal contrast between the suspected defect and non-defected areas was large enough to process data without image enhancement techniques. At various time intervals, the delamination was subjectively bound by a polygon on the thermal images and Equation 6-3 was used to determine delamination percent. Non-uniform heating, a function of the heater used for testing, did however provide a challenge in bounding the delaminated area on the pier cap, as the contrast between the delamination and thermal heating bands of the heater was difficult to distinguish.

To quantify the ground truth information for thermal image comparison, the simple polygon method was again utilized. Using the projected views from the thermal images as the total area, the suspected delamination marked by MDOT inspectors with spray paint was bounded by a polygon and the percent of delaminated area was calculated using Equation 6-1. For consistency, the polygon was constructed along the inside border of the spray paint closest to the suspected area of delamination.

Both the thermal infrared and optical cameras are recommended to be positioned at a normal angle to the surface of interest to achieve the most accurate results when using the polygon method for determining the percent of delaminated area. Due to the setup of this study and the position of the heater, both the thermal cameras and optical camera were positioned at an angle of approximately 10^{o}-20^{o} to the test surface. This positioning was adequate for comparing the MDOT ground truth information to the results of active IR thermography because the optical and thermal images were taken at the same perspective to the test locations.

6.6.2.2 Delamination Depth Estimation

To determine the feasibility of using the active IR surface heating method to predict the depth of delaminations on an in-service bridge, depth analysis procedures similar to those developed in laboratory studies were used and are described in earlier sections. All processing of thermal images was conducted in MATLAB. The notable difference between the processing of field data and laboratory data was the selection of a sound concrete background reference area. The background reference area for laboratory studies was selected as a box-shaped polygon surrounding the suspected area of delamination. This analysis shape was selected based on the shape of the simulated Styrofoam delaminations. Due to the geometry and position of delamination in thermal images collected during the field application, a box-shaped polygon could not be used as a reference area. Instead, an L-shape polygon was used as a background reference area. Because the relative shapes of delamination at each selected test location differed, the dimensions and orientation of the L-shaped polygon used during analysis varied. However, a thickness of 5 pixels was used for each of the L-shaped analysis areas for consistency. Figure 6-20 shows the analysis areas selected for a thermal image acquired by the FLIR SC640 during test B1 of the field demonstration.

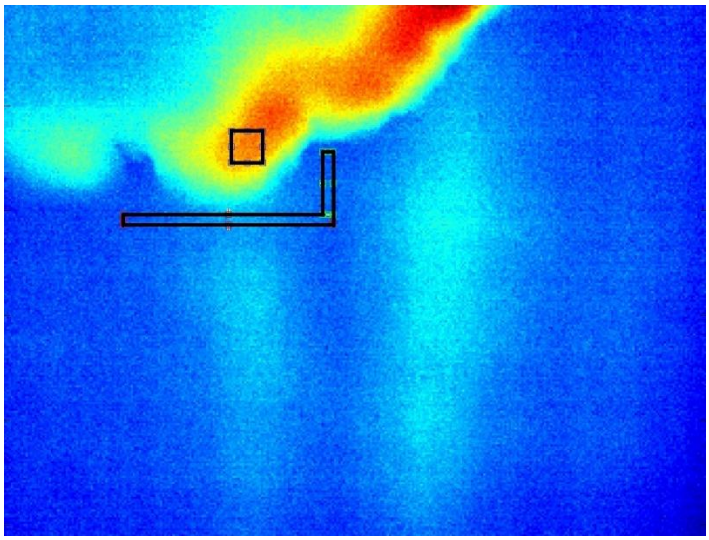

Figure 6-20: Analysis Areas Selected for Test B1 Captured by the FLIR SC640 Thermal Imaging Camera.

Once representative areas of delamination and sound concrete were selected, absolute contrast graphs were constructed. Due to the higher frame rate of the FLIR Tau 2 compared to the FLIR SC640, a moving average of 100 was calculated for this camera to reduce the effects of thermal noise. To determine if depth estimation was feasible, observation times were estimated from each of the absolute contrast plots constructed from data acquired by both thermal cameras used during testing. Because the diffusivity of the concrete used in the construction of the Franklin Street bridge was unknown, delamination depth was not directly estimated, however, previous laboratory studies confirm the relationship between observation time and delamination depth, making this method of determining the feasibility of depth estimation adequate for the objectives of this study (Vaghefi 2013).

6.7 Results and Discussion of Field Demonstration

The following sections present the findings of the field application of active thermography as related to estimation of delamination area and observation times of suspected delaminations at each selected test location on the underside of the bridge deck.

6.7.1 Area of Delamination

Delamination area analysis of the active IR thermography data was based on the visible contrast between delaminated areas and sound concrete in thermal images. For each of the tests conducted, the percent delamination was calculated for both the FLIR SC640 and FLIR Tau 2 every 5 minutes starting at the time the heater was shut off. This time was selected as the starting point of analysis because delaminations are not consistently visible before this point in active IR thermography testing. The maximum percent of delamination for all time step images at each test location is reported in Table 6-11. The data shows that at all testing locations and heat times, the delaminated areas determined by hammer sounding were larger than those detected by active IR thermography. In no test did the area of delamination detected by thermal imaging exceed 83% of hammer sounding results. Thermal images from the FLIR SC640 and FLIR Tau 2 infrared cameras can be seen in Figure 6-21 and include the test number, the maximum detectable delamination size bounded by an analysis polygon, and the acquired time of the thermal IR image from the beginning of the heat time.

It should be noted that the FLIR Tau 2 was not activated during test A1 until 18 minutes after the heater was shut off due to oversight. By the time acquisition initiated, surface anomalies such as spalls and cracking were no longer visible in the thermal images. As a result, the thermal images from the FLIR Tau 2 could not be correlated to the optical image taken at test location A and a total area could not be defined for quantifying ground truth information. The incomplete data is represented by a dash in Table 6-11. However, analysis procedures using the simple polygon method were conducted on the existing set of thermal data recorded by the FLIR Tau 2 during test A1.

Table 6-11: Percent Area Results of Active IR Thermography and Hammer Sounding.

	Test Number	*Maximum Delamination % by Active IR Thermography (%)*	*Delamination % by Hammer Sounding (%)*	*Area of Delamination by Active IR Thermography (ft^2)*	*Area of Delamination by Hammer Sounding (ft^2)*	*% Active IR Area of Hammer Sounding Area (%)*
FLIR SC640	A1	10.91	13.21	0.53	0.64	82.8
	A2	9.71	14.37	0.47	0.70	67.1
	B1	12.67	19.28	0.61	0.93	65.6
	C1	8.08	23.70	0.39	1.15	33.9
FLIR Tau 2	A1	10.37	-	0.62	-	-
	A2	7.92	18.45	0.47	1.10	42.7
	B1	19.02	28.56	1.13	1.70	66.5
	C1	23.47	40.30	1.40	2.40	58.3

- = incomplete data

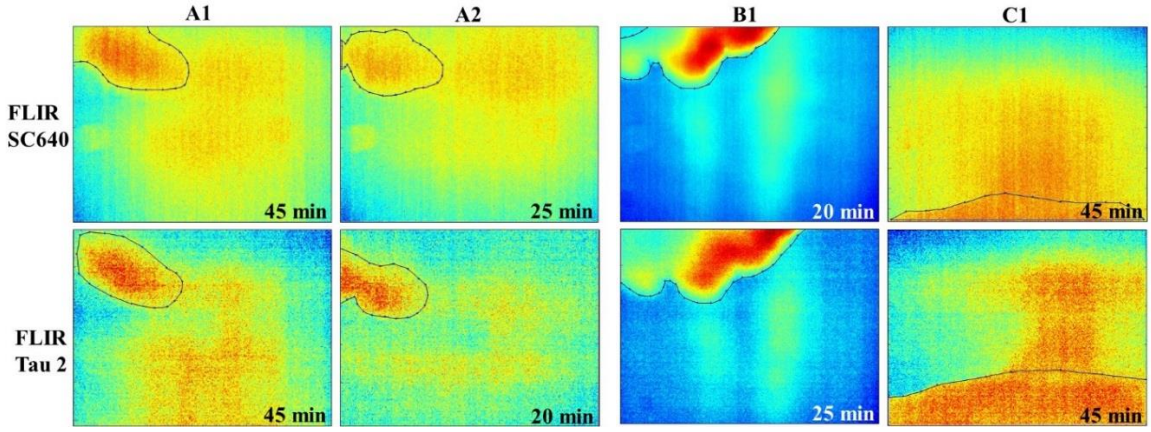

Figure 6-21: Maximum Delamination Areas using Simple Polygon Method for Thermal Image Processing.

While results above indicate hammer sounding predicts larger areas of suspected delamination than with active IR thermography, results also show that several limitations should be considered when detecting and quantifying delamination on concrete elements under a bridge. As previously noted, non-uniform heating adds difficultly to distinguishing the contrast between delaminated areas and areas of sound concrete. Laboratory studies have investigated thermal banding originating from the selected Solaira infrared heater which can be seen in Figure 6-21. For example, vertically oriented heat bands appear in test B1 and horizontal banding appears in test A2. Because of the subjectivity of selecting areas of suspected delamination, thermal banding had a direct effect on the absolute contrast and observation time of delaminations detected at each of the testing locations.

Another limitation to detecting delamination on the underside of a bridge can arise from thermal IR camera functionality. For this field application, two thermal IR cameras, a FLIR SC640 and FLIR Tau 2, were used to collect data. The FLIR SC640 has the ability to be manually focused on a test subject of interest while the FLIR Tau 2 does not contain this function. Because of the uniform temperature of the concrete test areas and the surrounding environment prior to active heating, it became especially difficult to focus the FLIR SC640 on the test areas. Improper focus of the test area may distort the thermal images resulting in less accurate analysis and results. To overcome this limitation, a small object was placed near the surface of the test locations prior to testing. The FLIR SC640 thermal IR camera was focused on this object to ensure image clarity. The object was then removed from the field of view of the camera and testing commenced.

One feature of the FLIR SC640 is that it contains an external display providing a live image to the operator and aiding in alignment of the camera with the test area. Without this ability to produce a live image, the FLIR Tau 2 must be carefully positioned to best capture the test area of interest. This limitation provides challenges for bridge inspectors who cannot be certain of the images they are capturing before post-processing of data. For future applications of active IR thermography, it is recommended that a computer program be developed to display data recorded by the FLIR Tau 2 in real time allowing areas of interest on bridge elements to be captured.

To ensure results from the active IR thermography tests could be compared to MDOT ground truth information, the thermal IR test locations were selected after inspectors completed a delamination survey on span 22W of the Franklin Street bridge. Test locations were selected based on the criteria that they contained areas of delamination and sound concrete areas. Because of this selection criteria and the availability of ground truth information at the time of testing, analysis procedures may have led to the bias detection of delamination.

Although the results of the thermal IR image analysis are subjective for this study and dependent on the operator, data does indicate the presence of similar delaminations at heating times of 15 and 5 minutes during tests A1 and A2. The percent delamination detected by hammer sounding varies for these two tests because the equipment was adjusted between tests causing slight changes in the captured area. Both thermal cameras detected a delamination of lesser area than hammer sounding.

6.7.2 Depth Analysis

To evaluate the performance of Active IR thermography and to investigate the feasibility of using this remote sensing technology to predict the depth of delaminations during field applications, absolute contrast graphs were constructed for all tests using data from both the FLIR SC640 and the FLIR Tau 2 thermal imaging cameras. Figure 6-22 and Figure 6-23 show the absolute contrast graphs from the four tests conducted on the Franklin Street bridge for the FLIR SC640 and FLIR Tau 2 respectively. The end of the heating phase is shown in the FLIR SC640 absolute contrast graphs by a vertical line. Because the FLIR Tau 2 was turned on and

began acquiring data at the end of the heating phase, the absolute contrast graphs for this camera represent only the cooling phase of testing. This starting time of acquisition for the FLIR Tau 2 was adequate for the objectives of this study as the observation time needed for depth analysis is determined from the cooling phase of testing. It should be mentioned again that the FLIR Tau 2 was turned on 18 minutes after the end of the heating phase due to oversight for test A2 and the data collected for this test is shown in Figure 6-23 (B).

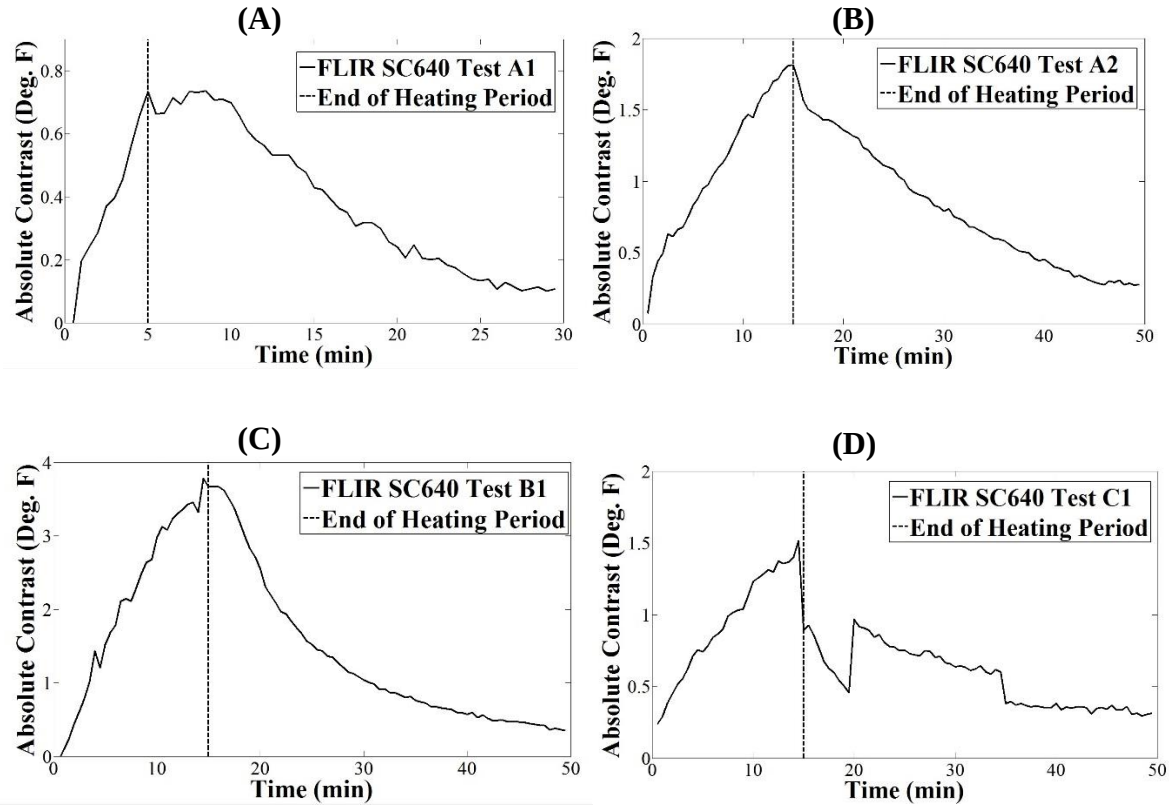

Figure 6-22: FLIR SC640 Absolute Contrast Graphs from Active IR Thermography Field Demonstration Testing (A) Test A1: 5 min. Heat Time (B) Test A2: 15 min. Heat Time (C) Test B1: 15 min. Heat Time (D) Test C1: 15 min. Heat Time.

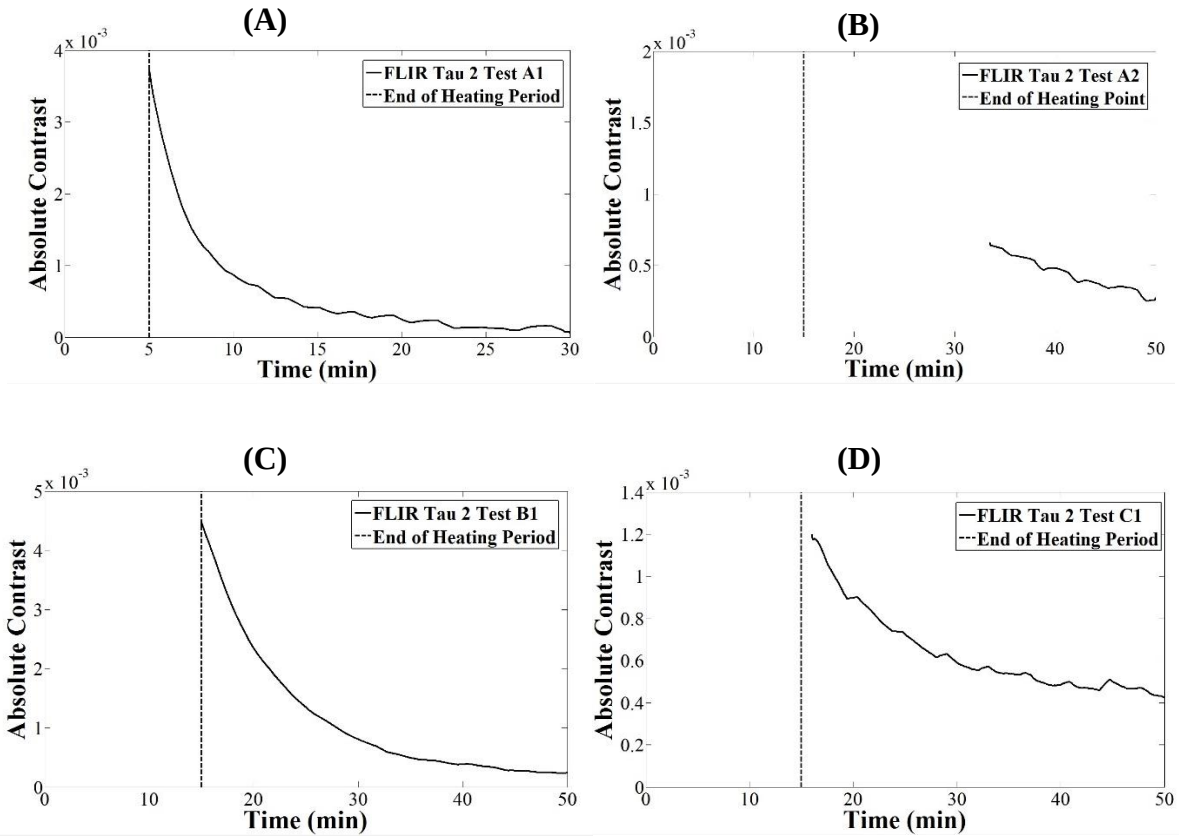

Figure 6-23: FLIR Tau 2 Absolute Contrast Graphs from Active IR Thermography Field Demonstration Testing (A) Test A1: 5 min. Heat Time (B) Test A2: 15 min. Heat Time (C) Test B1: 15 min. Heat Time (D) Test C1: 15 min. Heat Time.

Using the absolute contrast graphs constructed from data captured by both the FLIR SC640 and FLIR Tau 2 thermal cameras, the observation times for the selected delamination reference area were estimated for each test location. The estimated observation time is reported in Table 6-12. Observations of the absolute contrast graphs constructed from FLIR SC640 data show abrupt absolute contrast shifts at 20 min. and 35 min. for test C1 and were shown in Figure 6-22 (D). Due to this erroneous data, observation time could not be determined. To explain these temperature shifts, additional camera functions must be understood. The FLIR SC640 thermal imaging camera contains an internal lens shutter that automatically calibrates the thermal sensor to user defined parameters during data acquisition. It is hypothesized that the thermal camera did not calibrate correctly at 20 min. causing inaccurate shifted temperature readings until a successful calibration at 35 min.

Once observation times for each of the field tests were estimated, the depth of the delamination was estimated using the relationship between observation time, depth squared and thermal diffusivity presented in equation 6-2. The thermal diffusivity, δ, used to calculate depth was estimated from laboratory studies as 0.2219 in^2/min. It should be noted that this thermal diffusivity value corresponds to the concrete used to construct laboratory test slabs and is likely

different from the concrete used in the construction of the Franklin Street bridge. However, for the objectives and purpose of this study, the estimated diffusivity value is adequate for determining the feasibility of using active IR thermography for delamination depth estimation.

It should also be noted that field data shows delaminations on the bridge deck and pier cap that vary in depth. Variations in thermal contrast between areas above a delamination and areas of sound concrete support this observation. Due to this depth variation, the calculated depth for the field demonstration represents the average depth of the representative delamination area used to construct the absolute contrast graph. While the presented method of analysis allows for delamination depth estimates at relatively small areas, a more robust method should be developed to determine the depth across the entire delamination.

Table 6-12: Estimated Observation Times for Suspected Delaminations on the Franklin Street Bridge Deck and Pier Cap.

	Test Number	***Observation Time (min)***	***Corresponding Absolute Contrast (^{o}F)***	***Estimated Depth (in)***
FLIR SC640	A1	3	0.73	0.82
	A2	6.5	1.3	1.2
	B1	-	-	-
	C1	-	-	-
FLIR Tau 2	A1	-	-	-
	A2	-	-	-
	B1	-	-	-
	C1	-	-	-

Data shows that observation time can be estimated from data collected by the FLIR SC640 thermal camera at test location A from both the 5 min. and 15 min. heat time tests (A1 and A2 respectively). As previously discussed, estimated depth corresponds to the selected analysis areas. For this reason, the depth of the delamination calculated in tests A1 and A2 differ because selected analysis areas are not the same. Observation time could not be estimated using the current analysis techniques in any of the tests conducted at the second bridge deck location or pier cap (tests B1 and C1 respectively). It can also be seen in Table 6-12 that no observation times could be estimated from data acquired by the FLIR Tau 2 thermal camera.

While results from Table 6-12 confirm the use of active IR thermography to estimate the depth of delaminations in concrete bridge elements at test location A, several limitations should be considered when utilizing the described analysis method. Delaminations often form irregular shapes that are variable in depth. As a result, to estimate the depth at any given point of the delamination, the representative area used for absolute contrast calculations is limited in size to ensure a uniform depth in the specified region. The restricted size of the selected delamination

area provides little information about the actual characteristics and dimensions of a large subsurface defect, therefore analysis procedures must be repeated numerous times to quantify the entire delamination. This process may be time consuming and introduce additional interpretation errors due to the subjective nature of the analysis method used in this study. To more efficiently estimate delamination depth in the subsurface of concrete elements, other analysis methods should be further investigated that have automation capabilities allowing for a decreased analysis time.

6.8 Final Conclusions of the Active IR Thermography Inspection

Active IR thermography is a non-destructive condition assessment technique that is gaining popularity among different industries for evaluating and quantifying deterioration of concrete structures due to its simplistic testing and analysis procedures. In addition to remote sensing capabilities, this technology can be used to provide valuable information to inspectors for monitoring delamination growth with time. This study has investigated the potential of applying active IR thermography on concrete bridge elements to assist bridge inspectors in detecting and quantifying delaminations specifically on the underside of concrete bridge decks and piers not exposed to solar heating. The objective of this research was to investigate the feasibility of quantifying delamination area and depth for both laboratory and in-field applications while overcoming some of the limitations of passive infrared thermography. Active IR thermography testing was conducted on several concrete laboratory specimens to develop and provide a base for depth analysis procedures and to investigate several testing parameters. Enhancements to the testing procedure made in the laboratory allowed for the application of this non-destructive testing method on an in-service concrete highway bridge located in downtown Grand Rapids, MI.

Results obtained from initial laboratory testing provide evidence to verify the capabilities of active IR thermography to estimate depth of delaminations in concrete elements using a thermal impulse of 15 minutes using a 1500W heater. Data confirms the linear relationship between the square of the delamination depth and observation time as well as the empirical rule of infrared thermography that delaminations with a width-to-depth ratio greater than 2 and a depth of less than 2 in. from the surface can be accurately detected in thermal images. In addition, testing results demonstrate the effects of delamination size and depth on observation time. Observation time is especially important when selecting an effective time window for acquisition of thermal images to capture delaminations when they appear with maximum contrast to sound areas of concrete.

Completion of parametric laboratory testing revealed several testing variables affecting the thermal contrast between areas of delamination and areas of sound concrete including thermal impulse duration, heater distance from the surface of the concrete test specimen and thermal banding. Decreasing the thermal impulse duration from 15 min. to 5 min. decreased thermal contrast between areas of suspected delamination and areas of sound concrete, however,

delaminations exposed to the shortened impulse were still capable of detection using the selected analysis methods for this study.

One disadvantage of the heating method used in this was non-uniform heating of the concrete test specimens which influenced the selection of analysis areas and determination of observation time from absolute contrast graphs. Non-uniform heating can result from thermal banding originating from heating elements and from heat concentrations produced by decreased heater distances. In either case, selecting representative areas of delamination and sound concrete during analysis procedures becomes increasingly difficult and has a direct effect on absolute contrast. Further investigations are proposed to identify alternative, more appropriate heating sources for future active IR thermography applications.

Advancements to the active IR thermography testing procedure made in the laboratory allowed for testing of several areas on the underside of a concrete highway bridge deck and pier cap located in downtown Grand Rapids, Michigan. The intent of the field application was to address the feasibility of using active IR thermography on concrete bridge elements as a condition assessment method. Results show that active IR thermography is an appropriate non-destructive technique for detecting and quantifying the area of delamination on the underside of bridge decks and is a valuable inspection method for the bridge inspector's toolbox. Test results verify that, unlike passive infrared thermography, active IR thermography is not limited to a specific time window during the day for data collection and can be conducted during a cloudy day as exposure to sun light is not necessary to obtain delamination detection results. In addition, this field application confirms the feasibility of using active IR thermography for condition assessment on vertically oriented concrete bridge elements such as pier caps and the sides of bridge fascia. Furthermore, inclement weather on the test day (including light rain) did not deter data collection as long as tests were conducted in protected areas such as the underside of a bridge deck.

With the use of an external heater to overcome limitations presented by passive IR thermography such as specific testing time windows, active IR thermography can be used for inspection of bridge elements not exposed to the sun. Testing results from the field application show that a heat impulse of 15 min. delivered by the Solaira infrared heater is acceptable for detecting and quantifying subsurface defects. Preliminary results also show that using a shorter heat impulse duration of 5 min. is suitable for quantifying the area of delaminations on the underside of bridge decks and allows for reduced inspection times while using this condition assessment technique. The simplistic analysis method developed to compare MDOT ground truth information to thermal images acquired by the FLIR SC640 and FLIR Tau 2 provide an image processing base for future applications.

In all testing cases, MDOT hammer sounding was at minimum 17.2% greater than delamination areas detected by active IR thermography. Based on the statistics used for comparing hammer sounding to active IR thermography results, it can be concluded that MDOT bridge inspectors are conservative in their condition assessment techniques. However, the limitation of active IR should be considered including the delamination depth and width-to-depth ratio required for

detection using this technology and test set-up. To confirm hammer sounding is more conservative than active IR thermography, advanced thermal image processing should be further investigated. Numerous image enhancement techniques have shown potential to account for non-uniform heating and statistical analysis methods may provide less subjective, automated detection and quantification of subsurface defects.

In addition to determining delamination area using active IR thermography, including the use of reduced heating times, delamination observation times and depths were successfully calculated at test location A on the underside of the bridge deck using concrete thermal diffusivity determined in lab. While many limitations exist for the current depth analysis procedure presented in this chapter, including depth estimation of limited areas, it provides a base for future studies and analysis enhancements.

Results from this field demonstration also address the precision, cost and future capabilities of active IR thermography testing equipment. For all tests conducted on the Franklin Street bridge using both the FLIR SC640 and FLIR Tau 2 thermal cameras, data revealed less delamination per total area than the findings of MDOT inspectors. From these results, it is apparent that less expensive, more portable thermal infrared cameras show promise in detecting delamination area using active IR thermography and should be investigated before further application of this method. With ongoing advancements of technology, thermal cameras are becoming more portable and less expensive with little difference in image quality. Due to the similar performance of the FLIR Tau 2 with the FLIR SC640 in detecting delamination, small, less expensive thermal cameras may provide bridge inspectors with more accurate results than conventional non-destructive condition assessment techniques and allow greater access to bridge elements that cannot be captured using larger size equipment requiring mounting systems. However, the inability of the less expensive camera to focus or provide visual display maybe a deterrent. The field demonstration also confirmed the challenge of evaluating an entire deck underside with a small (3 ft by 3 ft) heating zone, concluding that this technology is most viable to evaluate a small location after an area of concern has been identified.

Furthermore, this research contributes to the current knowledge of the application of active IR thermography for concrete bridge inspection by using the surface heating method. While few previous studies focus on reducing inspection time and the portability of inspection equipment, this study concentrates on the application of active IR thermography to an existing concrete structure with the inspector in mind. Confirming the use of portable infrared heaters and handheld thermal cameras, this study provides evidence that heat times of as little as 5 minutes are capable of providing the necessary heat impulse to detect delaminations. In addition, the estimation of observation times from active IR testing confirms the feasibility of delamination depth estimation in both the laboratory setting and field application and serves as a base for future studies.

7. Project Outreach

Laboratory experiments and field applications of 3DOBS, BVRCS, passive IR thermography and active IR thermography have demonstrated success in the condition assessment of both the top and bottom decks of concrete highway bridges. To provide inspectors and end users the tools and knowledge to use the presented non-destructive remote sensing technologies for effective asset management, several training sessions were provided to MDOT personnel including inspectors, regional engineers, and photogrammetry experts. These training sessions are discussed below.

7.1 MDOT General Training Session

A general training session was conducted in Lansing, Michigan on October 16, 2014 to provide MDOT representatives with an overview of the test methodologies and equipment necessary for the application of each investigated condition assessment technique. With an objective of gaining an understanding of the field readiness and desire of technologies by current bridge inspectors, the three hour session included a presentation conducted by the principal investigators, a hands on equipment demonstration of the 3DOBS, BVRCS and active IR thermography systems and an implementation action plan discussion. The presentation slides from this training session are provided in Appendix G.

The group chose to explore the BVRCS in more depth because of its immediate field readiness, and hence requested an additional session specific to the BVRCS technology. The near highway speed system combining 3DOBS with passive thermography to detect spalls, cracks and suspected delaminations was also critiqued. Likewise, 3DOBS High Resolution system for detecting cracks as small as 1/32 in. was viewed by inspectors as needing guidance from the MDOT photogrammetry office prior to full implementation. A pilot study using the system for several MDOT bridges was suggested as a step towards implementation for scoping and detailed inspections. It was also suggested that the MDOT photogrammetry groups be trained on processing the 3DOBS data so inspectors could begin to use the system.

While the group showed interest in the idea of active thermography for detecting delaminations in areas not exposed to passive heating (sunlight), it was agreed that further study was needed before inspectors could confidently implement the system. Lightweight, portable heating systems, and hand held thermal and optical cameras will be key elements for future successful implementation. Data reduction and analysis methods can be enhanced for inspector use.

As a result of the general training session, two additional training sessions were scheduled to provide more extensive training for MDOT photogrammetry staff to understand the processing of 3DOBS data, and for inspectors to get hands-on experience with the BVCRS Bridgeviewer system, both of which were deemed field ready, deployable technologies.

7.2 Photogrammetry Training Session

A training session was held at the MTRI office in Ann Arbor to show the photogrammetry techniques used for 3DOBS on November 20, 2014. John Lobbestael, Frank Boston, and Kalvin Wixtrum from the MDOT photogrammetry department attended. This training session provided a walkthrough of the procedures to create a DEM and Orthoimage of a bridge deck from 3DOBS imagery using Agisoft PhotoScan. A sample dataset taken from a 3DOBS High-Res (Nikon D800) collect was used. Figure 7-1 depicts a general flow of data processing. John Lobbestael and Frank Boston were interested in working together on more application of 3D processing software in transportation. This included other areas of research that MTRI has done for MDOT including the use of UAVs with similar sensors to produce equivalent datasets.

7.3 BVRCS Training Session

A BVRCS training session was conducted at MTRI in Ann Arbor, Michigan on November 20, 2014, and led by MTRI staff members Colin Brooks, David Banach, and Rick Dobson. This session was based on the "BVRCS How To" manual and was presented to MDOT professionals, Eric Burns, Rich Kathrens, Dave Juntunen, and Kay Adefeso. The two-hour training session highlighted BVRCS equipment, use, and data processing methods. Additionally, a live demonstration highlighting how to process data was conducted, including how to link each photo to a GPS coordinate using GeoJot+ and how to hyperlink photos in ESRI ArcGIS Desktop software. The data used for this demonstration was collected during the June 6, 2014 data collection at the Merriman East U-turn Bridge in Livonia, Michigan. During this training session, questions were encouraged and answered. Lastly, a short demonstration on how to place the GoPro cameras on the hood of a vehicle was given outside of MTRI's office. Each MDOT professional in attendance was given a copy of the BVRCS How To manual, which is included in Appendix H.

At the conclusion of the BVRCS training session, MDOT officials obtained a better understanding into BVRCS equipment, data collection, data processing, and outputs. MDOT discussed potential ways to implement BVRCS equipment (especially the GoPro cameras) into daily bridge inspection methods both on the bridge deck and underneath the bridge. MTRI will potentially aid MDOT with data collection and processing when MDOT fully implements the BVRCS system. It was further suggested by Dave Juntunen that several of these technologies (3DOBS, BridgeGuard and BVRCS) be combined and evaluated on a state-wide basis. This would consist of a pilot study using the system on at least 20 bridges throughout the state to evaluate its ease of use and value added data for MDOT needs.

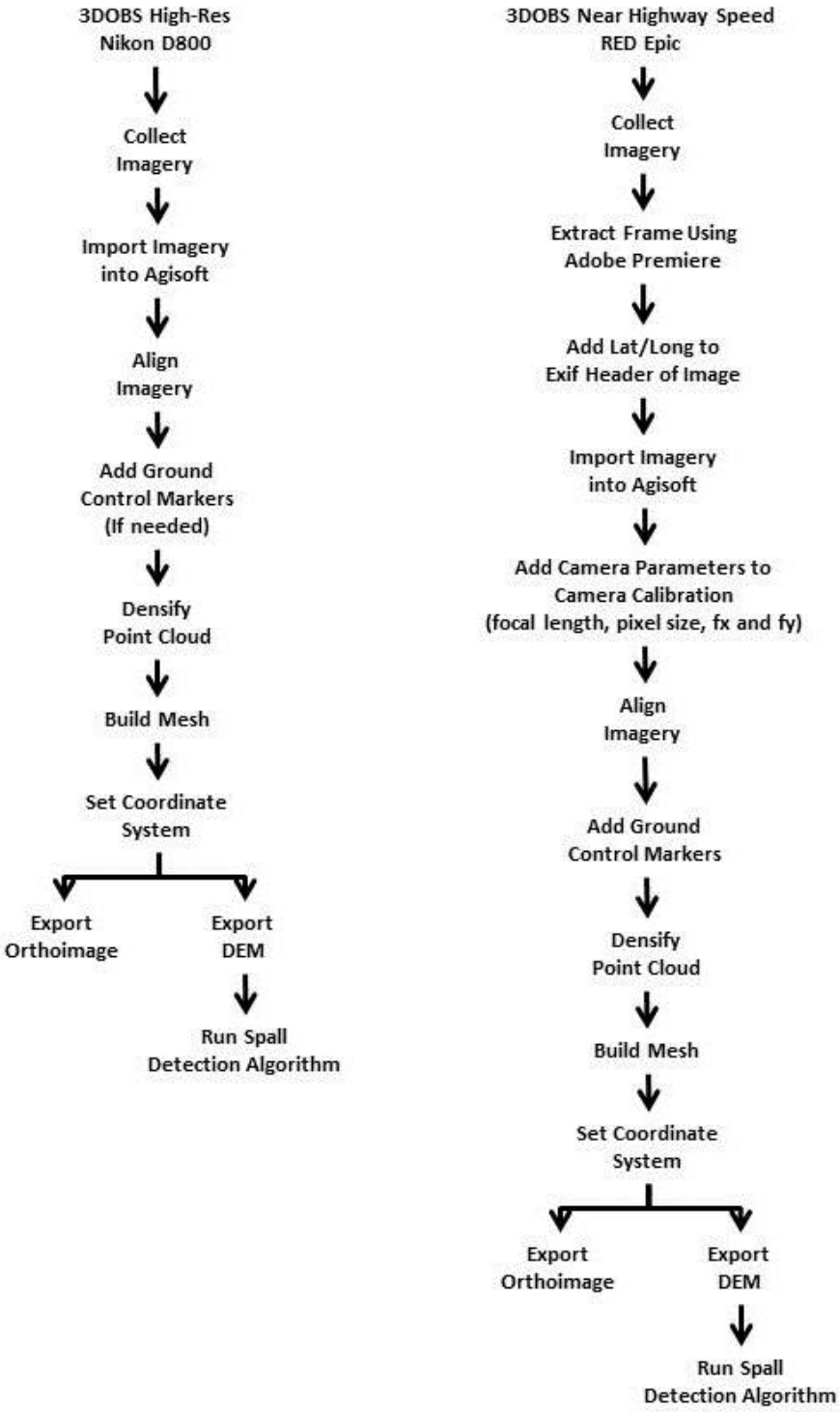

Figure 7-1: Flow Chart Showing the Processing Steps for the High Resolution and Near Highway Speeds Versions of 3DOBS.

8. MDOT NDE Bridge Condition Conclusions

8.1 Conclusions from Study

This research project investigated non-destructive evaluation (NDE) technologies, specifically remote sensing technologies including photogrammetry and thermography, for deployment at near highway speeds to assess the top surface condition of concrete bridge decks. The project also investigated an appropriate remote sensing technology of the evaluation of the underside of the bridge deck. Several non-destructive technologies were upgraded and combined including 3DOBS (3-D Optical Bridge-evaluation System), passive infrared (IR) thermography and BVRCS (BridgeViewer Remote Camera System) onto a single vehicle as an integrated system for condition assessment of the top surface of concrete bridge decks. Integrated data sets can lead to more effective asset management decisions through a more thorough understanding of deck condition. Collection techniques for active IR thermography were also demonstrated on the underside of a bridge deck affording a proof of concept demonstration for the ability to overcome some of the limitations presented with passive IR thermography.

BVRCS has proven to be a low cost, valuable tool for collecting a photo inventory of bridges providing information to inspectors and agencies. The previously implemented system utilizing Canon PowerShot cameras was upgraded to include GoPro cameras that have proved to be more rugged and easier to operate. The deployable system consists of two GoPros, a Garmin GPS and GeoJot+, which can be purchased for a total cost of approximately $1000. The GeoJot+ software allows for the creation of shapefiles consisting of interpolated points corresponding to the location each photo was captured. Each point is linked to a watermarked version of the collected photo that can be displayed in ArcMap or Google Earth.

The previous deployable 3DOBS system was upgraded into two separate versions to meet the needs of the project requirements to evaluate the top surface of concrete bridge decks: a near highway speed version which is capable of allowing the collection vehicle to travel at speeds up to 45 mph and a high-resolution version capable of detection and classification of cracking to as small as 1/32 in. The RED Epic was chosen for near highway speed collects due to its ability to collect 13.8 MP imagery at up to 60 fps while the Nikon D800 was chosen for high-resolution collects due to its 36.3 MP sensor. Both cameras can be mounted on the same vehicle mount, produce imagery that is processed in Agisoft PhotoScan and can be run through a spall detection algorithm. The tradeoff between the two is speed of the collection vehicle. The RED Epic allows for higher speed at moderate resolution (adequate for spall detection and general crack detection) while the Nikon D800 allows for higher resolution of crack detection at slower speeds.

When 3DOBS was combined with passive IR thermography on the same vehicle mount, both surface and subsurface conditions could be assessed with a single pass per lane. Both datasets were referenced to the same coordinates and could be viewed in GIS such as ArcMap. A total of eight separate data layers are generated from the collected imagery. These layers include an

orthoimage, DEM, hillshade of the DEM, LAS point cloud of the bridge deck, thermal mosaic, detected spalls layer, detected cracks layer, and potential delaminations layer. A combination of these layers would enable MDOT to perform change detection analysis on the distresses and provide objective data to help generate NBI ratings for the bridge deck.

Field demonstrations confirmed that under situations where the bridge deck is in good condition and contains very little or no distresses, it is difficult to reconstruct 3DOBS outputs without additional imagery overlap. For bridges with significant spalls or other features, only a single pass per lane is needed, as there would be enough 3D information in the imagery for accurate reconstruction. For bridge decks without major distress, additional drive-overs many be necessary to properly align imagery for condition evaluation.

Separately, these technologies can provide MDOT with a more detailed understanding of the condition of bridge decks. When combined, these three technologies would ensure MDOT could conduct bride deck inspections while keeping inspectors safe and away from traffic as well as eliminating the need to close down lanes and passing the time savings onto the traveling public.

Active IR thermography is a non-destructive condition assessment technique with simplistic testing and analysis procedures. This project focused on the application of this technology by using the surface heating method while keeping in mind inspection time and equipment portability. Results obtained from initial laboratory testing verify the capabilities of active IR thermography to detect and estimate depth of delaminations in concrete elements with a width-to-depth ratio greater than 2 and a depth of less than 2 in. using a thermal impulse of 15 minutes and a 1500W infrared heater. In addition, delamination detection using shorter heat times as little as 5 minutes were investigated and confirmed. Lab tests established the need for mounting upgrades prior to field applications resulting in the fabrication of two lightweight, portable mounts for both the heater and camera.

Advancements to the active IR thermography testing procedure made in the laboratory allowed for testing of several areas on the underside of a concrete highway bridge deck and pier cap located in downtown Grand Rapids, Michigan. Two thermal cameras, a high resolution FLIR SC640 and a lower resolution FLIR Tau2, were used to conduct testing as a means of comparison for low-cost equipment. Field deployment showed that this technology overcame limitations presented by passive IR thermography including specific testing time windows, the absence of sun and inability to test in inclement weather. A simplistic analysis method was developed to compare MDOT ground truth information to thermal images acquired by the two thermal cameras, and confirming that MDOT current practice is conservative. Testing results from the field application also showed that a heat impulse of 15 min. is acceptable for detecting and quantifying subsurface defects while using a shorter heat impulse duration of 5 min. is suitable for quantifying the area of delaminations.

Stakeholder input for implementation was gained through several outreach activities. A general training session was held to provide inspectors and end users the tools and knowledge to use the

presented non-destructive remote sensing technologies for effective asset management. Hands-on equipment demonstrations allowed attendees to have one-on-one discussions with researcher on the use, costs and benefits of the technologies. Outcomes included the request for two additional training sessions, one to review the data processing techniques for 3DOBS data with the MDOT photogrammetry group, and one session specifically to demonstrate the use of the BVRCS system for collecting a high-resolution geo-tagged photo inventory of a bridge deck. Training sessions confirmed that bridge inspectors are interested in using advanced technologies for routine, detailed and scoping inspections.

8.2 Recommendations for Further Research

Combining remote sensing technologies to assess the condition of a concrete bridge deck has been shown to be very useful to enhance bridge inspection. As the performance of cameras continues to advance, additional health indicators or condition state will be detectable. It is strongly recommended that MDOT keep abreast of changes in technology through additional interactions with the project team.

Deck cracking is a very real concern to bridge managers. Technology will advance to the point of refined crack detection (to as small as 1/32 in.) at near highway speeds or 1/64 in at slower speeds. Since the start of this project, new DSLRs are being developed with a resolution of 40+ MP and the RED Epic sensor has been upgraded from 13.8 MP to 19.4 MP and capable of 120 fps. These types of upgrades will only increase the ability to detect smaller cracks at faster speeds. Further research needs to include not only the assessment of enhanced camera performance, but also the development of an automated crack detection and classification algorithm. Building from related research would be an important component of automating crack detection. For example, the Transportation Research Board 2015 Annual Meeting has a dedicated poster session on automatic crack detection featuring the work of seven research teams, showing promise that this issue is tractable (see http://pressamp.trb.org/aminteractiveprogram/EventDetails.aspx?ID=32614). Similarly, an automated detection algorithm can be developed using thermal imagery to locate potential delaminations, building from current methods focused on analyst interpretation.

Active thermography was investigated as a method to assess the bottom surface condition of a bridge deck. Depth analysis procedures developed in lab were used on data collected in the field and results demonstrate the need for further research to accurately estimate delamination depth. Heating sources to cover larger areas or confined are areas should be investigated for use. Thermal cameras range in cost and performance; newer thermal cameras can be 1/10 the cost of ones purchased five years ago. This study used systems that were currently available for proof of concept testing and did not consider camera performance. Results of several cameras should be compared to determine the best equipment.

The use of unmanned aerial vehicles (UAVs) for condition assessment has a growing popularity. Remote sensing technologies, including optical, thermal, and LiDAR, have been successfully

demonstrated to MDOT through other research opportunities ("Evaluating the Use of Unmanned Aerial Vehicles for Transportation Purposes", 2013-067, No. 1, OR13-008, led by PI C.Brooks). Combining UAVs with the data fusion and common platform for technologies can enhance inspection for bridge decks, superstructures, and other transportation infrastructure. Pilot studies are recommended to demonstrate the optimal use of UAVs for condition assessment of bridge decks, in relation to vehicle-based and manual assessment, building from MDOT's recent research investment in this area.

As experts in remote sensing applications for transportation infrastructure, the project team is available to assist MDOT with their future research needs in an area of rapidly changing technology. Data processing techniques for assessment of a variety of health indicators are yet to be developed and can be applied to a host of situations including evaluation of steel and timber superstructures and substructures. Future research could address these additional bridge types and construction materials.

8.3 Recommendations for Implementation

An Implementation and Action Plan has been drafted to direct the Research Advisory Panel and other MDOT personnel in the steps necessary to implement the results of the research program. The draft plan is included in Appendix I. Data collection at near highway speed for the top of deck condition assessment and proof of concept testing for the underside of the deck was conducted for surface and subsurface evaluation. Recommendations are included for combining multiple remote sensing technologies into a single vehicle delivery. This section summarizes the implementation action plan.

The BridgeViewer BVRCS, a system shown to provide high resolution imagery using GoPro cameras to discern spalls and patchwork on a concrete deck while traveling at 45 mph and above, is near ready for deployment. The system is commercially available and low cost (less than $1000) , and can provide an assessment method comparable to visual inspection in a very short time. A hands-on demonstration session was provided for bridge inspectors and managers to begin implementation. It is recommended that MDOT begin with introducing the system into one region for all upcoming inspections. Inspectors will quickly learn the system operation and gain the benefit of having a high-resolution geo-tagged photo inventory of the bridge deck collected while travelling at highway speed without traffic interruption.

Top of deck evaluation at near highway speed can also include the detection of spalls, cracking, and suspected delaminations by combining 3-D photogrammetry and thermography data collections. A total of eight separate data layers generated from the collected imagery can assess the surface and subsurface condition of the deck. Imagery captured at near highway speed (45 mph) can detect spalls and delaminations, while imagery captured at slower speeds with higher resolution cameras can detect cracking to 1/32 in. It is recommended that these remote sensing technologies be integrated to the bridge inspector's suite of tools for inspection. Capital

investment in equipment, training of inspectors, and coordination with the MDOT photogrammetry office are necessary for implementation.

Common to the implementation of all these technologies, is the tough question that MDOT must assess thoroughly to fully understand the path to implementation. How will this data be used? Strategic discussions are needed within MDOT bridge management groups to explore the best strategies to utilize the data, such as whether time-history data can be used through a decision support system to predict service life for alignment of maintenance and repair funds, or how this information can be used to enhance the bridge preservation program. Pilot studies with an increased sample population will add confidence in the data and methodology for providing valuable information about the condition state of the concrete bridge deck.

Further development of the active thermography method is necessary prior to implementation for use in bridge inspection of concrete bridge decks. Studies should include variable heat sources and heating times for inspector convenience while optimizing data collection. Methods of analysis have been simplified, and upgraded equipment with improved resolution and lower costs should be considered. Most important, MDOT must decide where and when is the most appropriate use of the technology. While the method was demonstrated here for the bottom surface of a concrete bridge deck, any location where there is little to no solar heating may benefit from the use of active thermography.

MDOT is a leader in cutting edge research for enhancing bridge inspection. Proof of concept testing and field demonstrations for remote sensing technologies are necessary steps in the implementation of new systems and methodologies.

References

AASHTO (2011). AASHTO Guide Manual for Bridge Element Inspection. First Edition, American Association of State Highway and Transportation Officials.

AASHTO. (2008). "Bridging the Gap: Restoring and Rebuilding the Nation's bridges." Retrieved April, 2013, from ftp://ftp.mdt.mt.gov/research/LIBRARY/BTG-1-BRIDGING-GAP-AASHTO.PDF.

Abdel-Qader, I., S. Yohali, O. Abudayyeh and S. Yehia (2008). "Segmentation of thermal images for non-destructive evaluation of bridge decks." NDT & E International **41**: 395-405.

Abdel-Qader, I., S. Yohali, O. Abudayyeh and S. Yehia, 2008. "Segmentation of Thermal Images for Non-Destructive Evaluation of Bridge Decks." *NDT & E International*, 41, pp. 395-405.

ACI (2001). Protection of Metals in Concrete against Corrosion (ACI 222R). Farmington Hills, MI, American Concrete Institute.

Ahlborn, T. M., R. Shuchman, L. L. Sutter, D. K. Harris, C. N. Brooks and J. W. Burns (2012). Bridge condition assessment using remote sensors. Final project report, USDOT/RITA. Cooperative agreement # DTOS59-10-H-00001.

Arndt, R. W., 2010. "Square Pulse Thermography in Frequency Domain as Adaption of Pulsed Phase Thermography for Qualitative and Quantitative Applications in Cultural Heritage and Civil Engineering." *Infrared Physics and Technology*, 53, pp. 246-253.

ASTM (1997). ASTM D 4580 - 86: Standard Practice for Measuring Delaminations in Concrete Bridge Decks by Sounding, American Society of Testing Materials.

ASTM (2007). ASTM D4788-03: Standard test method for detecting delaminations in bridge decks using infrared thermography, American Society of Testing Materials.

ASTM, 2007, ASTM D4788-03: Standard Test Method for Detecting Delaminations in Bridge Decks using Infrared Thermography, American Society of Testing Materials.

Brown, J. R. and H. R. Hamilton, 2007. "Heating Methods and Detection Limits for Infrared Thermography Inspection of Fiber-Reinforced Polymer Composites." *ACI Material Journal*, 104(5), pp. 481-490.

Clark, M. R., D.M. McCann and M. C. Forde (2003). "Application of Infrared thermography to the non-destructive testing of concrete and masonary bridges." NDT & E International **36**: 265-275.

Engineering ToolBox. 2012. "Thermal Conductivity of Some Common Material and Gases." Retrieved October 30th, 2012 from http://www.engineeringtoolbox.com/thermal-

conductivity-d_429.html.

Federal Highway Adminstration (FHWA) (2006). Bridge Inspector's Reference Manual (BIRM). Washington, D.C.

FHWA (2006). Bridge Inspector's Reference Manual (BIRM). Washington, D.C., Federal Highway Administration.

FHWA. (2011). "National Bridge Inventory (NBI)." 2013, from http://www.fhwa.dot.gov/bridge/nbi/deck.cfm.

FHWA Bridge Preservation Guide, 2011. US Department of Transportation. Report No. FHWA-HIF-11042, McLean, VA.

Fu, G., Ed. (2005). Inspection and monitoring techniques for bridges and civil structures. Cambridge, England, Woodhead Publishing in Materials.

Ghosh, K. K. and V. M. Karbhari, 2006. "A Critical Review of Infrared Thermography as a Method for Non-Destructive Evaluation of FRP Rehabilitated Structures." *International Journal of Materials and Product Technology*, 25(4), pp. 241-266.

Gucunski, N., A. Imani, F. Romero, S. Nazarian, D. Yuan, H. Wiggenhauser, P. Shokouhi, A. Taffe and D. Kutrubes (2013). Nondestructive testing to identify concrete bridge deck deterioration. SHRP2. Washington, D.C.

Halabe, U. B., H. V. S. GangaRao and N. Perisetty, 2012, Infrared Thermography and GPR Techniques for Condition Assessment of RC Bridges. *NDT/NDE for Highways and Bridges: Structural Materials Technology (SMT)*. New York City, NY.

Henriksen, S., Ed. (1994). The glossary of mapping sciences. New York, NY, American Society of Civil Engineers.

Howard, G. B. and C. P. Sturos (March 2010). Data at Speed. Roads and Bridges. Howard, G. B., C. P. Sturos and T. M. Ahlborn (Feb 2010). On the fly over. Roads and Bridges.

Jana, D. (2007). Delamination - A State of The Art Review. Proceedings of the Twenty- Ninth Conference on Cement Microscopy Quebec City, PQ, Canada.

Jenson, J. (2007). Remote sensing of the environment: an earth resource perspective, Pearson Education, Inc.Jiang, R., D. V. Ja´uregui and K. R. White (2008). "Close-range Photogrammetry Applications in Bridge Measurement: Literature review." Measurement **41**(8): 823-834.

Kurita, K., M. Oyado, H. Tanaka and S. Tottori, 2009. "Active Infrared Thermographic Inspection Technique for Elevated Concrete Structures using Remote Heating System." *Infrared Physics and Technology*, 52, pp. 208-213.

Lamond, J. F. and J. H. Pielert, Eds., 2006. *Significance of Test and Properties of Concrete and Concrete-Making Materials.* STP-169d. Bridgeport, NJ, ASTM International.

Levar, J. M. and H. R. Hamilton, 2003. “Nondestructive Evaluation of Carbon Fiber-Reinforced Polymer-Concrete Bond using Infrared Thermography.” *ACI Material Journal*, 100(1), pp. 63-72.

Maas, H.-G. and U. Hampel (2006). "Photogrammetric techniques in civil engineering material testing and structure monitoring." Photogrammetric Engineering and Remote Sensing **72**(1): 7.

Maierhofer, C., A. Brink, M. Rolling and H. Wiggenhauser, 2002. “Transient Thermography for Structural Investigation of Concrete and Composites in the Near Surface Region.” *Infrared Physics and Technology*, 43, pp. 271-278.

Maldague, X. P. V. (1993). Nondestructive evaluation of materials by infrared thermography. London, Springer-Verlag.

Maldague, X. P. V. and P.O. Moore, 2001, *Nondestructive Testing Handbook: Infrared and Thermal Testing*, American Society of Nondestructive Testing.

Maldague, X.P.V., 1993, *Nondestructive Evaluation of Materials by Infrared Thermography*, London, Springer-Verlag.

McGlone, J. C., E. M. Mikhail, J. S. Bethel and R. Mullen, Eds. (2004). Manual of Photogrammetry. Bethesda, MD, American Society for Photogrammetry and Remote Sensing.

MDOT, 2003, Standard Specifications for Construction. Lansing, MI, Michigan Department of Transportation.

MDOT. (2007). "Pontis Bridge Inspection Manual." Retrieved January, 2013, from http://www.michigan.gov/documents/mdot/MDOT_BridgeDeckMatrix_withUncoatedBlackRebar_355077_7.pdf.

MDOT. (2008). "Bridge Deck Preservation Matrix." Retrieved July, 2012, from http://www.michigan.gov/documents/mdot/MDOT_BridgeDeckMatrix_withUncoatedBlackRebar_355077_7.pdf.

MDOT. (2009). "Project Scoping Manual." Retrieved July, 2012, from mdotwas1.mdot.state.mi.us/public/docs/scoping/Scoping_Manual.pdf.

MDOT. (2011). "Bridge Deck Preservation Matrix." Retrieved July, 2012, from http://www.michigan.gov/documents/mdot/MDOT_BridgeDeckMatrix_withUncoatedBlackRebar_355077 7.pdf.

MDOT. (2011). "Bridge Safety Inspection NBI Rating Guidelines." Retrieved January, 2013, from http://www.michigan.gov/documents/mdot/MDOT_BIR_Ratings_Guide_367482_7.pdf.

MDOT. 2008. "Bridge Deck Preservation Matrix." Retrieved July, 2012, from www.michigan.gov/documents/mdot/MDOT_BridgeDeckMatrix_withEpoxyCoatedRebar_355086_7.pdf.

MDOT. 2012. "Bridge Management and Inspection System." Retrieved May 2014 from http://mdotjboss.state.mi.us/mbrs/bridgeDashboard.do#no-back-button.

Moore, M., B. Phares, B. Graybeal, D. Rolander and G. Washer (2000). Reliability of visual inspection for highway bridges, NDE Validation Center/FHWA.

Pollock, D. G., K. J. Dupuis, B. Lacour and K. R. Olsen (2008). Detection of Voids in Prestressed Concrete Bridges using Thermal Imaging and Ground Penetrating Radar, Washington State University.

Ryan, T. W., R. A. Hartle, J. Eric Mann and L. J. Danovich (2006). Bridge Inspector's Reference Manual. Washington D.C., FHWA.

Spring, R., R. Huff and M. Schwoegler (2011). "Infrared Thermography: A Versatile Nondestructive Testing Technique." Materials Evaluation **69**(8): 935-942.

Starnes, M. A. (2002). Development of technical bases for using infrared thermography for nondestructive evaluation of fiber renforced polymer composites bonded to concrete. Civil and Environmental Engineering, Massachusetts Institute of Technology.

Starnes, M. A., N. J. Carino and E. A. Kausel, 2003. "Preliminary Thermography Studies for Quality Control of Concrete Structures Strengthened with Fiber-Reinforced Polymer Composites." *ASCE Journal of Materials in Civil Engineering*, 15(3), pp. 266-273.

Vaghefi, K. and T. M. Ahlborn, 2013. "Application of Active Infrared Thermography for Inspecting Existing Concrete Structures." *NDT & E International*, In review since October 2013.

Vaghefi, K., 2013, Infrared Thermography Enhancements for Concrete Bridge Evaluation. *Civil and Environmental Engineering*, Michigan Technological University. Ph.D.

Vaghefi, K., R. C. Oats, D. K. Harris, T. M. Ahlborn, 2011, Application of Thermal IR Imagery for Concrete Bridge Inspection. *PCI Convention and National Bridge Conference.* Salt Lake City, Utah, Prestressed/Precast Concrete Institute.

Vaghefi, K., R. C. Oats, D. K. Harris, T. M. Ahlborn, C. N. Brooks, K. Endsley, C. Roussi, R. Shuchman, J. W. Burns and R. Dobson (2012). "Evaluation of Commercially Available Remote Sensors for Highway Bridge Condition Assessment." ASCE Journal of Bridge Engineering **17**(6): 886-895.

Vaghefi, K., T. M. Ahlborn, D. K. Harris and C. N. Brooks (2013). "Combined Imaging Technologies for Concrete Bridge Deck Condition Assessment." ASCE Journal of Performance of Constructed Facilities Accepted April 2013.

Washer, G. (2010). Thermal Imaging of Damage in Bridge Soffits. NDE/NDT for Highways and Bridges: Structural Materials Technology, NYC.

Washer, G., R. Fenwick and N. Bolleni (2009 a). Development of hand-held thermographic inspection technologies. OR10-007.

Washer, G., R. Fenwick, N. Bolleni and J. Harper (2009 b). "Effects of environmental variable on infrared imaging subsurface features of concrete bridges." Journal of the transportation research board No. 2108: 107-114.